Networks and non-autonomous dynamics, with applications to cell energy metabolism

Joe Rowland Adams, MSci

This thesis is submitted for the degree of

Doctor of Philosophy

Undertaken at

Lancaster University

Department of Physics

Lancaster University

Lancaster, UK

November 2022

Abstract

Living systems are defined by their thermodynamic openness, by the fact that energy and matter are able to cross their boundaries. Without this capability to interact with their environment, living systems would be unable to support their life-sustaining functions. As a result of this continual interaction with its environment, the interior processes of a living system is forced to operate far from any equilibrium. Indeed, any system that is in equilibrium internally or with its environment could reasonably be characterised as a dead one.

The dynamics of systems that are operating far from equilibrium, however, are far from understood. In this thesis, we build on an existing framework for understanding these dynamics, based in the finite-time analysis of non-autonomous oscillatory processes. This approach is motivated by a key consequence of thermodynamic openness — to introduce time-dependence to the open system. We develop an original mathematical model for the energy metabolism of cells using inter-coupled networks of non-autonomous phase oscillators, with intra-network weighted coupling. The effect of each of this model's components on its dynamics and stability is numerically analysed. Experimental data of the metabolism of HeLa cells is analysed, finding the fundamental frequencies of this process. This analysis is used to demonstrate the capability of the model to reproduce the complex dynamics of the experiment, and this is contrasted to a comparable model of an alternative framework.

It is this capacity of non-autonomous oscillations to simply and deterministically produce apparently highly complex dynamics that justifies our application of them to this problem. We demonstrate it further by viewing them through the framework of statistical time-series analysis, finding that even a single non-autonomous oscillator can appear to

be $1/f^\beta$ noise in a power-spectral density estimation. Autonomous systems are shown to only present as noise when there are many of them, and hence it is the introduction of time-dependence that generates such complexity so readily. We demonstrate that this also occurs for coupled networks of non-autonomous oscillators, and in real experimental data. Analysis tools based in a finite-time framework, however, are shown to detect informative deterministic frequencies and couplings in both the numerical and experimental cases.

Overall, this thesis demonstrates that networks of non-autonomous oscillations are physically linked to living systems through the time-dependence introduced by thermodynamic openness. Additionally, it is shown that they are able to reproduce living systems' complex dynamics in a simple and usable way. Finally, it is established that much greater information about such an open system can be gained when they are analysed with this time-dependent deterministic framework in mind.

Contents

5   Summary and conclusions   170

List of Figures

List of Tables

Acknowledgements

First, I would like to thank my supervisor, Aneta. Without her support, guidance and encouragement, this thesis would not have been possible. I am extremely grateful for all her time and effort spent on this project and preparing me for an academic career.

Thanks also to my secondary and independent supervisors, Peter McClintock and Chris Arridge. They could always be relied upon to provide thoughtful and helpful comments and advice whenever asked. To all the other current and former students and postdocs in the nonlinear and biomedical physics group as well, who consistently provided a welcoming and helpful group culture. Particular thanks also to Julian Newman, for a very rewarding collaboration, and all his efforts to complete it in time for this thesis.

To all my Lancaster Labour comrades, for the regular social diversions that were oftentimes keeping me sane. In particular to Peter, who kept us going through the worst of lockdown.

To my mums, Helen, Lindsey and Jaqui, my dad Tony, and my sister Millie. They were always there to support me when I needed it, no matter what was happening in their own lives. An extra thanks, as well, to Lindsey, without whom I would not have even been accepted on to an undergraduate physics course.

And finally to my partner, Dan, who has been endlessly compassionate and caring every day, good or bad, for the last four years. None of this would have a purpose without you.

Declaration

This thesis is my original work and has not been submitted, in whole or in part, for a degree at this or any other university. Nor does it contain, to the best of my knowledge and belief, any material published or written by another person, except as acknowledged in the text. All quotations have been distinguished by quotation marks and the sources of information specifically acknowledged. This thesis is submitted for the degree of Doctor of Philosophy undertaken at Lancaster University (Lancaster, UK).

List of publications

The following publications are chapters in this thesis:

- Rowland Adams J, Stefanovska A. Modeling Oscillating Living Systems: Cell Energy Metabolism as Weighted Networks of Nonautonomous Oscillators. In Wood DR, de Gier J, Praeger CE, Tao T, editors, 2019-20 MATRIX Annals. Cham: Springer. 2021. p. 255-264. (Chapter 2)

- Rowland Adams J, Stefanovska A. Modelling cell energy metabolism as weighted networks of nonautonomous oscillators. Front. Physiol. 2021;11:613183. (Chapter 3)

- Rowland Adams J, Newman J, Stefanovska A. Distinguishing between deterministic oscillations and noise. Eur. Phys. J. Spec. Top. (in submission). (Chapter 4)

Work from this thesis has also been presented at the following scientific conferences and symposia:

- Rowland Adams J. The physics of a cancer cell's energy metabolism. Lancaster Cancer symposium. 10 July 2019. Lancaster, United Kingdom.

- Rowland Adams J. Modelling metabolic oscillations using nonautonomous oscillator networks. 9th International Congress on Industrial and Applied Mathematics. 15–19 July 2019. Valencia, Spain.

- Rowland Adams J. Network physics and cell metabolism in health and COVID-19. Lancaster University Science Week 2021. 12–16 April 2021. Online.

- Rowland Adams J. Modelling open systems with networks of nonautonomous phase oscillators. Dynamics Days Europe 2021. 23–27 August 2021. Online.

- Rowland Adams J. Deterministic noise. Stochastic Resonance 40. 13–15 September 2021. Perugia, Italy.

- Rowland Adams J. Chronotaxic systems and cell energy metabolism. FEPS European Physiology Day 2021. 12 October 2021. Online.

And in the following poster:

- Rowland Adams J. Modelling open biological systems with networks of nonautonomous oscillators. Physics meets Biology 2021. 26–28 July 2021. Online.

1. Introduction

It was thought for parts of the 20th century that all that remained for physics to address was the finer points of the subatomic and galactic scales, and that with the extension of the Standard Model into a theory of everything physics would be, in some sense, 'finished'. However with the advent and expansion of, among others, complexity and network science, the relevance of physics to significant unresolved questions has only expanded, including to a field much closer to home — living systems.

The study of living systems is the study of a symphony of interacting processes, cooperating in complex ways in spite of an impossibly noisy, constantly perturbing environment. On paper the interactions of these processes may appear profoundly fragile, and yet in reality they produce one of the most durable, persistent and adaptive phenomena on Earth — life. The question of how this happens has challenged an ever growing number of sciences, including, now, physics.

In this thesis we will focus on studying living systems as a collection of dynamical processes. This is to say, we are focused primarily on the function of a given process within a larger system. To take the example of the cell, which we will return to in Chapters 2 and 3, we examine how regularly, on what time scales, it produces energy and how this interacts with the time scales of its supply of molecules necessary to do so, and only secondarily where it is located within the cell, what the chemistry involved is, etc.

The aim of this approach is to be able to understand the potentially unexpected behaviour that emerges from these interactions in as simple a way as possible. This also allows us to draw on the significant and well-developed field of dynamical systems theory. In this

theory, we may represent a process with a differential equation, and then apply various analyses to find the solutions of this equation, and uncover these solutions' properties.

This is not to say that this is just a mathematical problem. The form of dynamical theory that it is most appropriate to apply is greatly informed by core disciplines of biology and physics. For the part of physics, a thermodynamic understanding of living systems is essential in order to construct such a model. Namely, we must recognise that living systems are thermodynamically open — both matter and energy are allowed to cross their boundaries. Without this, no living system would be able to acquire the molecules it needs for its essential processes, and nor is a system entirely isolating itself from the wider universe an easy thing to achieve.

The foremost implication of this openness is to engender a time-dependence in the evolution of the system; it no longer operates according only to its own internal processes, but is now affected by and dependent on an ever-changing external environment. In the language of dynamical systems, this means we are now dealing with non-autonomous systems.

The theory of non-autonomous dynamical systems offers an alternative to the established framework of autonomous theory being applied to systems of relatively few components, and statistical theory applied to relatively many, but has been traditionally neglected compared to this framework. One of the main aims of this thesis is to advance the finite-time framework, which analyses non-autonomous systems within finite-time, as opposed to assuming asymptotic time, to develop our understanding of non-autonomous systems as a whole, and their application to living systems specifically.

In addition to their interactions with a time-dependent environment, it is a prevalent property of living systems to exhibit an extensive network of interactions internally. It is this network from which the complex and adaptive macroscopic behaviours, i.e. the behaviours we are more likely to be able to experimentally measure, arise. It has already been shown in [1, 2] how individual processes and networks become more stable against external perturbation and give rise to time-dependent phenomena when non-autonomicity is introduced. But even with this recent work, and despite the fact that Kuramoto first introduced the oscillator model on which our work is based in 1975 [3],

the behaviour of non-autonomous networks of many forms is not understood. We will build on the recent work in this field by extending to interactions between such networks, an important step towards being able to replicate and understand the kind of processes actually occurring in living systems.

Another problem that has plagued our understanding of living systems, and many more systems besides, is noise in data. This phenomenon routinely obscures the features being investigated in experimental recordings, and much time and effort has gone into developing methods to reduce it. However, as easy as it is to assume that such noise is unwanted, it is not impossible that it can in fact provide useful information about the system. In this sense, it would not be 'noise', but dynamics of too great a complexity to be understood by whatever analysis method that is making it appear as noise. If this were so, then treating this phenomenon as complex dynamics, rather than noise, could result in much more information being obtained from a vast array of experimental measurements, perhaps most of all from living systems. In Chapter 4 in particular, we will explore the capacity of non-autonomous systems to produce such a phenomenon.

In summary, this thesis aims to advance our understanding of non-autonomous systems, particularly in the form of interacting networks of such processes, with a focus on their emergent dynamics. This is motived by an analysis of living systems, and we will apply these models to advance our understanding of important cellular metabolic processes. We will also investigate whether these models are responsible for some dynamics that are currently generally considered to just be noise.

1.1 Dynamical systems theory

Dynamical systems theory was developed to describe the evolution in time of a set of variables in a given phase space, that is, the space of all possible combinations of values of these variables. This evolution may be considered for either discrete time, where time is defined as some finite subset of the real numbers, or continuous time, where time is defined simply as the set of real numbers. In this thesis, we will consider only continuous time systems, which better represent the reality of how physical, and in particular living

systems, evolve. Mathematically, such a dynamical system can be described as

$$\dot{x}(t) = F(x(t), t). \tag{1.1}$$

The nature of the evolution described by a dynamical process may be characterised in a number of other ways, however. If the evolution is random, then we may consider the system to consist of a set of variables $\{X_t\}$, where the occurrence of each variable is associated with a certain probability. A fully deterministic process, in contrast, will obtain the set of state variable values $x(t)$ at the time t with 100% probability, as described by Eq. 1.1. These two distinctive mechanisms of time evolution can also be combined, by the addition of some random function, X_T, valued at each time t, to Eq. 1.1—

$$\dot{x}(t) = F(x(t), t) + X_t. \tag{1.2}$$

In this form therefore, the deterministic change in the variables $x(t)$ will be additionally influenced by random variables, and so is not guaranteed to obtain the same state at the same t, while still following some fundamental deterministic pattern. Here, we will consider exclusively deterministic processes and deterministic processes with random additions. These, again, best reflect our understanding of living systems as being governed by deterministic laws, sometimes perturbed by random environmental factors. The extent to which this latter supposition is true will be further discussed in Chapter 4.

The final property of the evolution of a dynamical system we will discuss here is time-dependence. Autonomous dynamical systems are ones in which their evolution does not depend explicitly on time, i.e.

$$\dot{x}(t) = F(x(t)). \tag{1.3}$$

This is in contrast to Eq. 1.1, where F depends explicitly on t, and is referred to as a non-autonomous dynamical system.

1.1.1   Stability of dynamical systems

The stability of dynamical systems is one of the key considerations of the field. It is one of the main analyses through which we can understand and explain the mathematical behaviour of a dynamical system, and by extension any physical system it may represent.

This is particularly the case when explicit analytical solutions to the systems are not known. In this subsection we will review the foundational concepts of this theory, and the conditions in which well-established methods can be applied. This is largely based on the reviews presented in [4–6].

Equilibrium points, limit cycles and stability

The solution of a differential equation such as Eq. 1.1 gives the values of the state variables $x(t)$ for which $\dot{x}(t) = 0$. In other words, these are the values of $x(t)$ that, if reached, will not change in time if unperturbed. These are referred to as equilibrium points. The values of these points are often sought in an effort to understand the dynamics of the system under study, and this method for studying a dynamical system is hence heavily reliant on our ability to solve the associated differential equations. As such, the mathematical tools available to solve more complex differential equations often form a barrier to better understandings of physical systems.

A key question for the analysis of the dynamics of a physical system, beyond just the existence and value of equilibria points, is the stability of these points. An equilibrium point is said to be asymptotically stable if, when the system is perturbed from this point, the perturbation decays to zero in finite time. If the perturbation instead remains in some neighbourhood of the equilibrium point, but does not return to it, then it is called Lyapunov stable, or neutrally stable. If neither of these behaviours hold, and the perturbation grows unboundedly, then it is unstable.

For a system that is linear and autonomous, the stability is simply given by the associated eigenvalues — an equilibrium point is asymptotically stable if the corresponding eigenvalues have negative real parts, unstable if they have positive real parts and neutrally stable if they are imaginary or zero. For nonlinear autonomous systems it is common to linearise about an equilibrium point by calculating the Taylor expansion of a perturbation from this point, which leads to

$$\dot{x}(t) \approx J(x_f) \cdot x(t). \tag{1.4}$$

The stability in the vicinity of this equilibrium point is then once again given by the eigenvalues of the Jacobian $J(x_f)$. This approach does not, however, in general hold for non-autonomous nonlinear systems.

For a multi-dimensional system, it is possible to find not just equilibria points, but also limit cycles. This occurs when F permits a set of solutions that forms a closed trajectory in phase space such that $x_f(t_1) = x_f(t_1 + t_2)$ for some times t_1 and t_2. This also extends similar definitions of stability, where they now simply consider trajectories perturbed from any point on the cycle, rather than a single equilibrium point.

Limit cycles, while of particular relevance to this thesis, are but one example of a whole class of dynamical objects – attractors. These are sets of points in phase space that attract neighbouring points into the subset in forward time, and appear in many variations, including limit cycles and chaotic attractors. This class of objects will be discussed further in Section 1.7.

Phase and synchronisation

If one is primarily concerned with the dynamics of a system that includes periodic oscillations, it is common to disregard the amplitude state variables, under the proviso that they vary only minimally, and instead describe it in terms of a single variable — the phase. This reduces the formulation of the system to just considering its current position in some repeating cycle of undefined amplitude. If the system is reduced to a single phase, a.k.a. a one-dimensional phase system, as will initially be considered here, representation of any amplitude dynamics of the original system will be lost entirely. Hence if these amplitude dynamics are significant to the functioning of the system, a one-dimensional phase representation will provide only a partial picture of the full dynamics. Mathematically, Eq. 1.1 would then be described in terms of a natural frequency, $\omega(t)$,

$$\dot{\theta} = \omega(t), \tag{1.5}$$

with a phase θ through the time derivative $\dot{\theta}$, assuming that F describes a periodic oscillation, and that it includes no interactions with other systems. For an autonomous system, alternatively, we would have a constant natural frequency such that —

$$\dot{\theta} = \omega. \tag{1.6}$$

This simplification is particularly useful when considering the interaction of oscillatory processes. As the models of this thesis are ubiquitously based in the dynamics of interacting oscillations, we will adopt a phase framework from this point onwards.

The simplest form of interacting oscillatory processes is an oscillator with frequency ω_1 driven by an external force with frequency ω_2 and a coupling strength ϵ, like so —

$$\dot{\theta} = \omega_1 + \epsilon \sin(\theta - \omega_2 t). \tag{1.7}$$

Even in this simple case, there is the possibility of a new phenomenon not seen in the uncoupled systems we have considered thus far — synchronisation. This is when, due to the external driving force, the oscillator begins oscillating with the frequency of the driver. This is also an equilibrium point, i.e. in this case, once it occurs it persists indefinitely, assuming no change in external influences. The conditions under which this is possible is best understood by considering a rotating frame with respect to the driver. This frame is defined as the difference between the driven phase, defined by $\dot{\theta}_1 = \omega_1 t$, and the driving phase, defined by $\dot{\theta}_2 = \omega_2 t$,

$$\dot{\phi} = \omega_1 - \omega_2 + \epsilon \sin(\phi), \tag{1.8}$$

where ϕ denotes this phase difference $\theta_1 - \theta_2$. Here, it is evident that an equilibrium point is only possible when $|\omega_1 - \omega_2| \leq \epsilon$. Hence, only when then natural frequencies are sufficiently close and the driving is sufficiently strong. Synchronisation is a common mechanism through which physical and living systems can operate their oscillatory processes harmoniously with other internal processes, and external perturbations. Understanding when and how this happens is therefore crucial to answering the further question of why, which is crucial to truly understanding a system.

Mutual synchronisation can also take place between two oscillators that are bi-directionally coupled to one another with coupling strengths F_1 and F_2, of the form —

$$\begin{cases} \dot{\theta}_1 = \omega_1 + F_1 \sin(\theta_1 - \theta_2), \\ \dot{\theta}_2 = \omega_2 + F_2 \sin(\theta_2 - \theta_1). \end{cases} \tag{1.9}$$

A rotating frame of the difference between these two phases can once again be adopted, which tells us that synchronisation is possible in this case when $|\omega_1 - \omega_2| \leq F_1 + F_2$.

Once considering more than two processes, as is often the case in physical systems that are not yet fully understood, it can be more convenient to adopt the formalism of networks. In this framework, each oscillator process is now considered as a network node, and the interactions between them as network edges. More information on the application of network science to the dynamics of physical systems can be found in [7].

In particular, the Kuramoto model, which we now introduce, was specifically designed to understand the interactions of oscillators through a simple network lens. In this model all-to-all coupling is considered, that is to say, every oscillator is influenced by and influences every other. Mathematically, a network of N oscillators can be described using the coupling strength K as

$$\dot{\theta}_i = \omega_i + \frac{K}{N} \sum_{j=1}^{N} \sin(\theta_i - \theta_j). \tag{1.10}$$

In this formulation, the coupling K is taken to be constant and identical between each oscillator pair (i, j), but this does not have to be the case. In Chapters 2 and 3 non-identical coupling weights will be considered. Here, as in the previous example of two coupled oscillators and a single driven oscillator, this coupling is specifically phase coupling. That is, coupling that results in adjustment of the oscillator's phase, and not amplitude.

Taking advantage of the application of network theories, an order parameter of this network can also be characterised. This is defined as

$$re^{i\Psi} = \frac{1}{N}\sum_{i=1}^{N} e^{i\theta_i}. \tag{1.11}$$

Here, Ψ is the average phase of the network, and the order parameter r characterises the level of coherence between the phases of the oscillators in the network. If the oscillator phases are initially spread equidistantly around the circle and then transition towards being equal, the order parameter will begin at zero and approach one. In this way, it can be understood as a measure of the level of synchronisation between oscillators within a network.

1.1.2   Non-autonomous oscillations

As techniques, such as the ones we have outlined in the previous subsection, for analysing autonomous systems are much better understood and developed than for non-autonomous ones, it is natural to try to find ways to apply them to the latter. It is a common misconception that this can be accomplished through the autonomous extension, whereby a non-autonomous system is reduced to an autonomous one by incorporating time as just another dimension. This is done as follows—

$$\begin{cases} \dot{\tau} = 1, \\ \dot{x}(t) = F(\tau, x(t)). \end{cases} \tag{1.12}$$

The dynamical features that we would then aim to study in this new autonomous system, equilibria points, limit cycles, etc., are bounded objects. However, in the process of the autonomous extension, while we have made a time-independent system, we have also made an unbounded one [8]. Hence, to understand the dynamics of non-autonomous systems they must be analysed as non-autonomous systems, and to do so alternative techniques are required. In 1.7, we will outline some of the recent developments in this alternative approach to non-autonomous systems.

1.2   Statistical physics

When modelling or analysing a physical system, it is just one approach to treat it as deterministic, and attempt to discern the pattern or law that governs its evolution.

Another is to assume that there is no such deterministic rule in this evolution, and that it is in fact random, with each subsequent value occurring with some probability. This is not necessarily because the given system is expected to be genuinely random, but in most cases rather that its dynamics is considered too complex for its deterministic laws to be derivable. Or alternatively, that the system's evolution can be well predicted by treating it as random regardless of whether its fundamental physical laws are deterministic or random. Both of these, and the entire statistical approach that we will review here, are of course intimately connected to the concept of dynamical noise, which we will discuss more specifically in Section 1.5, and is the focus of Chapter 4.

The latter of these two cases, the idea that a system may be well described by a statistical model, is applied particularly for systems where there are a large number of components with many degrees of freedom. In such systems, the microscopic states of each individual component may be calculable, but are too numerous to enlighten how the system behaves as a whole. Instead, macroscopic properties of the system are thought to provide a better understanding of the system's dynamics. These systems of many components and many degrees of freedom are extremely common in the study of life and the natural world more generally, and the application of a statistical framework to understand them, in part or in whole, has become commonplace [9–12].

The model of statistical physics is intimately connected to thermodynamics. They each concern many of the same system variables, and the statistical approach to calculating key thermodynamic measures, such as entropy, have become almost ubiquitous. In thermodynamics, these variables can be categorised as extensive or intensive. An extensive variable depends on the size of and/or amount of matter in the system, such as the mass and volume. An intensive variable, meanwhile, does not depend on the mass of the system. This includes temperature and pressure.

At the foundation of this field is the study of canonical ensembles, which relate various, traditionally time-independent, variables. These are constructed for three different thermodynamic situations—

1. the microcanonical, where the energy, E, number of particles, N, and volume, V are constant, and the joint probability density function, ρ, is investigated.

2. The canonical ensemble, where the temperature, T, number of particles, N, and volume, V are constant, and the partition of the probability of each microstate of the system occurring, Z, is investigated.

3. The grand canonical ensemble, where the temperature, T, chemical potential, μ, and volume, V are constant, and the partition of the probability of each microstate of the system occurring, $\mathcal{Z}$, is investigated.

The three-dimensional classical mechanical microcanonical ensemble for a slice of the energy of the system from E to $E + \Delta$ has been found to be

$$\rho(q, p) = \frac{1}{\Gamma(E, V, N)}, \tag{1.13}$$

where

$$\Gamma(E, V, N) = \int \int d^{3N}q d^{3N}p. \tag{1.14}$$

q_N is the Nth generalised coordinate of the system, and p_N is the Nth momentum. This is defined only for isolated systems in equilibrium, where there can be no change in energy or matter.

The canonical ensemble considers the same system, except with the addition of being thermodynamically coupled to a heat bath. Hence, the temperature of the system must now remain constant, but energy may be exchanged with the bath. This ensemble can be written as

$$Z = \sum_i \exp -\frac{E_i}{k_B T}, \tag{1.15}$$

where i is a given microstate, E_i is the energy of this state and k_B is the Boltzmann constant.

Finally, the grand canonical ensemble arises from systems that are isolated other than for being in thermodynamic equilibrium with a reservoir. Crucially, the number of particles is allowed to vary. It can be defined as

$$\mathcal{Z} = \sum_i \exp \frac{N_i \mu - E_i}{k_B T}. \tag{1.16}$$

The concepts from this field of particular relevance to Chapter 4, to whether living systems are best understood deterministically or statistically, relate to the role of time in statistical properties. We will now briefly review them.

1.2.1 Ergodicity

The idea of ergodicity is that, given enough time, most trajectories of a stochastic (or indeed deterministic) process will eventually have eventually visited any given subset of the phase space for a fraction of time proportional to its measure. Hence, the measure is able to represent a probability distribution of the location of a trajectory of the system in the phase space at a given time t. Mathematically a ergodic stationary stochastic process can be defined, for a measurable space $(X, \mathcal{B})$, a measurable bounded continuous observable function h and a probability measure μ, for any set $A \in \mathcal{B}$, as

$$\frac{1}{t} \int_0^t h(x(s)) \, ds \to \mathbb{E}_\mu[h] \quad \text{as} \quad t \to \infty. \tag{1.17}$$

Put another way, the time average estimate of a sample trajectory of such a process will converge to the ensemble average $\mathbb{E}_\mu[h]$. A process possessing this quality hence allows the consideration of only a typical trajectory of the process to derive its aggregate behaviour. This therefore justifies the use of a single time-series as a representative realisation of an ergodic stochastic process, and for its long-time-asymptotic properties to be judged from only a finite series. It follows from this that ergodicity is a crucial property for a stochastic system to possess if it is going to be analysed in an asymptotic time framework.

1.2.2 Stationarity

A stationary stochastic process is one whose statistical properties are time-invariant, that is, they do not change under translation in time. More specifically, the cumulative distribution function D of the probability distribution of the stochastic process $\{X_t\}$ consisting of $n \in \mathbb{N}$ samples obeys the equality

$$D\left(X_1, X_2, \cdots, X_n\right) = D\left(X_{1+\tau}, X_{2+\tau}, \cdots, X_{n+\tau}\right), \tag{1.18}$$

subject to some translation in time $\tau \in \mathbb{R}$. This can hence be seen as a statistical physics equivalent to the concept of autonomous processes in deterministic dynamical systems theory. Correspondingly, the notion of a non-stationary process is defined as

one where Eq. 1.18 does not hold, and is hence to stationary processes and autonomous is to non-autonomous.

In further similarity, applying stationary distributions and constructing stationary models is by far the more common approach when studying physical systems. This is once again partly a function of the much more developed theory concerning stationarity, compared to non-stationarity. This is to the extent that it is not uncommon, upon encountering what appears to be a non-stationary process, to try to transform it into a stationary one. There are therefore many well-known examples of stationary stochastic processes, and of main concern in Chapter 4 will be one such of these, $1/f$ noise.

1.3   Thermodynamics

The most immediate question posed by thermodynamics when considering a dynamical system is whether that system is thermodynamically isolated, closed or open. Thermodynamically isolated systems can exchange neither matter nor energy with their environment, and are therefore difficult to construct in practice. Indeed, a strictly isolated system could not occur at all in nature. Closed systems can exchange energy but not matter. Autonomous dynamical systems can therefore often be appropriate for representing a closed system. The limited amount of interaction with the environment does not usually lead to time-dependence, and allows for the possibility of a thermodynamic equilibrium or steady state relationship between the system and its environment, i.e. for the dynamical system to exhibit equilibria points and/or invariant attractors. Finally, open systems allow both matter and energy to cross their boundaries [13]. In this section, we will review how this makes thermodynamically open systems the most suited to describing living systems, and the key developments in thermodynamics concerning such systems.

1.3.1   Characterising living systems

We have mentioned already that thermodynamically closed systems are able to exchange energy with their environment, and therefore potentially reach a thermal equilibrium with this environment. A closed system in such a state could, however, still remain distinct from this environment thanks to its hard boundary when it comes to matter.

But this is not a possibility for an open system due to its ability to transfer matter with its environment. An open system that is in equilibrium with its environment no longer maintains any meaningful distinction from that environment, and must have no functioning internal processes that are distinct from external ones. Therefore, living systems must not only be open, but out of equilibrium; the only way for 'living' systems to maintain an equilibrium with its environment is for it to die.

Open systems that are not in equilibrium with their environment, but instead in a steady state, are defined as maintaining flows of energy and matter across the system boundaries, as is characteristic of non-equilibrium behaviour, but flows that are constant in time. Such states were among the first to be considered in the shift from studying thermodynamic equilibrium to non-equilibrium because they could be considered to be 'near equilibrium', as we shall discuss further later. However, these states are still not able to completely capture the behaviour of living systems. It is a significant challenge to living systems that their environment is continuously changing, and this challenge requires that the systems themselves also adapt to accommodate this. As such, living systems do not consume necessary molecules from their environment nor expel waste products at constant rates, but in a time-varying manner according to their own internal demands and the current state of their environment. Such a dynamic cannot be characterised by a 'near equilibrium' steady state.

In summary, in the language of thermodynamics living systems are best characterised as far from equilibrium thermodynamically open systems. These are systems that exchange matter and energy with their environment, and do so in a continuously changing, time-dependent manner, without ever reaching an environmental equilibrium.

1.3.2 Entropy far from equilibrium

One of the most crucial variables for studying equilibrium, or the lack thereof, in thermodynamic systems is associated with the second law of thermodynamics — specifically, entropy. Entropy was first defined by Clausius for reversible processes in isolated systems, as the ratio between an increment of heat transferred and the temperature. This led to the conclusion that the entropy of isolated system can only ever increase, and will reach

its maximum when the system is in internal equilibrium. These findings also naturally extended to reversible processes in closed systems.

The original statistical description of entropy was introduced by Boltzmann as

$$S = -k_B \sum_i p_i \ln p_i, \tag{1.19}$$

for all the states p_i of the system, and the Boltzmann constant k_B. For Boltzmann, like all of the original framework of statistical thermodynamics, was only intended to characterise the maximum entropy of a system in thermodynamic equilibrium. This was due in large part to the relative ease of measuring the thermodynamic variables of an equilibrial system.

Describing entropy away from equilibrium, in particular in open systems, was distinctly more difficult due to the quite different behaviour of these systems compared to equilibrial ones. A significant development in this direction were the Onsager reciprocal relations, which extended relationships between key thermodynamic variables to apply beyond a strict equilibrium [14]. However, these were only found to hold near to equilibrium, and not far from it, and to be additionally broken by time-irreversibility, as in, say, a non-autonomous process. Hence defining the macroscopic entropy of a far from equilibrium system remains an open question in thermodynamics.

The initial formulation of entropy by Clausius, and the conclusion that it is maximal for equilibrium systems, also led to an interpretation of entropy as a measure of order. In this view, equilibrium either between the internal processes of the system or between the system and its environment is a state of total disorder. The conclusion of this in concert with the second law of thermodynamics is that systems, and indeed the universe, only ever become more disordered, particularly as they are subject to environmental influences.

This implication could be questioned, however, given the evidence from the natural world. As life has developed it has not become more ordered, rather the opposite. Living systems have in fact evolved to maintain ever more intricate and complex systems that maintain their internal order in often disordered environments. One answer to this apparent contradiction was offered by Prigogine, who coined the term 'dissipative structures' to describe open systems where entropy is produced and expelled to facilitate ordered internal processes [15, 16]. Hence, while methods to precisely calculating the

15

thermodynamic macroscopic entropy of far from equilibrium systems may not currently be known, characterisations such as this offer a way to understand the process of entropy production.

1.3.3 From equilibrium to non-equilibrium

Developing a framework through which far from equilibrium systems can be characterised, analysed, and ultimately have their behaviour predicted is one of, if not the most, significant open questions of thermodynamics, and consequently dynamical systems. There have been many significant contributions to this goal. We will discuss further the contributions of dissipative structures, by Ilya Prigogine, and synergetics, by Hermann Haken, and briefly how the contribution of this thesis fits in these contexts.

Dissipative structures, as was introduced in the previous subsection, may be an organised structure of matter or energy. They may exist only when the system is far from equilibrium and the system is open to continual flux of energy and matter from its environment. These structures are produced by the fluctuations, i.e. minor perturbations away from the average, in system variables characteristic of open systems. In a system near equilibrium these fluctuations would decay, or relax, until the variable has returned to the stable average, and the system as a whole is once again in equilibrium. But, far from equilibrium, these fluctuations relax much more slowly, and may establish a feedback loop if they interact nonlinearly. If there are sufficient fluctuations this feedback may reach a critical point, creating a new ordered state far from equilibrium, i.e. a dissipative structure [17].

Dissipative structures arose primarily as an explanation of chemical phenomena. Synergetics, on the other hand, had its origins more in control theory, and hence is framed initially in terms of forcing between subsystems and systems. Synergetics applies when a system consists of many subsystems, and when the behaviour of the system as a whole cannot be described by linear combination of its subsystems. Hence, like in dissipative structures, the concerned system exhibits complex behaviour as a result of nonlinear interactions of its components. Rather than examination of the microscopic fluctuations of the system, the theory of synergetics is based in analysis of a key macroscopic variable — the order parameter of the system. This parameter is less complicated to derive than

the microscopic properties of the system when its relaxation time is much greater than that of the subsystems. It additionally plays an important role in the dynamics of the system through the slaving principle, that the subsystems adiabatically follow this order parameter. This allows the order parameter it to characterise the macroscopic evolution of the system, and for the microscopic evolution of the subsystems to be disregarded without increasing the complexity of the macroscopic dynamics. This principle furthermore defines the analysis as a finite-time one — this adiabatic condition can only be maintained for a slow, continuous variation of time. These conditions hence draw further analogy to dissipative systems. Where there fluctuations are required to relax slowly, in synergetics the same requirement is placed on the order parameter [18].

Common to both of these systems is the incorporation of time into their framework. In contrast to equilibrium theory, the system is not reduced to some macroscopic variables that are invariant until the system is in some way changed, these far from equilibrium approaches are forced to closely track the continual change of their chosen parameters in time, resulting from the system's constant interaction with its environment. We propose that it is this time-dependence that is the key characteristic of far from equilibrium systems, that these systems are defined by their lack of rigid stationary stability that can be relied upon to simplify equilibrium systems. The framework of finite-time analysis, the close tracking of the evolution of a quantity in time, of time-dependent systems that we build on in this thesis is therefore, we believe, not just a contribution to the abstract dynamics of non-autonomous differential equations, but towards a fundamental framework for the behaviour of systems far from equilibrium.

1.4   Complexity

Complexity has been a field rapidly growing in interest, with many attempts to categorise systems at the forefront of research under a common framework. Despite this, there is no consensus on what exactly makes a system complex or simple. Nonetheless, some common themes from otherwise differing definitions can be identified.

The most common concept associated with complexity is the idea of the system as a whole being more than the sum of its parts. This is, in other words, the theory that a

complex system should give rise to emergent macroscopic behaviour that cannot be immediately reduced to a result of its components [19]. Some form of interactions between components within the system is a common way for this phenomenon of emergence to arise, and hence the existence of these interactions often forms part of a definition of complexity [20, 21].

Another frequently occurring aspect of definitions of complexity is many components or degrees of freedom. This is once again linked to the idea of emergence — the argument being, that only for a system with many components could such a phenomenon take place. An exception to this is often provided for chaotic systems, which are are almost always identified as being complex [22–24].

Periodic systems, however, are not considered to be complex because of the predictability and apparent simplicity of a basic oscillation. However, synchronisation of interacting oscillatory components is very much an emergent behaviour of such a system, and is far from easily predictable from these components alone in non-trivial cases. In Chapters 3 and 4 we will explore the capacity of these systems to produce complex dynamics, and in particular in Chapter 4 their capacity to do so while consisting of only very few components.

1.4.1 Measuring complexity

Just as there is no clear consensus on a definition of complexity, there is also, unsurprisingly, a variety of disparate methods for measuring the degree of complexity of a system.

Entropy is considered to be a related but different measure to complexity, through its association with order and disorder. A highly ordered state, similar to basic periodicity, is considered to be simple, as is a highly disordered state that lacks structures to produce coherent dynamics and can be well-predicted by statistical models. Maximal complexity is therefore associated with an entropy in between the latter's minimum and maximum values [23, 24].

There are two main types of quantitative complexity measures, besides the variety of methods of entropy calculation. The first, including algorithmic information content and

logical depth, considers the information contained within, or the computational resources required by, the shortest possible computational program that can produce equivalent data to the studied system [25, 26]. The second, which includes effective measure complexity and thermodynamic depth, is based more directly in the data collected from the studied system. They are concerned with the information content of the time-series data itself, whether it be the amount of information required to predict the evolution of the series, or the amount of information a point in a time-series carries about its past [23, 24, 27]. A key difference between these two measures is how they treat randomness, which we will discuss further in the next section.

1.5   Noise

In Section 1.1 we briefly discussed that fully deterministic formulations are far from the only kind of dynamical system. In this section we will outline the role of random processes in physical models, in particular the place of noise in data science.

Noise in data is a phenomenon relevant to a huge range of scientific fields and physical systems including, of particular interest in this thesis, the study of living systems and cellular processes [28]. Despite, or perhaps because of, this ubiquity of relevance there is no easy consensus on its definition. The most commonly used, non-exclusive, definitions can be summarised as follows:

1. Noise is a random process [29–35] that can be defined by

    (a) an uncorrelated evolution [33, 36],

    (b) incoherence [37, 38],

    (c) a lack of deterministic reproducibility [39].

2. Noise is any behaviour that cannot be explained by consideration of the physical system itself [34, 40–43].

But in practice, perhaps the most concise summary of what is commonly considered to be noise in data is anything that the observer considers should not be present, and that does not provide any useful information. This is with the exception of certain desirable

effects of noise, for instance in stochastic resonance noise assists a multistable system in making equilibria transitions [44].

It is in part this tendency to categorise as noise that which is not currently understood that has led to considerations of randomness forming such a large part of the treatment of physical systems. It is as a result entirely commonplace, for example, to filter experimental time-series to remove assumed-noise. In the world of modelling, it is similarly common to include noise terms in the system's evolution, usually in the form of additive noise [45]. In Chapter 3 we will assess the ability of an entirely deterministic physical model to generate complex behaviour reflective of experimental data, and in Chapter 4, the ability of the current framework for analysing noise to correctly identify non-autonomous determinism.

1.5.1   Noise and complex dynamics

At the fundamental physical level, at least until the advent of quantum mechanics, noise was still considered to be a product of deterministic processes. In this sense, noise is a complex dynamic, the deterministic origins of which cannot be uncovered from the available data with the available tools. Noise is currently considered to have two main origins: a high-dimensional system of large numbers of non-chaotic, autonomous processes [29, 46–48], and low-dimensional chaotic systems evolving on a fast time scale [49–52].

From this view of noise as a complex dynamic, it is not hard to see why noise and random processes have been a significant part of the conversation about the numerical calculation of entropy. It has been of much debate whether pseudorandom behaviour is truly complex, or whether evidently deterministic structures conveying much more significant amounts of information is a more accurate characterisation of complexity [53]. In the former position, noise is associated with a highly disordered state, which is traditionally considered to be highly entropic. The latter position however is partly driven by the conception of entropy as a measure of the information content of a time-series. We saw this idea feature in some of the techniques for calculating entropy mentioned in the previous section, but it is most famous in the form of Shannon entropy [54].

In some entropy calculation methods both complex deterministic and random systems would be assigned a high value. However, many newer measures would assign a lower value to the latter, on the basis that a random system conveys less information than a complex deterministic one [55]. This corresponds again to some of the ideas of the previous section that random processes are not necessarily complex, and can often be easily described and predicted by statistical models. Multiscale sample entropy, in particular, was developed to assign similarly low entropy values to highly ordered deterministic and uncorrelated random dynamics by calculating the sample entropy for multiple different time scales [56, 57]. Through this method, time-series without correlations on longer time scales, e.g. random noise, would be distinguished from those that do, e.g. deterministic dynamics evolving over a range of time scales.

1.6   Numerical methods

When seeking to understand the behaviour of a dynamical system, obtaining an analytical expression of its solutions and their stabilities is the ideal scenario. Such an analysis provides unambiguous answers to any related question we could pose. However, for the systems we will be dealing with in this thesis — coupled networks of non-autonomous nonlinear oscillators — methods for obtaining these solutions are not currently well understood. This is not to say that there are no developments in this area; for example, in [58], a finite-time framework for analytically understanding the stability of 1-dimensional non-autonomous cyclic processes was recently introduced. However, even in this case, higher-dimensional non-autonomous systems remain analytically unsolved.

In this and other cases where full solutions are not forthcoming, it is natural to turn to numerical methods. For differential equations, which form the basis of the dynamical systems we are studying, as was discussed in Section 1.1, the most important of these is numerical integration. In this method, the value of the differential equation, a.k.a. the amount by which the studied quantity changes at a given time, is calculated for a set of time points. The first thing to note is that as the systems we discussed in Section 1.1 were defined over continuous time, this procedure maps the system onto a discrete time. This is similar to the process of strobing, pioneered by Poincaré, and the Poincaré map, but where there the discrete times are determined by the evolution

of periodic dynamics, here they are selected only with some reference to the potential accuracy of their produced solution.

As a result of this mapping, we are no longer dealing with a 'true' solution, but an approximation of the trajectory of the variable through time. This of course implies that some approximations may be better or worse than others, which is largely determined by two aspects of the method — the algorithm through which each new value is calculated, and the intervals of discrete time for which they are evaluated. For the latter, it is crucial that a sufficiently close set of intervals are chosen that all the fast-time scale dynamics is able to be seen from the resulting data. This is an idea elaborated further by the concept of the Nyquist frequency [59, 60]. It is also essential however that the intervals are not so close that slower-time scale dynamics are hard to discern through the sheer volume of the data. Nor indeed that the procedure becomes too computationally demanding. Some methods discard with a constant interval altogether, and instead aim to adapt it between each step in time to suit the current accuracy requirements of the system, with reference to a notion of the relative error of various different intervals. For the question of different algorithms, a vast number of approaches have been developed, many of which are reviewed in [61]. We will now discuss in more detail the algorithms used in this thesis.

1.6.1   Numerical integration

Numerical integration is based in the estimation of the change in a function $y(t)$ between the point t_n and a future point $t_{n+1} = t_n + h$ according to the differential equation $\dot{y} = f(t, y(t))$, for some chosen constant h. At the most basic level, assuming some starting value y_0 is known, future values may be estimated by the first-order Euler method

$$y_{n+1} = y_n + hf(t_n, y_n). \tag{1.20}$$

Here, first-order means that the final estimation is calculated from only one 'step' forward in t, a.k.a. for one addition h. Higher order algorithms may be used to increase the accuracy of the estimation, while involving more calculations and therefore compu-

tational resources. For example, the fourth-order Runge-Kutta method, which is used in Chapters 2 and 4, and parts of Chapter 3, proceeds as follows:

$$y_{n+1} = y_n + \frac{h}{6}(k_1 + 2k_2 + 2k_3 + k_4),$$

$$k_1 = f(t_n, y_n),$$

$$k_2 = f\left(t_n + \frac{h}{2}, y_n + \frac{hk_1}{2}\right),$$

$$k_3 = f\left(t_n + \frac{h}{2}, y_n + \frac{hk_2}{2}\right),$$

$$k_4 = f(t_n + h, y_n + hk_3). \tag{1.21}$$

The size of the steps forward in time, h, may also be decreased to increase the estimation accuracy, similarly at the expense of computational resources as more calculations will be required to reach the same final time.

So far we have discussed differential equations dependent only on time and one other variable, x. However, x may instead be replaced by a set of variables of any size without altering the algorithm, provided that these variables do not depend on one another. The more complicated case is when they are instead mutually dependent. If we differential equations $\dot{y} = f(t, y(t), x(t))$, $\dot{x} = g(t, x(t), y(t))$, for instance, then our fourth-order Runge-Kutta method must be altered to:

$$y_{n+1} = y_n + \frac{h}{6}(k_1 + 2k_2 + 2k_3 + k_4),$$

$$x_{n+1} = x_n + \frac{h}{6}(l_1 + 2l_2 + 2l_3 + l_4),$$

$$k_1 = f(t_n, y_n, x_n),$$

$$l_1 = g(t_n, x_n, y_n),$$

$$k_2 = f\left(t_n + \frac{h}{2}, y_n + \frac{hk_1}{2}, x_n + \frac{hl_1}{2}\right),$$

$$l_2 = g\left(t_n + \frac{h}{2}, x_n + \frac{hl_1}{2}, y_n + \frac{hk_1}{2}\right),$$

$$k_3 = f\left(t_n + \frac{h}{2}, y_n + \frac{hk_2}{2}, x_n + \frac{hl_2}{2}\right),$$

$$l_3 = g\left(t_n + \frac{h}{2}, x_n + \frac{hl_2}{2}, y_n + \frac{hk_2}{2}\right),$$

$$k_4 = f(t_n + h, y_n + hk_3, x_n + hl_3),$$

$$l_4 = g(t_n + h, x_n + hl_3, y_n + hk_3). \tag{1.22}$$

This may be expanded by the same procedure for however many dependent variables are present in the system, and is an essential variation to enable the consideration of interacting processes.

A further key consideration when numerically integrating differential equations is the extent to which they may be 'stiff'. Stiffness refers to the degree of instability of the equations, such that small parameter changes may cause a significant change. In the methods discussed thus far, also called 'explicit' methods, this would hence require a small step size and high order. An alternative approach, 'implicit' methods, were developed specifically for this problem. Instead of estimating the value of the differential equations at one parameter step forward, implicit methods construct an equation to be solved dependent on both the current and next step. For example, this approach transforms Equation 1.20, the 'forward' Euler method, to

$$y_{n+1} = y_n + hf(t_{n+1}, y_{n+1}), \tag{1.23}$$

the 'backward' Euler method. The change to introducing a dependence on y_{n+1} on both sides of the equation results in an algebraic equation, dependent on the form of f, that must be solved for each step.

In much of the numerical integration of Chapter 3 an implicit algorithm, Matlab's ode15s [62], is used. This algorithm integrates an equation $\dot{y} = f(t, y)$ via

$$hf(t_{n+1}, y_{n+1}) = (1 - \kappa)\gamma_s \nabla^{s+1} y_{n+1} + \sum_{m=1}^{s} \gamma_m \nabla^m y_n, \qquad (1.24)$$

where $s \in [1, 5]$ is the order of the algorithm, κ is a scalar parameter, $\gamma_s = \sum_{j=1}^{s} \frac{1}{j}$ and ∇ is the backward difference formula, so that $\nabla^m y_n = \sum_{i=0}^{m} (-1)^i \binom{m}{i} y_{n-i}$ and $\binom{m}{i}$ is the binomial coefficient.

These have all been examples of fixed-step and fixed-order algorithms. There is an increasing number of alternate methods that instead vary their step size and order according to the region of the parameter space of the differential equations the algorithms find themselves in at that moment, in as far as that can be determined. This can allow these methods to choose a large step size and low order when the equations vary little over large parameter changes, saving computational resources, and a small step size and high order when the inverse is true, ensuring accuracy.

The key part of adaptive step size and order algorithms is their ability to estimate the error introduced by different steps and orders, and thus judge what the most appropriate selection of each is. If the error is estimated poorly, then significant errors and unnecessary computational demands may be introduced.

In ode15s, the relative error between different step sizes is estimated through interpolation of the backwards differences, using the saved solutions $y(t_n - jh)$ for $j \in [0, s]$, calculated as

$$p(t) = y(t_n) + \sum_{i=1}^{s} \nabla^i y(t_n) \frac{1}{i! h^i} \prod_{m=0}^{i-1} (t - t_{n-m}). \qquad (1.25)$$

This is used to construct a backwards difference matrix

$$D = [\nabla p(t_n), \ldots, \nabla^s p(t_n)], \tag{1.26}$$

which can be compared to the same calculated for a different step size, h^*,

$$D^* = [\nabla^* p(t_n), \ldots, \nabla^{*s} p(t_n)]. \tag{1.27}$$

The relative error is defined through two further matrices, U,

$$U_{jr} = \frac{1}{j!} \prod_{m=0}^{j-1} (m - r), \tag{1.28}$$

where $r \in [1, s]$, and R,

$$R_{jr} = \frac{1}{j!} \prod_{m=0}^{j-1} \left(m - r\frac{h^*}{h} \right), \tag{1.29}$$

by considering $D^* = DRU$. If this relative error calculated by RU is within the defined tolerance, the algorithm may then increase h, or alternatively if the error of the current step size is outside of the tolerance compared to a smaller step size, h may be reduced.

1.6.2 Time-series analysis

Once a numerically integrated time-series of a variable has been produced, it is often necessary to apply further analysis to be able to understand its dynamics. When these dynamics are expected to be oscillatory, analysis that makes reference to the time-frequency domain is ideal. This is in particular for non-autonomous oscillations, where the ability to see how any frequencies develop in time is key to understanding the system. We will discuss this further predominantly in Chapter 4.

One of the original analysis methods of the time-frequency domain is the windowed Fourier transform. This is defined as

$$G_s = \frac{1}{2\pi} \int_0^\infty \exp\left(i\xi t \right) \hat{s}(\xi) \hat{g}(\omega - \xi) d\xi, \tag{1.30}$$

where $\hat{s}(\xi) = \int_{-\infty}^{\infty} s(t) \exp(-i\xi t) dt$ is the Fourier transform of the component $s(t)$, ξ is the frequency domain integration element and ω is the frequency at which the transform is evaluated. The window function, $\hat{g}(\xi)$ tapers the time-series to smooth out the transition from zero to non-zero amplitudes at the beginning and end of the series. This is necessary for (inevitably) finite time-series to reduce the extent to which an otherwise sharp transition between these regions may introduce artificial spectral content. A common form of this function is a Gaussian window, defined as

$$\hat{g}(\xi) = \exp\left(-\frac{f_0^2 \xi^2}{2}\right), \tag{1.31}$$

where f_0 is the frequency resolution parameter. This resolution parameter determines the relative resolution of the time and frequency domains.

A drawback of the windowed Fourier transform, however, is that the application of a window of a fixed size in the time domain will provide worse resolution of some frequencies than others. If a long window is used, then a reasonable resolution at low frequencies will be obtained, but there will be a poor time domain localisation of high frequencies in particular. Conversely if the window is short, there will be good time domain localisation of the high frequencies, but poor estimation of the lower frequencies.

The wavelet transform is intended as a solution to this problem. It is similarly defined as

$$W_s = \frac{1}{2\pi} \int_0^{\infty} \exp(i\xi t) \hat{s}(\xi) \hat{\psi}^* \left(\frac{\omega_\psi \xi}{\omega}\right) d\xi, \tag{1.32}$$

where ω_ψ is the frequency at the peak of the wavelet. ψ^* is the wavelet window function, which unlike the windowed Fourier transform window, adopts a different time domain length for each frequency. In this thesis, we will use the lognormal wavelet, which additionally takes advantage of the logarithmic relationship between frequency and time, and is defined as,

$$\hat{\psi}^*(\xi) = \exp\left(-\frac{(2\pi f_0 \ln \xi)^2}{2}\right). \tag{1.33}$$

We will also make use of higher-order analysis, specifically the wavelet bispectrum as defined in [63], to investigate coupling relationships between functions. For the functions $x, y, z \in L^{\infty}(\mathbb{R}, \mathbb{R})$, this is defined as

$$B_{\psi^*, xyz}(A) = \int_{\mathbb{R}^3} 1_A(\exp(\xi_1), \exp(\xi_2), t) b_{\psi^*, xyz}(\exp(\xi_1), \exp(\xi_2), t) d(\xi_1, \xi_2, t), \tag{1.34}$$

27

where 1_A is the indicator function of the input set A. The local logarithmic-frequency wavelet is

$$b_{\psi^*,xyz}(f_1, f_2, t) = D_{\psi^*}\left(\frac{f_1}{f_1+f_2}\right)^{-1} W_{\psi^*,x}(f_1, t) W_{\psi^*,y}(f_2, t) \overline{W_{\psi^*,z}(f_1+f_2, t)},$$

(1.35)

for the frequencies f_1 and f_2. Finally, the normalisation factor is

$$D_{\psi^*}\left(\frac{f_1}{f_1+f_2}\right) = \int_0^\infty \int_0^\infty \frac{\hat{\psi}^*\left(\frac{f_1}{\xi_1}\right) \frac{f_2}{\xi_2} \frac{f_1+f_2}{\xi_1+\xi_2}}{\xi_1 \xi_2} d\xi_1 d\xi_2.$$

(1.36)

When analysing in the time-frequency domain, it is important to consider an additional question of precision, beyond just the accuracy of the numerical integration that led to this point. Namely, precision in the time domain and precision in the frequency domain are related by a version of the Heisenberg uncertainty principle. That is to say, for some frequency domain precision $\Delta\omega$ and some time domain precision Δt, we have

$$\Delta\omega\Delta t \geq 1.$$

(1.37)

This is because to exactly determine the value of a frequency mode, a sufficient window must be considered so as to capture at least one period, but the longer this window, the more time points this frequency will be assigned to, i.e. the less well time-localised the frequency mode will be. The wavelet transform handles these competing requirements particularly well by adapting its resolution for different parts of the time-frequency domain, and hence it plays a significant role in the analysis conducted in this thesis.

The final question we will address in this section is that of statistical significance. This is the process of determining whether the value an analysis method has assigned to a particular point in a given domain is significant, and not something that could be easily replicated by analysis of another time-series without the same dynamics. In ideal experimental circumstances, this may be done by comparison to a control group. This comparison is intended to clarify the extent to which results are due to randomness or uncertainty, rather than being genuine. However in numerical analysis of differential equations, or experiments where a control group is not available, comparison time-series, a.k.a. surrogates, can be constructed from the analysed time-series itself. To do this, many methods have been developed to re-arrange time-series in such a way that certain

properties are maintained, such as the amplitude, but the dynamics described by the sequencing of the points is removed. An in-depth review of many of these methods, and the wider process of determining statistical significance in the context of non-autonomous dynamics, is provided in [64]. In this thesis, we adopt the wavelet iterative amplitude adjusted Fourier transform approach outlined there. The algorithm to conduct this procedure is outlined below.

1. Calculate a maximal overlap discrete wavelet transform (MODWT) of the time-series, which decomposes the time-series into the time-series of its constituent time scales.

2. (a) Randomly shuffle each scale time-series.

   (b) Calculate the Fourier transform of each shuffle, and replace the Fourier amplitudes with those of the original scale time-series. This is done in order to preserve the power spectrum of the original time-series.

   (c) Rescale these Fourier transforms to match the distribution of the original scale time-series.

   (d) Repeat the previous two steps with the result of step 2(c) becoming the input of step 2(b), until the output is the same as the input.

   (e) This final output is taken as the result of this stage of the process.

3. Calculate the mirror image of the output surrogate for each scale time-series. The closest match of each surrogate and its mirror image to the original scale time-series is taken was the final surrogate for that scale.

4. Calculate the inverse MODWT of the surrogates to recompose each scale surrogate into a single composite time-series. This gives a single surrogate of the original time-series.

5. Repeat the entire process for the number of desired surrogates.

1.7   Contemporary research

As was set out in the introduction, the two primary subjects on which this thesis is based are non-autonomous dynamical systems, and to a lesser extent, network science. The study of both of these fields has been rapidly growing in recent years. In this section, we review some of the developments most relevant to our aim of understanding living systems through the lens of networks of non-autonomous processes.

1.7.1   Characterising thermodynamically open systems

The most immediate and fundamental question considered by this thesis is how to best mathematically and physically characterise thermodynamically open systems. We have discussed already the contributions of dissipative structures and synergetics to this question. Here, we will review significant recent developments, before introducing the point of view that we will adopt in this thesis.

Statistical mechanics

It was originally hoped that dissipative structures may be able to explain the thermodynamic behaviour of all complex, far-from equilibrium systems. However, the theory is still fundamentally based in the system exhibiting a linear response to external influence, specifically through its connection to the linear Onsager reciprocal relations. In reality, nonlinear responses are extremely common, if not ubiquitous for real systems.

In [65], an extension of the concept of dissipative structures not based in linear responses was suggested, named dissipative adaptation. This theory is derived from comparing all possible trajectories between two states of the system. Through this it is speculated that those trajectories that have absorbed, as opposed to dissipated, the most externally performed work that are the most likely to occur. The implication of this is that systems will at time form structures that are minimally dissipative, and absorb sufficient external work as to transform into a new state, and then dissipate their gained heat so that the systems remain in this new state. A quantitative measure of the change in probability of a time-reversed trajectory ocurring because of heat dissipation was suggested in [66],

30

where

$$\frac{p_{i \to j}(t)}{p^*_{j \to i}(\tau - t)} = \exp\left(\frac{Q_{\text{diss}}}{k_B T}\right), \tag{1.38}$$

and $p_{i \to j}(t)$ is the probability of a trajectory of the system from state i to j, $p^*_{j \to i}(\tau - t)$ the probability of the same trajectory reversed from a time τ, Q_{diss} the dissipated heat, k_B the Boltzmann constant, and T the temperature. This was developed further in [65] by considering the relative probability of a forward trajectory from state i to j, and from i to k

$$\frac{p_{i \to j}(t)}{p^*_{i \to k}(t)} = \exp\left(-\frac{E_{kj}}{k_B T}\right) \frac{p^*_{j \to i}(\tau - t)\langle \exp\left(-\frac{W_{\text{abs}}}{k_B T}\right)\rangle_{ik}}{p^*_{k \to i}(\tau - t)\langle \exp\left(-\frac{W_{\text{abs}}}{k_B T}\right)\rangle_{ij}}, \tag{1.39}$$

where $E_{kj} = E_j - E_k$ is the energy difference between the states k and j, $W_{\text{abs}} = Q_{\text{diss}} + E_{ij}$ is the work absorbed to move from state i to j, and $\langle \cdot \rangle_{ij}$ indicates the average of the quantity over all microtrajectories from state i to j. Hence, this demonstrates that the more work is absorbed along a trajectory, the more likely that trajectory is to take place. In [65], the states resulting from these preferred processes are associated with those best adapted to the influence of the environment, and the processes are therefore also associated with the mechanism by which these unexpected behaviours can emerge from complex systems.

[67] adopts an alternate approach to developing a framework for the thermodynamics of open systems. While still based in a probabilistic view of transitions between states, it seeks to build up from the microstates, to the mesoscopic and finally to the macroscopic view of a many-body open system. This system is thermodynamically coupled to multiple reservoirs and subject to an external drive, intended to simulate thermodynamic openness.

Some of the most significant results of [67] were to derive the probability of far from equilibrium fluctuations across spatial scales. For microscopic states, this was found to be

$$\ln \frac{p\left(\beta^{(1)}\delta w_{\boldsymbol{\lambda}}, \left\{\delta j_{\mathbf{f}}^{(\nu)}\right\}, \left\{\delta j_e^{(\nu)}\right\}\right)}{\tilde{p}\left(-\beta^{(1)}\delta w_{\boldsymbol{\lambda}}, \left\{-\delta j_{\mathbf{f}}^{(\nu)}\right\}, \left\{-\delta j_e^{(\nu)}\right\}\right)} = \beta^{(1)}\left[\delta w_{\boldsymbol{\lambda}} - \Delta a_1^{\text{eq}}\right]$$

$$+ \sum_{\nu=1}^{L}\left[\beta^{(\nu)}\delta w_{\mathbf{f}}^{(\nu)} + \left[\beta^{(1)} - \beta^{(\nu)}\right]\delta e^{(\nu)}\right]. \tag{1.40}$$

Here, $p\left(\beta^{(1)}\delta w_{\boldsymbol{\lambda}}, \left\{\delta j_{\mathbf{f}}^{(\nu)}\right\}, \left\{\delta j_e^{(\nu)}\right\}\right)$ is the probability of simultaneously observing the microscopic non-autonomous work $\beta^{(1)}\delta w_{\boldsymbol{\lambda}}$, the microscopic time-integrated autonomous work currents $\left\{\delta j_{\mathbf{f}}^{(\nu)}\right\} \equiv \left(\beta^{(1)}\delta w_{\mathbf{f}}^{(1)}, \ldots, \beta^{(L)}\delta w_{\mathbf{f}}^{(L)}\right)$ and the microscopic time-integrated energy currents $\left\{\delta j_e^{(\nu)}\right\} \equiv \left(\left[\beta^{(1)} - \beta^{(2)}\right]\delta e^{(2)}, \ldots, \left[\beta^{(1)} - \beta^{(L)}\right]\delta e^{(L)}\right)$. The work/energy currents referred to here are current elements in that they are vectors of the instantaneous work done on the reservoirs/energy change in the reservoirs, and if unwound further in time would represent the flow of these quantities. $\tilde{p}$, meanwhile, is the probability of the time-reversed processes. The superscript (ν) indicates the quantity is with respect to the νth reservoir, $\beta = \frac{1}{k_B T}$, k_B is the Boltzmann constant, T is temperature and $\delta w_{\boldsymbol{\lambda}}$ is the infinitesimal work resulting from the external driving protocol $\boldsymbol{\lambda}(t)$. The subscript $\mathbf{f}$ indicates the quantity results from the non-conservative force vector associated to the νth reservoir, $\delta e^{(\nu)}$ is the infinitesimal energy change of the νth reservoir and $\Delta a_1^{\text{eq}} = -\frac{1}{\beta^{(1)}}\ln\sum_{\alpha}\exp\left(-\beta^{(1)}e_{\alpha}(\boldsymbol{\lambda}_t)\right) + \frac{1}{\beta^{(1)}}\ln\sum_{\alpha}\exp\left(-\beta^{(1)}e_{\alpha}(\boldsymbol{\lambda}_0)\right)$ is the change in the global microscopic equilibrium free energy with respect to the reference reservoir $\nu = 1$, and e_{α} is the energy of the α microstate.

As the number of units in the model is increased, there will be increasing numbers of microstates with equal energies and occupation numbers, leading these states to be energetically identical. It is also assumed these states are kinetically identical through their coupling to the same reservoirs. Therefore, these states can be grouped into a new single mesostate. Through this process, increasing number of units can in fact result in decreasing degrees of freedom as this regime is entered. The corresponding mesoscopic equation to Eq. 1.40 is

$$\ln\frac{P\left(\beta^{(1)}\delta W_{\boldsymbol{\lambda}}, \left\{\delta J_{\mathbf{f}}^{(\nu)}\right\}, \left\{\delta J_E^{(\nu)}\right\}\right)}{\tilde{P}\left(-\beta^{(1)}\delta E_{\boldsymbol{\lambda}}, \left\{-\delta J_{\mathbf{f}}^{(\nu)}\right\}, \left\{-\delta J_E^{(\nu)}\right\}\right)} = \beta^{(1)}\left[\delta W_{\boldsymbol{\lambda}} - \Delta A_1^{\text{eq}}\right]$$

$$+ \sum_{\nu=1}^{L}\left[\beta^{(\nu)}\delta W_{\mathbf{f}}^{(\nu)} + \left[\beta^{(1)} - \beta^{(\nu)}\right]\delta E^{(\nu)}\right], \quad (1.41)$$

where the newly-capitalised variables are simply mesostate versions of their microscopic lowercase versions. These are obtained by coarse-graining from the q^N microstates of the N units, where q, $N \in \mathbb{Z}^+$, to the N units.

The macrostate is obtained in the limit $N \to \infty$. In order to define fluctuations, which can scale exponentially with N, in this regime, a path-integral formalism was

applied. This approach allows a re-definition of the work currents, energy current and equilibrium free energy according to $\delta\mathcal{X}_Y = \lim_{N\to\infty}\frac{\delta X_Y}{N}$, where $X \in \{W, E, \Delta A^{\text{eq}}\}$ and $Y \in \{\boldsymbol{\lambda}, \mathbf{f}, 1\}$, respectively. The fluctuation probability hence becomes

$$\lim_{N\to\infty}\frac{1}{N}\ln\frac{P\left(\beta^{(1)}\delta W_{\boldsymbol{\lambda}}, \left\{\delta J_{\mathbf{f}}^{(\nu)}\right\}, \left\{\delta J_E^{(\nu)}\right\}\right)}{\tilde{P}\left(-\beta^{(1)}\delta E_{\boldsymbol{\lambda}}, \left\{-\delta J_{\mathbf{f}}^{(\nu)}\right\}, \left\{-\delta J_E^{(\nu)}\right\}\right)} = \beta^{(1)}[\delta\mathcal{W}_{\boldsymbol{\lambda}} - \Delta\mathcal{A}_1^{\text{eq}}]$$

$$+ \sum_{\nu=1}^{L}\left[\beta^{(\nu)}\delta\mathcal{W}_{\mathbf{f}}^{(\nu)} + \left[\beta^{(1)} - \beta^{(\nu)}\right]\delta\mathcal{E}^{(\nu)}\right]. \quad (1.42)$$

Quantum mechanics

One of the major fronts in this area is how to incorporate the notion of thermodynamic openness into a quantum mechanical framework. Traditional quantum theory, much like thermodynamics, is built on the concept of equilibrium, which cannot be expected in an open system. It additionally makes extensive use of Hamiltonian systems, which are required to be time-reversible, which does not in general hold for thermodynamically open systems. One approach to deal with this complication is to conceive of the system as entangled with a bath (also referred to as a reservoir). This bath has infinitely many degrees of freedom and is initialised in a state of thermodynamic equilibrium. The total Hamiltonian then becomes

$$H_{\text{tot}} = H_S + H_B + H_I, \quad (1.43)$$

where H_S and H_B are the Hamiltonians of the system and the bath, respectively, and H_I is the Hamiltonian of the interactions between them. The reduced quantum density matrix of the system, $\rho_S(t)$, is derived by averaging over the elements of the bath in the total density matrix, $\rho_{\text{tot}}(t)$. $\rho_S(t)$ reflects the dynamics of an open system, where there is no irreversible attainment of an equilibrium as the system can transform from pure states to mixed states. $\rho_{\text{tot}}(t)$ meanwhile obeys standard quantum mechanical principles, in particular the Liouville equation

$$i\hbar\dot{\rho}_{\text{tot}}(t) = [H_{\text{tot}}, \rho_{\text{tot}}(t)]. \quad (1.44)$$

This provides a solution to the system density matrix, thereby incorporating far from equilibrium behaviour into the quantum mechanical framework. This solution is

$$\rho_S(t) = \mathsf{Tr}_B\left[U(t, t_0)\rho_{\text{tot}}(t_0)U^\dagger(t, t_0)\right], \quad (1.45)$$

where Tr_B is the trace over the degrees of freedom of the bath, and $U(t, t_0) = T \exp\left(-\frac{i}{\hbar} \int_{t_0}^{t} H_{\text{tot}}(t')dt'\right)$ is the standard time-evolution operator and T is the time-ordering operator. An outline of a thermodynamically open approach to quantum mechanics is provided in [68], and applications of this approach can be seen in [69, 70].

A system-bath approach was also used in [71], to adapt the notion of dissipative adaptation to the quantum world. This considers a three-level lambda system, i.e. two states $|a\rangle$, $|b\rangle$ and an excited state $|e\rangle$, with transition frequencies ω_a and ω_b between the states $|a\rangle$ and $|e\rangle$ and $|b\rangle$ and $|e\rangle$, respectively. The initial state is an arbitrary mixture of $|a\rangle$ and $|b\rangle$. This system is entangled to an infinite bath at absolute zero temperature, which leads to spontaneous emission rates Γ_a between $|a\rangle$ and $|e\rangle$ and Γ_b between $|b\rangle$ and $|e\rangle$. A single photon pulse incident on the bath is then considered. The transmission probability resulting from this pulse is found to be

$$p_{a \to b}(\infty) = \frac{\Gamma_b}{\Gamma_a + \Gamma_b} \frac{\langle W_{\text{abs}} \rangle_a}{\hbar \omega_a}, \tag{1.46}$$

with a corresponding reverse transmission probability of $p_{b \to a}^* = 0$. In other words, the transmission from $|a\rangle$ to $|b\rangle$ results in a pure quantum state, which is associated here with the order observed in complex open systems. The probability of this transmission, with 0 probability of reversing, is found to be higher the more work is absorbed in the process of the transmission.

Deterministic dynamics

In [72], control theory is applied to model the dynamics of open systems in terms of their inputs and outputs. The basis of this approach is the linear system

$$\dot{x}(t) = Ax(t) + Bu(t), \tag{1.47}$$

$$y(t) = Cx(t). \tag{1.48}$$

$x(t) \in \mathbb{R}^n$ is the state of the system, $u(t) \in \mathbb{R}^m$ is the input and $y(t) \in \mathbb{R}^m$ is the output. A, B and C are constants controlling the influence of the current system state on the future state, the influence of the input on the future state, and the influence of the current state on the system output, respectively. The pairs (u_i, y_i), for $i = 1, \ldots, m$, are then 'ports', which connect the system to others. A may additionally be expressed as incorporating some resistance, R, within these ports, for example $A - R$. Hence,

when interacting with other systems, there is some notion of loss, and the interaction is dissipative if R is K-symmetric and positive semi-definite, i.e. for some symmetric positive-definite matrix K, $KR = R^T K \geq 0$, and where $H(x) = \frac{1}{2} x^T K x$, $H(x)$ being the storage function of the system. In the case of a linear input-output system dissipatively coupled to some unspecified other system or environment, the equilibrium solution $x = 0$ where there is no input, $u(t) = 0$, is asymptotically stable. In other words, the system outputs until it reaches equilibrium with this environment, and then remains in this equilibrium unless perturbed. This is the classically expected case of a one-directional open system.

To consider cases where there is non-zero input, the change in the microscopic state vector $x(t)$ is re-written as a stochastic Langevin equation. If the ports are considered to to be connected to an infinite heat bath, which is always in equilibrium and has unchanging temperature, of temperature T_j

$$\dot{x}(t) = \left(A - \sum_j R_j \right) x(t) + Bu(t) + \sum_j \sqrt{2T_j} F_j w_j(t). \qquad (1.49)$$

Here, $R_j = F_j F_j^T K$ is the resistive element of the port (u_j, y_j) and $w_j(t)$ are independent Gaussian white noise processes. The macroscopic behaviour of the system, however, can be expressed deterministically in terms of the deterministic covariance matrix $X(t)$

$$\dot{X}(t) = AX(t) + X(t)A^T - \sum_j R_j X(t) - \sum_j X(t)R_j^T + 2\sum_j R_j K^{-1} T_j. \qquad (1.50)$$

The energy balance of the system, the change in the storage function, is then

$$\frac{d}{dt} H(x(t)) = -\sum_j \mathsf{Tr}\left(X(t)KR_j X(t)K \right) + \sum_j T_j \mathsf{Tr}\left(KR_j X(t) \right). \qquad (1.51)$$

This is all to say, that the infinite heat bath inputs a heat flow into the system that drives the system into a repeating cycle, i.e. the system is in a steady state.

A similar deterministic dynamical approach to the above focuses on port-Hamiltonian systems. These are based in the theory of Hamiltonian dynamics, which considers a mechanical system in the form

$$\dot{q} = \frac{\partial H}{\partial p}(q, p), \tag{1.52}$$

$$\dot{p} = -\frac{\partial H}{\partial q}(q, p) + B(q)f, \tag{1.53}$$

$$e = B^T(q)\frac{\partial H}{\partial p}(q, p). \tag{1.54}$$

$q = (q_1, \dots, q_k)^T$ are the generalised coordinates of the system, $p = (p_1, \dots, p_k)^T$ are the corresponding generalised momenta, $H(q, p)$ is the Hamiltonian function representing the total energy of the system, $B(q)f$ is the generalised external forces resulting from an input force $f \in \mathbb{R}^m$ and $e \in \mathbb{R}^m$ is the energy balance of the system.

The transformation to port-Hamiltonian systems was motivated by a need to analyse relatively more complex open systems, and achieved through an integration with network model theories. Specifically, a structure matrix is introduced, which allows network interactions within the system, and between the system and its environment. This can be formulated as

$$\dot{x} = J(x)\frac{\partial H}{\partial x}(x) + g(x)f, \tag{1.55}$$

$$e = g^T(x)\frac{\partial H}{\partial x}(x), \tag{1.56}$$

where $x = (x_1, \dots, x_n) \in \mathcal{X}$ are the local coordinates of the system on the n-dimensional manifold $\mathcal{X}$, $J(x)$ is the $n \times n$ structure matrix and $g(x)$ is the input matrix, governing the external interactions [73]. This has been applied to many mechanical systems, such as to develop a control method to optimise the electricity storage of hybrid car batteries [74]. Recent research has suggested the approach could be additionally adapted to allow for finite-time systems, which expand its applicability to, among others, biological systems [75].

We have reviewed here multiple approaches that seek to construct a non-equilibrial thermodynamics from consideration of the fundamental microstates. Whether stochastic, deterministic or quantum mechanical, all of these approaches have found it necessary to couple their systems to some reservoirs or baths. This extension of the system has

been required because all of these approaches have been based in the conservation of mass and energy. This is because in isolated systems, all matter and energy flow can be tracked while still only mathematically treating the system itself. In open systems, however, energy and matter must be allowed to leave and enter the system to and from the environment, but to maintain conservation, this means the environment too must be brought into the mathematical formalism. This can prove a significant complication, and a significant part of why there is no well-established thermodynamics of these systems.

Rather than take this approach, we will focus on the phases of the processes we consider. These phases are not quantities that are exchanged between the system and the environment, regardless of whether the system is isolated, closed or open, and so there is no difficulty concerning conservation. This construction also considers the dynamics, rather than the statistics or mechanics of the system. An advantage of this difference is that the dynamics of complex open systems, at least at the macroscopic level, are often much more easily observed than their fluctuations of mechanical quantities, and more readily mathematically definable than their statistical thermodynamics. Understanding the dynamics of a system is additionally crucial to understanding its function and purpose, in a way that cannot always be derived from statistical properties alone.

The nature of this modelling approach being centred around the phase, rather than amplitude, dynamics is also derived from a certain view of the physical world. We consider at a fundamental level the universe to be constructed out of oscillations. These oscillations form an extremely efficient way of transmitting energy and information, and it is conversely inefficient to suppress them. They may, however, be combined to construct amplitude oscillations and fluctuations at the more macroscopic level we commonly observe. The corollary of this is that even when a macroscopic observable may appear non-oscillatory, it remains possible that is constructed from a superposition of oscillations with sufficiently differing phases that their fundamental oscillatory nature is not obvious. This hence forms another motivation for our treatment of open systems as formed of dynamical phase oscillators, and their mean-field as a key physical observable.

Finally, it was common to all the treatments of open systems we have presented here to consider the role of time-irreversibility in these systems. This forms the core of the theory, indeed, in the case of dissipative adaptation in [65]. There, and in the quantum

version of [71], an adapted state is defined as one that is irreversible under time reversal. Similarly, in [67], the probability of time-forward and reverse fluctuations were found to not be in general equal. The incorporation of time is taken a step further in [68], where the governing quantum density matrix is found to be time-dependent, and [72], where all inputs, outputs, and resulting macroscopic variables are also time-dependent. This is seen perhaps most clearly in [67], where the transformation to an open system is made by the introduction of a time-dependent forcing, and results in non-autonomous work currents. The link between open systems and time-dependence, with a characterisation of environmental influences being time-varying and leading to time-dependent system behaviour, can hence be seen to be a common one, whether it is more or less explicit in any given model. In our approach, we make this link by considering exclusively non-autonomous phase oscillations.

1.7.2 Oscillator networks

The study of networks has been adopted by a huge number and increasing number of fields, in particular those seeking to understand physical systems, where interactions are inevitable. This has, naturally, led to many developments in the understanding of networks, some of which we will review here.

In particular, we are concerned with the dynamics of networks of oscillatory processes. For this purpose, the study of order and synchronisation within such a network is a key concern. We have already reviewed the notion of an order parameter for networks of Kuramoto oscillators in Section 1.1, where the level of synchrony between oscillating nodes is characterised by a single amplitude of the mean field. An alternative procedure was proposed in [76] for networks of autonomous Kuramoto oscillators, which aims to provide more detailed information about the relationship between nodes by defining a time-averaged correlation between them,

$$\rho_{ij} = \langle \cos\left(\theta_j(t) - \theta_i(t)\right)\rangle. \tag{1.57}$$

Hence, the matrix whose ith, jth element is given by ρ_{ij} measures not just a global notion of synchronisation, but whether each individual oscillator pair has become correlated.

The main purpose of this measure in [76] is to facilitate an optimisation procedure for designing a network architecture that produces the desired dynamics. Once the required form of the correlation matrix is identified, the network weights that would produce this matrix can be reasonably straightforwardly derived. However, this requires that the correlations between whatever physical system the network nodes represent can be realistically determined.

Observing various order parameters of a system and developing methods to produce them are not the only way such variables can be used to understand a dynamical system. For instance, in [77] the transition from a low to high value of the order parameter is studied as a phase transition. The theory of phase transitions was originally developed to understand discontinuous critical transitions in physical systems, such as the evaporation of a liquid into a gas, or the alignment of spins in an Ising model of a 2D lattice, both of which are considered in [77]. Similarly, the sudden transition from a largely desynchronised to largely synchronised state in an oscillator network may be viewed in this way.

The phenomenon of universality has also long been studied in phase transitions, that is, that seemingly regardless of their physical differences, many systems are theorised to have the same exponents of their critical transition points. However, experimental findings have often not been in precise agreement with these theories. In [77], it is argued that this results from mean field approximations used in deriving these theoretical exponents that are not physically justified, in particular for systems with dominant local interactions and variations in local density. These are not, however, complications that apply to networks of all-to-all coupled Kuramoto oscillators. In such networks, each oscillator's dynamics are manifestly governed by a mean field comprising every other oscillator in the network. It was indeed shown in [78] for an autonomous oscillator network that a critical transition from relative desynchronisation to synchronisation occurs under increase of the coupling strength, and that this can be predicted through a mean field approach.

It has been a common theme of the work reviewed in this section so far that it has considered only autonomous oscillations, and the complications to instead considering non-autonomous ones are not to be underestimated, as we will discuss further in the rest of this section. For instance, critical transitions in networks of autonomous processes

are usually permanent so long as all parameters are kept constant. However, in a non-autonomous one, the time-variation of these parameters may allow them to repeatedly cross and un-cross the critical boundary. The impact this might have on the dynamics of a network of Kuramoto oscillators has not been explored. Similarly in [76], the procedure for determining the required network weights to produce the desired correlation dynamics depends on the mean of the differences between the frequencies of each pair of nodes being zero. This does not in general hold for time-dependent frequencies, however. The inclusion of non-autonomous oscillators therefore requires a comprehensive reconsideration of any network analysis designed with autonomous ones in mind.

Much of the current work in network science is also focused on the topology of these networks, and seeking to make it reflective of the physical system being modelled. This is feasible in, for instance, the study of the relationship between regions of the brain, as in [76], where there are not too many nodes and the dynamics of each one can be individually measured. Not so much, however, in the energy metabolism of cells as we will study here, where what precise physical component is represented by network nodes is less clear, and cannot be individually measured in vivo by any currently existing techniques. Nevertheless, we will outline in Chapters 2 and 3 the efforts we have made to incorporate the physical interactions of cell metabolic processes into the topology of our networks.

Due to these aforementioned complications, in this thesis we focus on well-established theories of order in all-to-all coupled networks of Kuramoto oscillators, but investigate them in the novel context of non-autonomous oscillations, and with feasible topological alterations where they are physically justifiable.

1.7.3   Non-autonomous processes

In Section 1.1 we discussed how the same analyses that have been developed for autonomous systems cannot be effectively applied to non-autonomous systems. In the extended phase space of the latter, incorporating time as an additional dimension alongside the phase space of the former, relevant objects such as fixed points no longer necessarily determine the dynamics of the entire space, but often only a single slice in time in which they exist. Time-dependence therefore requires new conceptualisations of

these objects that account for time-variability, and new methods for identifying them. How best to adapt techniques developed for autonomous systems, or to develop ones bespoke to non-autonomous systems, has remained an open question.

A main concern of the study of dynamical systems is identifying phase space surfaces of stability and instability, which can provide an understanding of the dynamics of the system over a region of its phase space, or even the entire space, and are therefore extremely useful for predicting the behaviour of a dynamical system for different initial conditions. There are several ways to conceptualise these key behaviours in non-autonomous systems, some of which we will now review.

Attractors

Perhaps the most straightforward dynamical objects to imagine in non-autonomous systems are attractors, given their presence in autonomous systems as well. In non-autonomous systems, these come in two forms — forward attractors and pullback attractors. For a given function $f : \mathbb{Z}^2 \times \mathbb{R}^n \to \mathbb{R}^n$ and an n-manifold of initial conditions C, if

$$\text{dist}\left(f\left(t; t_0, C\right), A\right) \to 0 \text{ as } t \to \infty, \tag{1.58}$$

for some invariant manifold A (that is to say, a manifold for which $f\left(t; t_0, x_0\right) \in A$ if $x_0 \in A$), then A is a forward attractor and C is within its basin of attraction.

A pullback attractor on the other hand is a manifold B for which

$$\text{dist}\left(f\left(t; t_0, C\right), B\right) \to 0 \text{ as } t_0 \to -\infty. \tag{1.59}$$

I.e. rather than the system inevitably approaching the manifold as time moves forward as in the case of the forward attractor, the evolution of the system tends towards the manifold as it is initialised at earlier and earlier times.

In an autonomous system, these concepts are one and the same — any manifold that attracts a trajectory of the system as time moves forward will also be approached as the

system is initialised at progressively earlier times. This is because autonomous systems do not depend on time as a physical quantity, and trajectories initialised at an earlier time will evolve in the precisely same manner as those at a later time, all other parameters being the same. This is not the case for non-autonomous systems, where the concepts of forward and pullback attraction become uncoupled [8, 79–81].

It has also been shown that non-autonomous pullback attractors can be global [82, 83]. Such attractors, also called maximal pullback attractors, are defined as

$$\text{dist}\left(f\left(t; t_0 - j, C\right), B\right) \to 0 \text{ as } j \to -\infty \ \ \forall \ t_0 \in \mathbb{Z} \ \& \ \forall \ B \in \mathbb{R}^d, \qquad (1.60)$$

where d is the dimension of B. This is in contrast to forward attractors, which are not necessarily unique. Instead, the intersections of forward attractors may create larger and larger basins of attraction for larger and larger invariant manifolds, which may or may not span the entire phase space.

While the establishment of these dynamical objects for non-autonomous systems is a significant step forward, identifying them in any given system is still far from trivial. They also do not necessarily determine the entirety of a system's dynamics. This is particularly true in finite-time, as opposed to the asymptotic times over which such attractors are defined, as will be discussed more later in this section.

Hyperbolicity

The hyperbolic dynamics of systems are often sought for their ability to simplify the study of a system. This occurs when some of the derivatives expand or contract in such a way that a study of those alone reveal local, or even global, dynamics.

One such concept is normally hyperbolic invariant manifolds. These have long been studied for autonomous systems as generalisations of hyperbolic fixed points, which are 2-dimensional fixed points with a stable and unstable manifold. A normally hyperbolic invariant manifold, therefore, is one where trajectories on the manifold remain there, but those normal to it either return to it (when they are along the associated stable manifold) or diverge from it (when they are along the associated unstable manifold). The dynamics tangential to the manifold are dominated by the stable and unstable

manifolds of the normal directions, and hence all dynamics in the vicinity of such a manifold can be predicted by studying only the manifold itself. This reduction of the dynamical system from many trajectories to a single manifold is therefore a highly related concept to Haken's slaving principle. As was reviewed earlier in this chapter, the slaving principle similarly allows for a reduction from considering many microscopic dynamics to a single enslaving macroscopic order parameter.

This property of normally hyperbolic manifolds was proved in the foundational work of [84]. There, the existence of a invariant manifold $\bar{M} = M \cup \partial M$ was established. This $\bar{M}$ is a C^r compact and connected manifold embedded in $\mathbb{R}^n$, and overflowing invariant under X, where X is a C^r vector field on $\mathbb{R}^n$. Overflowing invariant means that $X|M$, the vector field X that is restricted to the manifold M, is tangent to M and X is never tangent to ∂M. The manifold $\bar{M}$ was proved to be diffeomorphic to $\bar{M}_Y$, i.e. to have a structure-preserving mapping between the manifolds, where Y is a C^r vector field in a C^1 neighbourhood of X if $\nu(m) < 1$ and $\sigma(m) < \frac{1}{r}$ for all $m \in M$. Here,

$$\nu(m) = \inf\{a : \frac{\frac{|||w_0||}{||w_{-t}||}}{a^t} \to 0 \ \text{ as } t \to \infty \ \forall w_0 \in N_m\}, \tag{1.61}$$

where N_m is the bundle of vectors normal to TM, the tangent space of M. And,

$$\sigma(m) = \inf\{s : \frac{\frac{||w_0||^s}{||\nu_0||}}{\frac{||w_{-t}||^s}{||\nu_{-t}||}} \to 0 \ \text{ as } t \to \infty \ \forall \nu \in T_m M \ \& \ w_0 \in N_m\}. \tag{1.62}$$

Additionally, the stability of these invariant manifolds was proved in [84], with reference to the hyperbolic splitting of vector bundles. Specifically, M_Y is diffeomorphic to M if there is a hyperbolic splitting of $TR^n|M$ with $\sigma^-(m) < \frac{1}{r}$ and $\sigma^+(m) < \frac{1}{r}$. In this definition,

$$\sigma^-(m) = \lim_{t \to \infty} \frac{\ln ||D(F^{-t}|M)(m)||}{-\ln ||\pi^- DF^t(F^{-t}(m))|N^-||}, \tag{1.63}$$

where F^s is the flow $x(s)$ such that $\dot{x}(t) = X(x(t))$ and $x(0) = x$, and D is the derivative with respect to space variables. Additionally, the superscripts $-/+$ denote the splitting under the forward/backward flow, respectively, and $\pi^{-/+}$ is the projection on $N^{-/+}$. Finally,

$$\sigma^+(m) = \lim_{t \to -\infty} \frac{\ln ||D(F^{-t}|M)(m)||}{-\ln ||\pi^+ DF^t(F^{-t}(m))|N^+||}. \tag{1.64}$$

This hence adds a notion of stability due to hyperbolic splitting, in addition to more conventional asymptotic stability.

This was more recently considered for non-autonomous systems, through the argument that such a manifold persists under sufficiently small perturbation, such that a similar nearby manifold may be considered if the inclusion of time is conceptualised as an external perturbation [85]. More specifically, non-autonomous systems of the form

$$\dot{\theta} = \Theta(\theta, r, t) \tag{1.65}$$

$$\dot{r} = R(\theta, r, t) \tag{1.66}$$

$$\dot{t} = 1, \tag{1.67}$$

where $r \in \mathbb{R}^n$ and $\theta \in M$ for some compact manifold M, were considered. It was proved that for any $r \in \mathcal{B}_\epsilon := \{r \in C^1 \; : \; |r|_1 \leq \epsilon(\eta)\}$, i.e. any point within a closed ball $\mathcal{B}_\epsilon$ of radius $\epsilon(\eta)$ in the phase space of r, where $\epsilon(\eta)$ places an upper bound on the solution $\tilde{r}$ of $\dot{r}$, there is a unique $\tilde{r} \in \mathcal{B}_\epsilon$. There is additionally a contraction in the norm $||\cdot||_{t_0}$ $\tilde{T} : \mathcal{B}_\epsilon \to \mathcal{B}_\epsilon$ such that $r \mapsto \tilde{r}$. This norm is defined as

$$||r||_{t_0} := \sup_t |\Phi(t_0, t)| \exp^{-\gamma|t-t_0|} |r(t)| < \infty, \tag{1.68}$$

where Φ is the principal matrix solution of the system $\delta\dot{\theta} = \delta\theta \int_0^1 \Theta_\theta(\lambda\theta_1(t) + (1 - \lambda)\theta_2, r, t)d\lambda$ and $\gamma \in (\gamma_-, \gamma_+)$ where $\gamma_\pm = \frac{1}{2}\kappa \pm \sqrt{\frac{\kappa^2}{2} - |R_\theta||\Theta_r|V}$. If r is the fixed point of $\tilde{T}$ and θ is the solution of $\dot{\theta}$, then there is a normally hyperbolic invariant manifold $\tilde{\rho}(\theta_0, t_0) = r(t_0)$.

Techniques for estimating hyperbolic dynamics, centred on calculation of the finite-time Lyapunov exponent spectrum, were considered in [86]. A Lyapunov exponent spectrum can be defined by considering a perturbation from a trajectory $x(t)$ initially along a direction v_0 with a magnitude $\delta \in \mathbb{R}$, leading to a new perturbed trajectory $x_\delta(t)$. A different finite-time Lyapunov exponent may then be calculated for each direction v_0, up to n such directions for an n-dimensional system, via the limit

$$\lambda = \lim_{\delta \to 0} \frac{1}{T} \ln \left(\frac{||x_\delta(t) - x(t)||}{|\delta|} \right), \tag{1.69}$$

which describes how the perturbation evolves over a finite time interval $[0, T]$, for ever decreasing amplitude of perturbation. The finite-time Lyapunov exponent is generally

referred to as the maximal exponent of the spectrum, λ_1, with the rest of the spectrum ordered as $\lambda_1 \geq \lambda_2 \geq \cdots \geq \lambda_n$. The maximal exponent is then used to characterise the stability of the unperturbed trajectory $x(t)$ as follows—

$$\begin{cases} \lambda_1 > 0 & x(t) \text{ is unstable,} \\ \lambda_1 = 0 & x(t) \text{ is neutrally stable,} \\ \lambda_1 < 0 & x(t) \text{ is stable.} \end{cases} \tag{1.70}$$

There is not, however, a universal procedure for identifying hyperbolic manifolds, and their applicability to non-autonomous systems does not hold for all magnitudes of time-dependence. Like all such study of behaviour in the vicinity of fixed points or invariant manifolds, the dynamics along the normal manifolds are currently only understood through the linearisation of the system, and thus restricted in their accuracy to a certain, not too large, region around the hyperbolic manifold [87, 88].

Chronotaxic systems

Chronotaxic systems, introduced in [1], consist of a process subject to a non-autonomous driving. For instance

$$\begin{cases} \dot{x} &= g(x, p(t)) \\ \dot{p} &= f(p), \end{cases} \tag{1.71}$$

where $p \in \mathbb{R}^n$ and $x \in \mathbb{R}^m$.

Rather than the process becoming synchronised to the driving only so long as it inhabits an equilbrium point in the phase space of their rotating frame, as in the case where both constituent parts are autonomous, the position of this equilibrium point now moves as the natural frequency of the driver varies in time. In doing so, the driver forms a moving point attractor, $x^A(t)$, which attracts the oscillator to its continually varying position, resulting in a non-autonomous version of a limit cycle Γ_0. That is to say

$$\lim_{t_0 \to -\infty} \left| x\left(t, t_0, x_0\right) - x^A(t) \right| = 0, \tag{1.72}$$

where $x \in \mathbb{R}^n$ and t_0 is the time at which the system is initialised. A trajectory that meets the point attractor will become invariant,

$$x(t, t_0, x^A(t_0)) = x^A(t). \tag{1.73}$$

Hence, an oscillator that becomes synchronised to this moving point attractor will become stabilised against perturbations. As we can see from Eq. 1.72, this is in fact a time-dependent pullback attractor [89].

This phenomenon can be seen in Fig. 1.1. Three trajectories are initialised neither on the limit cycle nor the point attractor. In each frame, the simulation is advanced by 2.5 s — the point attractor moves, and the trajectories are pulled towards the cycle it is tracing.
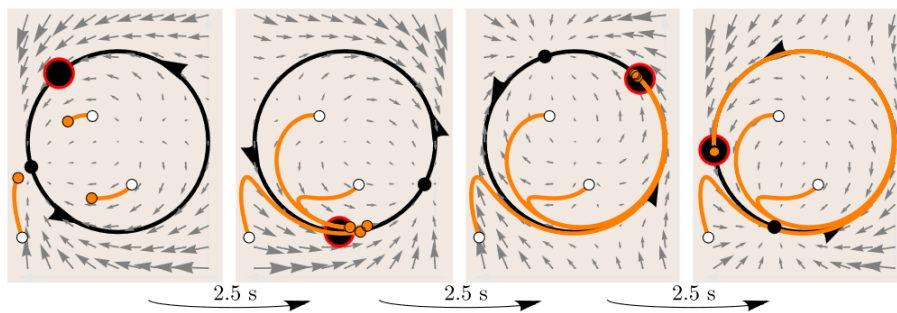
Figure 1.1: Numerical simulation of a chronotaxic system. Three initial states are shown by white dots, their trajectories by orange lines, and their current position by orange dots. The moving point attractor is shown by the black disc with a red outline, and the limit cycle it produces is represented by the black circle. The vector flow is also shown by the grey arrows. Each subsequent pane of the figure shows a 2.5 s advancement of the simulation, starting at the left. Reprinted with permission from [1].

This capacity of time-variability to create a more stable system is highly applicable to living systems in particular, where the ability of processes to continue despite environmental perturbations is essential and time-dependence is ubiquitous.

Thus far we have considered the dynamics of systems defined over indefinite times. However, such a definition cannot include living systems, which are born and then inexorably die in a finite span of time. We will therefore now consider finite-time analysis, which

considers the dynamics of systems over finite time intervals, and dynamical phenomena derived from this framework. We will see that even when a system may be extendable to indefinite time, an analysis over finite-time can uncover dynamics that would be missed if only the asymptotic time behaviour of the system was considered. This demonstrates precisely why this framework is more suited to living systems — it is the behaviour of living systems over appreciable human time scales in which we are interested.

Lagrangian coherent structures

Lagrangian coherent structures are another concept of invariant manifolds, this time conceived with finite-time analysis from the start. The theory was largely developed from fluid dynamics, particularly the idea of material surfaces, where a parcel of fluid moves through a fluid flow without losing its mass, but possibly changing shape. This parcel when tracked in time can therefore be seen as a surface, which is analogised to a manifold in the theory of Lagrangian coherent structures.

A material surface is considered a Lagrangian coherent structure when it attracts or repels trajectories near it over a finite time interval. Such manifolds are not necessarily unique, locally or globally, and are conventionally only referred to as attracting or repelling if they are locally the strongest attractor or repellor. When a locally repelling and a locally attracting material surface are local to one another, they are collectively referred to as a hyperbolic Lagrangian coherent structure. At this point, the similarities to normally hyperbolic invariant manifolds are obvious, and hyperbolic Lagrangian coherent structures are similarly sought for to explain their local dynamics. A key difference, however, is the origins of the latter in finite-time dynamical theory. An attracting/repelling Lagrangian coherent structure is only necessary invariant and attracting/repelling over the finite time interval for which the system is defined.

The ridges of the finite-time Lyapunov exponent field have been used to identify hyperbolic Lagrangian coherent structures in first 2- [90], and then n- [91], dimensional systems with non-autonomous dynamics [92, 93].

In [91], Lagrangian coherent structures are defined for $n \in \mathbb{Z}^+$ dimensions. This is done under the consideration of the non-autonomous dynamical system

$$\dot{x}(t) = v(x(t), t), \tag{1.74}$$

where $x \in \mathcal{D} \subset \mathbb{R}^n$, $\mathcal{D}$ being the domain of v, with the flow map $\phi_t^T : x(t) \mapsto x(t+T)$. Here, T is the time the system is being mapped to by the flow, which may be positive or negative. The finite-time deformation tensor associated to this system is then

$$\Delta(x,t;T) = \frac{d\phi_t^T(x)^*}{dx} \frac{d\phi_t^T(x)}{dx}, \tag{1.75}$$

where * denotes the transpose. This operator has n eigenvalues $\lambda_n \in \mathbb{R}^+$, and the corresponding finite-time Lyapunov exponent

$$\sigma(x,t;T) = \frac{1}{|T|} \ln \sqrt{\lambda_{\mathsf{max}}(\Delta(x,t;T))}. \tag{1.76}$$

This is defined in terms of the maximum eigenvalue of Δ, λ_{max}.

A repelling Lagrangian Coherent structure is then defined as a differentiable manifold $\mathcal{M} \subset \mathcal{D}$ of codimension 1, that is, of 1 dimension less than $\mathcal{D}$. This manifold exists when

1. There are $n-1$ $\lambda_n < 1$, and 1 $\lambda_n > 1$.

2. The unit nomrla vector $\hat{n}(x)$ to the manifold $\mathcal{M}$ is orthogonal to the gradient $\nabla \sigma(x,t;T)$.

3. $\Sigma(\hat{n},\hat{n}) < 0$ and for all unit vectors $\hat{u}$ such that $|\langle \hat{u}, \hat{n} \rangle \neq 1$, $\Sigma(\hat{n},\hat{n}) < \Sigma(\hat{u},\hat{u})$. Σ is the second derivative of σ.

An attracting Lagrangian Coherent structure, meanwhile, is defined in the same manner, but for the reverse time. I.e. when $T < 0$.

There have also been investigations suggesting several possible problems with this approach in certain systems however. These include that forms of Lagrangian coherent structures other than hyperbolic may not be distinguished from the hyperbolic [94] and that finite-time Lyapunov exponents calculated through a sliding window of time may not be Lagrangian, due to non-negligible flux [95].

Intermittent synchronisation

Another synchronisation phenomenon unique to non-autonomous systems playing out in finite time is intermittent synchronisation, notably discussed in [2, 96, 97]. Where for chronotaxic systems the ability of time-variability to transform an equilibrium point

into a moving point attractor is considered, intermittent synchronisation arises from re-examining the conditions for which synchronisation is possible in the same model as Eq. 1.71. In the previous section, we saw that synchronisation may occur within a region of frequency-coupling parameter space, where the frequency of the oscillator and the driver are sufficiently close and the coupling is sufficiently strong for the oscillator to become synchronised to the driver. If the frequency of the driver is now allowed to vary in time, the parameter space region where synchronisation is possible will expand. In these newly-synchronisable boundary regions, synchronisation is possible for some points in the variation of the driver, but not others. Therefore if the system's parameters exist in this region, the oscillator will be synchronised to the driver at some times and not others, a.k.a. it will be synchronised intermittently.

In [2], this is mathematically derived for a system of N phase coupled identical oscillators subject to an external driving,

$$\dot{\theta}_i = \omega + D \sum_{j=1}^{N} A_{ij} \sin(\theta_i - \theta_j) + \gamma \sin(\theta_i - \theta_0(t)), \tag{1.77}$$

where A_{ij} is the adjacency matrix element, which determined whether oscillators i and j are coupled, D is the network coupling strength and γ is the strength of the driving on each oscillator in the network. The external driving is determined by the differential equation $\dot{\theta}_0 = \omega_0(1 + kf(\omega_m t)$, with a natural frequency ω_0 and time-dependent frequency modulation determined by the function f, amplitude k and frequency ω_m. The system viewed in the rotating frame $\psi_i = \theta_i - \theta_0(t)$ is

$$\dot{\psi}_i = \Delta\omega(t) + D \sum_{j=1}^{N} A_{ij} \sin(\psi - \psi_j) + \gamma \sin\psi_i, \tag{1.78}$$

which reduces the degrees of freedom of the system by 1.

The system is then linearised around the solution $\tilde{\psi}(t)$, to obtain

$$\delta\dot{\psi}_i = -D \sum_{j=1}^{N} L_{ij} \delta\psi_j + \gamma \delta\psi_i \cos \tilde{\psi}(t), \tag{1.79}$$

where $L_{ij} = A_{ij} - \sum_{j=1}^{N} A_{ij}\delta_{ij}$ and δ_{ij} is the Kronecker delta. This linearisation can then be used to derive the Lyapunov exponent spectrum

$$\lambda^\alpha(t) = \begin{cases} -D\Lambda^\alpha - \sqrt{\gamma^2 - \Delta\omega(t)^2} & \forall t : \gamma > |\Delta\omega(t)| \\ -D\Lambda^\alpha & \text{else}, \end{cases} \tag{1.80}$$

where $\alpha = 1, \ldots, N$ and Λ^α are the eigenvalues of the Laplacian L_{ij}. Hence, as t varies such that $|\Delta\omega(t)|$ moves across the value of γ, the condition determining the stability in Eq. 1.80 will alternate. This alternation can potentially result in a change in sign of the Lyapunov exponent, and therefore the stability of the system.

In addition to giving rise to a new form of synchronisation, this results in an expansion of the region in parameter space for which synchronisation can occur compared to an equivalent autonomous system. This is because while the limits of the region where synchronisation would occur now result in intermittent synchronisation, so too do the regions just beyond the previous limits of synchronising parameters. In this way, systems that permit this phenomenon are once again well suited to describing living systems — the increased ability of a system to synchronise is an important part of functioning in a perturbative environment.

Finite-time dynamics of slow forcing

We have already discussed that finite-time dynamics is an analytical framework that considers systems over a finite interval of time, regardless of whether that system is extendable beyond this interval, and that Lagrangian coherent structures have formed a major component of this result. The results indicating the existence of intermittent synchronisation highlighted a new frontier in this analysis — that of slowly time-varying external forcing — which was recently developed further in [58, 98].

In those references, a finite-time analysis of the Adler equation was developed, which describes the phase difference between a Kuramoto oscillator and an external periodic driving as follows —

$$\dot{\phi}(t) = G(t) - \epsilon \sin\left(\phi\left(t\right)\right). \tag{1.81}$$

The time-dependence of G is taken to be slow relative to the dynamics of ϕ, and so $G(t)$ is replaced with $G(\eta t)$, with the additional restriction that $t \in \left[0, \frac{1}{\eta}\right]$. When analysed as $\eta \to 0$, the separation between the fast timescale of $\phi(t)$ and the slow of $G(\eta t)$ becomes maximal. In this case, this is therefore not just a finite-time analysis, but a slow-fast one. In this framework, it was shown in [58] that the dynamics of $\dot{\phi}(t)$ become dominated

by its solutions on the slow manifold, which take on global stability properties. It was further shown that if at such a solution

$$
\begin{cases}
\frac{\partial \dot{\phi}}{\partial \phi} < 0 & \text{then the solution is hyperbolicly stable,} \\
\frac{\partial \dot{\phi}}{\partial \phi} > 0 & \text{then the solution is hyperbolicly unstable,} \\
\frac{\partial \dot{\phi}}{\partial \phi} = 0 & \text{then the solution is non-hyperbolic.}
\end{cases}
\tag{1.82}
$$

Applied to Eq. 1.81, this framework found, through the calculation of finite-time Lyapunov exponents, that the system transitions from neutrally stable to stable as the amplitude of the time dependence within $G(\eta t)$ is increased. Furthermore, the value at which this transition occurs depends on the length of the time interval over which the system is studied. Once again, this demonstrates the physical role of time in a non-autonomous system, and the importance of analysing the system in finite time.

There remains, however, no holistic and self-consistent theory for the dynamics of non-autonomous systems, as much as the recent approaches reviewed here have begun to indicate paths towards one. In this thesis therefore, we will adopt numerical analyses of non-autonomous systems based as much as possible in the finite-time framework that we have reviewed in this section. In Chapters 2 and 3, a numerical approach will be adopted due to the considered system being considerably beyond the current forefront of analytically understood solutions, and in Chapter 4 so as to inform how such systems may appear when present in real, experimentally measured data. But in both cases, we will pay careful attention to the physical nature of time, the necessity of which has been demonstrated by the results of this section. In Chapter 4, we will additionally demonstrate the advantages of this finite-time approach, and the risks of it not being adopted.

2. Modelling oscillating living systems: Cell energy metabolism as weighted networks of non-autonomous oscillators

Cells are an archetypal example of thermodynamically open systems. They necessarily exchange energy and matter with their environment; essential ions must be brought in to facilitate their life-sustaining processes, and waste products must be expelled to prevent the cell from bursting. This capability is facilitated largely by ion channels. These consist of both passive channels, which allow ions to pass in and out of the cell, following the conventional laws of tending towards equilibrium, and active channels, which expend energy to move ions against the electrochemical gradient and perturb the internal cellular environment away from equilibrium. It is only through this perturbation that a cell survives — if it were to reach equilibrium with its environment, it would no longer have the internal balance necessary for its processes to function. Hence, they are far from equilibrium systems as a result of their thermodynamic openness.

The energy required to power these active ion channels is provided by the cell's energy metabolism. This is conducted by glycolysis and oxidative phosphorylation, producing adenosine triphosphate (ATP), which is supplied to the ion channels. Glycolysis is performed by enzymes in the cytosol of the cell, consuming primarily glucose, and oxidative phosphorylation is undertaken in the mitochondria, consuming primarily oxygen. These processes are also highly inter-linked to one another, and consist of multiple connected

versions of themselves. In other words, they may be considered to be networks that are coupled to one another.

The supply of oxygen and glucose to the cells is also not constant; the cardiovascular system that moves them through the blood stream and into the extracellular environment has long been understood to be oscillatory, and indeed to have time-dependent frequencies [99]. As a result, it is for more efficient for the aforementioned metabolic processes that rely on these metabolites to also oscillate in a time-dependent manner, rather than attempt to convert their oscillatory input into a constant output.

Contemporary kinetic models of the glycolytic process have suggested that an overall oscillatory nature may be an inevitable result of the manner in which the process is constituted under normal living state parameters. In [100], for example, it is shown that if the constituent processes interact linearly and without feedback the overall process will operate in a steady state. However, once nonlinear interactions and feedback loops between the sub-processes are accounted for, as is expected from experimental observation, glycolytic oscillations should be expected. Alternate model approaches have come to a similar conclusion, such as the control theory method employed in [101]. There, trade-offs between the robustness of the process, its ability to withstand parameter perturbation and meet variable demand, and its efficiency are found to inevitably result in oscillations. This results primarily from the consideration of autocatalysis, with the more significant this aspect of the overall process is, the more oscillatory glycolysis becomes.

Observing this experimentally, however, has been less consistent. The initial observation of glycolytic oscillations was in yeast cells [102], and similarly anaerobic conditions remain the most common circumstance in which to observe these oscillations in vitro [103]. This is by no means exclusively the case, for example they have also been observed in aerobic muscle cells and beta-cells, to name a few [104–106], and will be discussed in the context of cervical cancer cells in this chapter. Cancerous cells are known to disfavour aerobic metabolism compared to healthy cells, but this is not to the extent of a complete exclusion of oxidative phosphorylation. In these examples it can certainly be said however that these cells are far from a healthy state or their conventional living environment and parameters. This is a pervasive problem in the investigation of living systems; the only methods that exist to closely study their internal processes necessitate

removing them from their environment at best, and severely damaging them at worst, and risking fundamentally altering their behaviour as a result. The fact that oscillations in *in vitro* experiments appear more often in anaerobic conditions or for specific parameter manipulations is quite possibly linked to this fact [105, 107–114]. As is increasingly suggested by a variety of modelling approaches, oscillations likely require a full range of interactions and access to metabolites that can (so far) only be maintained in *in vivo* conditions. This is one potential explanation for the gap between models' convergence around the expectation of oscillatory behaviour, and experiments' inconsistent results.

Another explanation is the difficulty in identifying and classifying oscillations in such experimental data. While this may not be challenging for the simplest analytical equations, the potential nonlinear superposition of many different oscillatory modes, introduction of time-dependent modulation and inevitable inclusion of noisy variations and imperfect measurement in a much more complex experiment require specialist analysis techniques to discern. The gulf between the results different analysis tools can give on this question of oscillation or noise is considered more fully in Chapter 4, but is highly relevant to the consideration of analysing metabolic processes in this and the next chapter also.

The case of oxidative phosphorylation oscillations is rather more straightforward. The cyclic nature of this process has been expected since the discovery of the Krebs cycle, a key part of mitochondria's metabolic process, and has been observed in many experiments [115–119].

The further question, beyond that of the existence of oscillations, is how oscillations may communicate, and thereby can be considered to be interacting. First, we can consider there to be multiple glycolytic oscillations within a single cell; glycolytic enzymes co-locate to produce ATP in multiple different parts of the cytosol [120]. There have been multiple chemical exchanges suggested for how glycolytic oscillations may be synchronised between different cells, including acetaldehyde, pyruvate and ethanol [104], with acetaldehyde accumulating the most evidence in favour [112, 121–123]. Communication within the cell is far harder to study however, with the cytosol in particular being one of the most complex parts with many different processes all occurring simultaneously. So without any hard evidence one way or the other, in this and the following chapter we

assume internal glycolytic communication to operate in a similar manner to external, in that it is based in diffusive molecular exchange.

The picture is similar for oxidative phosphorylation. It is even clearer that there will be many processes occurring in the cell, as it takes place in each mitochondrion, of which a typical cell has many. It is also challenging to measure the communication of healthy, living mitochondria within a cell, but there has been observations of nano tunnel structures connecting them, which may be used for this purpose, as well as the inevitability of common input and output regulation [115, 117, 124–127]. We hence make a similar assumption of molecular exchange being a mechanism of oxidative phosphorylation communication.

As a result of all of these factors, which we will further expand upon in this and the next chapter, we propose that the dynamics of cell energy metabolism are an appropriate candidate for the application of finite-time analysis and to be modelled with non-autonomous oscillator networks. This analysis and model forms the basis of this chapter, where it will be introduced and justified. In Chapter 3 fundamental behaviour of the model will be analysed and a comparison to another model will be made in the context of a real cellular metabolism experiment.

The process of constructing system models is significantly affected by the transition from thermodynamically closed to open systems. In closed systems, the conservation of mass is a reliable constant, and thus forms a core principle of all attempts to model these systems. These models cannot be applied to open systems, where conservation of mass does not hold. We hence develop new models that break from this traditional framework from new first principles, which will be outlined in further detail in this chapter.

Of course, this is not to say models of open systems must be entirely non-conservative. If every variable was so, then the system as a whole would no longer be meaningfully deterministic. Instead of mass, we will assume the possibility of a conservation of some phase of the system. A contrast of these two modelling approaches will be reviewed and detailed further in Chapter 3.

Joe Rowland Adams and Aneta Stefanovska, 2019–2020 MATRIX Annals

Abstract

Oscillations are a common feature throughout life, forming a key mechanism by which living systems can regulate their internal processes and exchange information. To understand the functions and behaviours of these processes, we must understand the nature of their oscillations. Studying oscillations can be difficult within existing physical models that simulate the changes in a system's masses through autonomous differential equations. We discuss an alternative approach that focuses on the phases of oscillating processes and incorporates time as a key consideration. We will also consider the application of these theories to the cell energy metabolic system, and present a novel model using weighted non-autonomous Kuramoto oscillator networks in this context.

It is increasingly clear that a wide variety of biological processes are rhythmic in nature, from glycolysis within a cell to the heart pumping blood throughout the body [99, 108]. Replicating this fluctuating behaviour poses a challenge to many traditional modelling methods, which can rely upon approximations of the system as thermodynamically closed and linear, and which examine the system asymptotically in time. Such models may only generate oscillations at particular parameter selections and modulations, oscillate with a high degree of stability, and exist in a steady state within most of their parameter space. This is in contrast to much of what has been observed of oscillating living systems, where the oscillations continually fluctuate in their frequency and amplitude, and continue until the death of the system itself [105, 107–110, 112–116, 127–133]. We will present and discuss a different approach that rethinks how fluctuating biological systems are best modelled, applied to the cell energy metabolic system.

2.1 Principles of an alternative approach

In Table 2.1 we outline the key principles that form our method for modelling oscillating living systems, which we discuss further in this section.

It is easy to see that biological systems are open: without being able to exchange mass and energy across its boundary a cell would die, the blood would not be oxygenated by

Table 2.1: Summary of the principles informing our modelling approach contrasted to those of mainstream approaches

Mainstream principles	Our principles
Open systems can be modelled as perturbed closed systems	Open systems can only be fully represented by open models
Oscillations result from instability of a dynamical system	Oscillations are inherent to the dynamics of open systems. Living systems continuously exchange energy and matter with the environment and each process is characterized by self-sustained oscillators on a certain time-scale
Nonlinear systems can be recombined from linear systems	Nonlinear systems are best understood by nonlinear models
Time variation in living systems is often due to noise, and can be averaged out over asymptotic time	Time variation in living systems is often deterministic, and must be modelled as non-autonomous to reflect the full system dynamics

the lungs, and neurons would not receive the energy they need to fire [99, 134–136]. While it can be mathematically simpler to treat these systems as closed off to their environment, doing so is not modelling them in their healthy, existing state, but instead a dead or dying one. The first principle of our approach is therefore to allow the modelled system to be open. As a result, the quantities of our model are not the mass of elements involved, but the instantaneous phases of the concerned processes.

Oscillations can often be considered as a perturbation of a system away from its 'natural' steady state. However, an attempt to remove oscillations from an otherwise oscillatory system would be equivalent to destroying the system itself: oscillations not only allow a compartmentalisation of otherwise conflicting processes, but play a significant role in the exchange of information and regulation throughout living systems [128]. Therefore we instead treat them as an intrinsic result of the openness of living systems.

While modelling systems' interactions linearly similarly significantly simplifies the mathematics, it does not reflect the biological reality. Biological systems endemically exhibit transitions in behaviour disproportionate to environmental changes [137], and so we propose to model them as nonlinearly interacting phase oscillators [4].

The fourth key principle of our approach is that living systems should be studied according to the time scales in which they actually exist and function. Analysing the properties of a system in an asymptotic time frame can erase dynamics that exist for only short times. Lucas et al., for example, demonstrated that non-autonomous phase oscillators may synchronise intermittently, and that this is missed when using asymptotic methods [2].

This variation of frequency of oscillation is seen throughout biology [116, 128, 132, 133], and hence our model considers nonlinearly interacting phase oscillations with non-autonomous frequencies, analysed on finite time scales.

2.2 Modelling a cell's energy metabolism

Our model brings together these four principles to examine the oscillations of the energy metabolism of a single cell. The focus of this model is the production of ATP, a key molecule in maintaining cellular functions, by glycolysis, consuming glucose, and mitochondrial oxidative phosphorylation (OXPHOS), consuming oxygen [134, 135]. We build on the work of Lancaster et al. [138], who modelled each metabolic process as a singular non-autonomous phase oscillator. This model is based on the theory of chronotaxic systems, which characterises non-autonomous oscillations as a method for stabilising against external perturbations [1]. We extend this to include multiple oscillators of each process, transforming the glycolytic and OXPHOS processes into weighted networks of Kuramoto oscillators [6]. We also incorporate the findings of Lucas et al. [2], deterministically varying the frequencies of the oscillations.

This model is represented diagrammatically in Fig. 2.1. It consists of four main elements - two weighted Kuramoto networks of phase oscillators representing glycolysis and OX-PHOS, and two sets of phase oscillators driving these networks, representing glucose and oxygen.
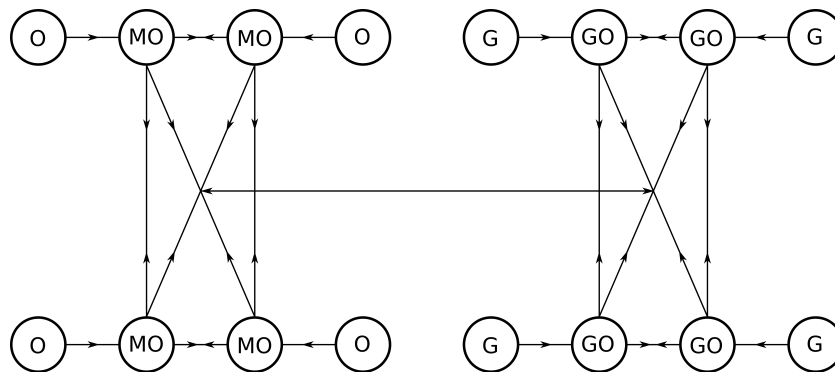
Figure 2.1: Oscillator model diagram, where each circle represents a glycolysis (GO), glucose (G), mitochondrial OXPHOS (MO) or oxygen (O) oscillator, and each line a coupling.

That these processes are oscillatory has been extensively established by experimentation, and further, that they may do so non-autonomously [105, 107–110, 112–116, 127–133, 138]. The networks of the model reflect the

fact that glycolysis occurs in a cell distributed throughout the cytosol, undergoing multiple different reactions simultaneously, and that these reactions appear to communicate through the exchange of acetaldehyde molecules [112, 120–123]. Similarly, cells contain multiple mitochondria, each undergoing OXPHOS, communicating through molecular exchange, common regulation and inter-mitochondrial nano tunnels [115, 117, 124–127]. The weighting of these networks, such that neighbouring oscillators influence one another more strongly than those more separated, reflects the spatial distances between these individual processes, and the diffusive nature of their molecular-exchange-driven communications.

We now introduce the mathematical formulation of these elements, beginning with the concept of phase oscillators. These are derived from ordinary differential equations that exhibit self-sustaining oscillations in their state dynamics. Phase, in this circumstance, is defined as the position of the equation along its oscillatory cycle at a given time. The frequency here refers to the velocity of this phase, which we allow to vary in time. We choose to focus on phase as the building blocks of our model, initially discarding the amplitude of the oscillations. This is because at a microscopic level the oscillator is a unit defined with a phase only, while the amplitude is built at a mesoscopic level, resulting from the mean field of the network.

The oscillators' phase can be further defined in the immediate region around its oscillations in state space through the use of isochrons. Isochrons connect all points in the region adjacent to a stable cycle with the one point on the cycle that, after a time, will first meet the perturbed points back on the cycle as the perturbation decays. Thus all these points are defined by the same phase [4, 5].

For non-autonomous oscillators we may also make this extension of definition, by considering each state in time as an autonomous system of slightly different frequency to the ones proceeding and following it. So long as the cycle of each autonomous system exists in the region of attraction of the system proceeding it, we may define the former's phase via the isochrons of the latter system. This assumption hence requires

that the change in the oscillator's frequency over time remains small in comparison to the frequency itself [8].

Having defined phase in the region of non-autonomous cycles, we can consider methods of coupling oscillators. Because our approach focuses on the frequencies and phases of the systems involved, phase coupling is used to model the effects of the biological processes on one another. Through this form of coupling, oscillatory systems perturb one another's phase in a backwards or forwards direction, depending on the comparative directions of oscillation of the two systems. Too strong coupling, however, can perturb the phase beyond the region defined by isochrons. Therefore in order for the perturbed system to remain in the region of its original cycle, where phase is defined, we must further require that that the coupling generating the perturbation is only weak [4, 5, 139].

We may now consider the equations of the model. First, the glycolysis and OXPHOS intra-network connections are defined as

$$
\dot{\theta}_{GONi} = \frac{K_{GO}}{N} \sum_{j=1}^{N} W_{ij} \sin\left(\theta_{GOj} - \theta_{GOi}\right),
$$

$$
\dot{\theta}_{MONi} = \frac{K_{MO}}{M} \sum_{j=1}^{M} W_{ij} \sin\left(\theta_{MOj} - \theta_{MOi}\right), \tag{2.1}
$$

where the subscript GO represents the glycolytic network and MO the OXPHOS, N the number of glycolytic oscillators, M the number of OXPHOS oscillators, K_X the relevant network coupling strength and θ_X the phase.

The weighting of edges within the glycolytic and mitochondrial networks consists of more heavily weighting shorter edges, where the nodes are positioned equidistantly around a ring. Mathematically, for $i \leq \frac{N}{2}$

$$
W_{ij} = \begin{cases} \dfrac{W}{|i-j|}, & \text{for } j \in \left[1, i + \frac{N}{2} - 1\right], \\[4mm] \dfrac{W}{|j - N - i|}, & \text{for } j \in \left[i + \frac{N}{2}, N\right], \end{cases} \tag{2.2}
$$

and for $N \geq i > \frac{N}{2}$

$$
W_{ij} = \begin{cases} \dfrac{W}{|i-j|}, & \text{for } j \in \left[i - \frac{N}{2} + 1, N\right] \\[4mm] \dfrac{W}{|j + N - i|}, & \text{for } j \in \left[1, i - \frac{N}{2}\right] \end{cases} \tag{2.3}
$$

where i denotes the index of the node under consideration, j the index of the node at the other end of the corresponding edge, N the number of nodes in the network, W a constant to be chosen, and W_{ij} the resulting weighting of the edge connecting nodes i and j.

Next, the glucose and oxygen driving are defined as,

$$
\begin{aligned}
\dot{\theta}_{GOGi} &= \epsilon_G \sin\left(\theta_{GOi} - \theta_{Gi}\right), \\
\dot{\theta}_{MOOi} &= \epsilon_O \sin\left(\theta_{MOi} - \theta_{Oi}\right),
\end{aligned} \tag{2.4}
$$

where the subscript G represents the glucose driving and O the oxygen, and ϵ_X represents the coupling strength of the relevant driving.

Finally, the inter-network interactions arise through coupling each network to the mean field of the other [140], such that

$$
\begin{aligned}
\dot{\theta}_{GOMOi} &= F_{GO} r_{MO} \sin\left(\Psi_{MO} - \theta_{GOi}\right), \\
\dot{\theta}_{MOGOi} &= F_{MO} r_{GO} \sin\left(\Psi_{GO} - \theta_{MOi}\right),
\end{aligned} \tag{2.5}
$$

here F_X is the intra-network coupling strength, r_X the Kuramoto order parameter, where $r_X e^{i\phi} = \frac{1}{N} \sum_{k=1}^{N} e^{i\theta_{Xk}}$ and ϕ is the phase of the mean field arising from the network, such that $r_X = 1$ indicates a totally ordered network, while $r_X = 0$ a totally disordered one. Further, the average phase of network X is $\Psi_X = \frac{1}{N} \sum_{i=1}^{N} \theta_{Xi}$.

The four governing differential phase equations therefore are,

$$\dot{\theta}_{Gi} = \omega_{Gi}(t),$$
$$\dot{\theta}_{Oi} = \omega_{Oi}(t),$$
$$\dot{\theta}_{GOi} = \omega_{GOi}(t) + \dot{\theta}_{GONi} - \dot{\theta}_{GOGi} + \dot{\theta}_{GOMOi},$$
$$\dot{\theta}_{MOi} = \omega_{MOi}(t) + \dot{\theta}_{MONi} - \dot{\theta}_{MOOi} - \dot{\theta}_{MOGOi}, \qquad (2.6)$$

where $\omega_X(t)$ is the time-varying natural frequency of oscillator X. The signs of the inter-network coupling terms are opposite to represent the inhibitory effects of OXPHOS on glycolysis, and the excitatory effects of glycolysis on OXPHOS [138].

We offer in Fig. 2.2 a comparison between an output of this model and an experimental observation of cellular glycolysis. This experiment was conducted by Amemiya et al., who optically measured the NADH fluorescence, a by-product of glycolysis, of batches of HeLa cells cultured under a variety of glucose starvation conditions [132]. The model output is the combined Kuramoto order parameter of the glycolytic and OXPHOS networks, defined as $\Psi_{GOMO} = \frac{1}{(N+M)} \left(\sum_{i=1}^{N} \theta_{GOi} + \sum_{j=1}^{M} \theta_{MOj} \right)$. The parameter values this simulation was conducted under are given in Table 2.2.

Table 2.2: Parameters used in the simulation to generate the output displayed in Fig. 2.2

Parameter	Value(s)
ϵ_G	[0.1, 0.26]
ϵ_O	0.01
K_{GO}	1
K_{MO}	1
F_{GO}	0.05
F_{MO}	0.05
ω_G	[0.0465, 0.0465] Hz
ω_{GO}	[0.0838, 0.1045] Hz
ω_{MO}	[0.0543, 0.0677] Hz
ω_O	[0.0258, 0.028] Hz
N	100
M	100
W	1
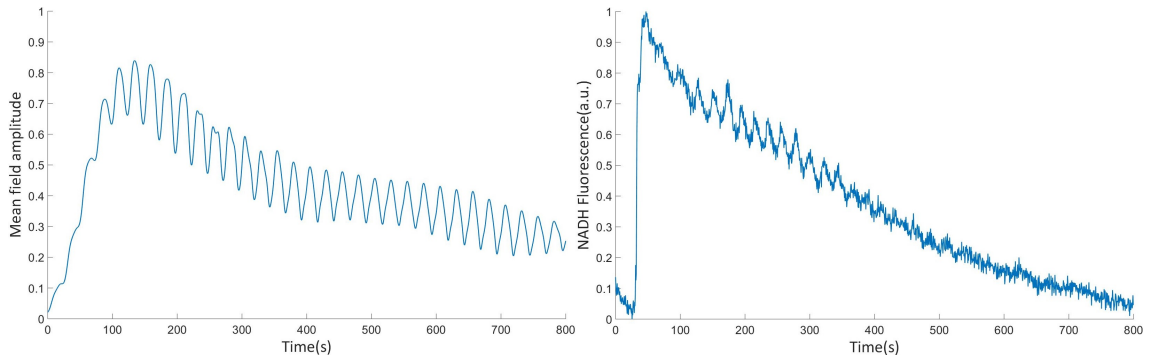
Figure 2.2: Sample output of the model (left) and the NADH fluorescence of a single HeLa cell from the Amemiya et al experiment, normalised to within the range [0, 1] (right) [132]. The model output is represented by the combined Kuramoto order parameter of both the glycolytic and OXPHOS networks.

2.3   Outlook

Modelling oscillating biological systems in their living state is a complex task. In order to reproduce every oscillation, variation of frequency, and different regime of stability a system offers, oscillations and nonautonomicity must be built in to the foundations of a model.

Using this approach, we can replicate oscillatory biological data in all its variety with only small changes to model parameters, that can themselves be matched to experimental measurements. Investigating the parameters at which various combinations of the oscillators of the model synchronise, and the transitions between these relationships, can also reveal a significant amount about a biological system. Each of these regimes can be understood as a healthy or pathological state of the system, revealing the breakdown of which mechanisms can be identified with which diseases [138].

Further, analysing the synchronisation of non-autonomous oscillator networks in finite time has already uncovered the new phenomenon of intermittent synchronisation [2]. Investigation of the metabolic model we have presented here, which introduces multiple networks and more complex forms of coupling, promises yet more unseen stabilisation behaviours.

3. Modeling Cell Energy Metabolism as Weighted Networks of Non-autonomous Oscillators

Joe Rowland Adams and Aneta Stefanovska, Frontiers in Physiology (2021)

Abstract

Networks of oscillating processes are a common occurrence in living systems. This is as true as anywhere in the energy metabolism of individual cells. Exchanges of molecules and common regulation operate throughout the metabolic processes of glycolysis and oxidative phosphorylation, making the consideration of each of these as a network a natural step. Oscillations are similarly ubiquitous within these processes, and the frequencies of these oscillations are never truly constant. These features make this system an ideal example with which to discuss an alternative approach to modelling living systems, which focuses on their thermodynamically open, oscillating, nonlinear and non-autonomous nature. We implement this approach in developing a model of non-autonomous Kuramoto oscillators in two all-to-all weighted networks coupled to one another, and themselves driven by non-autonomous oscillators. Each component represents a metabolic process, the networks acting as the glycolytic and oxidative phosphorylative processes, and the drivers as glucose and oxygen supply. We analyse

the effect of these features on the synchronisation dynamics within the model, and present a comparison between this model, experimental data on the glycolysis of HeLa cells, and a comparatively mainstream model of this experiment. In the former, we find that the introduction of oscillator networks significantly increases the proportion of the model's parameter space that features some form of synchronisation, indicating a greater ability of the processes to resist external perturbations, a crucial behaviour in biological settings. For the latter, we analyse the oscillations of the experiment, finding a characteristic frequency of 0.1–0.2Hz. We further demonstrate that an output of the model comparable to the measurements of the experiment oscillates in a manner similar to the measured data, achieving this with fewer parameters and greater flexibility than the comparable model.

3.1   Introduction

Analysing the energy metabolism of a cell can be key to understanding more about its functions, states and health. A malfunctioning metabolism is indicative of a wide range of pathological states, from diabetes, to Alzheimer's, to cancer [141–144]. A healthy metabolism also plays a significant role in other higher order processes through its production of adenosine triphosphate (ATP), which, for example, allows the generation of a membrane potential. The membrane potential is itself crucial for a variety of functions, including maintaining the cell's structural integrity and the firing mechanism of neurons [145, 146].

Cellular ATP is generated mainly through glycolysis in the cytosol, consuming glucose, and oxidative phosphorylation (OXPHOS) in the mitochondria, consuming oxygen [134, 135]. Like many biological processes, experimental observations have established that these reactions are oscillatory [105, 107–110, 112–115, 127, 129–131, 138]. Not only this, but there is further evidence to suggest these oscillations may be non-autonomous [116, 128, 132, 133, 147, 148]: that their frequencies vary over time. Modelling this behaviour is a challenge for many traditional techniques, which often rely on perturbations of a steady state to give rise to oscillations, and the addition of noise to simulate non-autonomous variation. We present here an alternative approach to mod-

elling non-autonomous oscillations in living systems, and what we can learn from such models.

The time variation of biological oscillations is often neglected, even where the existence of oscillations is acknowledged. Many modelling theories assume this variation to be due to noise, arising either from experimental methods or from the complexity of the system's interactions, and therefore that it can be averaged out when considered over asymptotic time. Time sensitive analysis of such data can show that the variation in a process's oscillations, induced by interactions with its surroundings and otherwise, is often deterministic [2, 96]. Lucas et al. [2, 96] further showed that allowing for this deterministic variation in a model's architecture, and analysing it over the finite time scales within which biological systems actually exist, can reveal dynamics that would be missed in a solely asymptotic approach. In particular, an intermittent synchronisation, where oscillators are synchronised at some times and not others, without any change of parameters, can only exist when oscillations are allowed to be non-autonomous and only found when they are analysed with finite time techniques.

The origins of our cellular metabolism model lie in the work of Lancaster et al. where glycolysis and OXPHOS are each represented by bi-directionally coupled non-autonomous Kuramoto oscillators [6], and each driven by a non-autonomous oscillator depicting the supply of glucose and oxygen, respectively [138]. This model was built on the theory of chronotaxicity [1], which studies the effects of non-autonomicity to stabilise oscillators in spite of perturbations, an important ability for biological processes.

However, like most biological processes, neither glycolysis nor OXPHOS are a single process, but many [118, 144, 149–151]. Glycolysis occurs distributed throughout the cytosol, while OXPHOS is localised within the many mitochondria of the cell. These processes further communicate between themselves as well as one another. Glycolysis was found to signal inter- and intra-cellularly through the exchange of acetaldehyde [112, 121, 123, 152], while OXPHOS is thought to interact in many possible ways, including molecular exchange, common regulation and inter-mitochondrial nano tunnels [120]. Here, we extend the Lancaster et al. model [138] to consider glycolysis and OXPHOS as all-to-all coupled networks of oscillators. These networks are furthermore weighted such that oscillators closer to each other around a ring are connected more strongly than

those further from one another, to reflect the nature of molecular exchange over a range of distances. We also draw from the work of Petkoski et al., who introduced a method of phase coupling through mean fields of ensembles of oscillators [153, 154].

We present here a summary of the Lancaster et al. non-autonomous oscillator model for cell energy metabolism [138], the details of its adaptation to weighted networks of oscillators, informed throughout by our alternative approach to modelling oscillating living systems. We will discuss further the analysis that had and can be done on these models, and what they can reveal about the biology of the cellular production of ATP and its role in wider processes.

3.2   Materials and Methods

Our modelling approach consists of four main principles, which are summarised in Table 3.1. We consider the cell to be the minimal functioning biological unit: processes within the cell cannot be isolated and still function and more macroscopic functions can be built from a cellular level, but the cell itself can survive provided the appropriate molecular supply in its environment. It is crucial however that the cell is able to expel waste and absorb needed molecules. This makes the cell a thermodynamically open system: matter and energy must cross its boundaries in order for the cell to survive. One of the principles of our approach is therefore to treat the cell and its internal processes as open, constructing a model that does not impose a constant mass on the system. While many models make mass their subject, it is much easier to achieve the aim of an open system by focusing the phase of the processes instead, and so in our model we consider the phase of oscillations.

Our second principle is to treat oscillating systems as not just a temporary perturbation from a steady state, but as fundamentally defined by their oscillations. We therefore do not construct our model as a non-oscillating set of processes and subsequently find sets of parameters that induce oscillations, but set oscillations as the foundation of the model by representing each process with a phase oscillator. Cellular processes are also inevitably characterised by their nonlinearity [137], and modelling these nonlinearities is

Table 3.1: Summary of the principles informing our modelling approach contrasted to those of mainstream approaches

Mainstream principles	Our principles
Open systems can be modelled as perturbed closed systems	Open systems can only be fully represented by open models
Oscillations result from instability of a dynamical system	Oscillations are inherent to the dynamics of open systems. Living systems continuously exchange energy and matter with the environment and each process is characterised by self-sustained oscillations on a certain time-scale
Nonlinear systems can be recombined from linear systems	Nonlinear systems are best understood by nonlinear models
Time variation in living systems is often due to noise, and can be averaged out over asymptotic time	Time variation in living systems is often deterministic, and must be modelled as non-autonomous to reflect the full system dynamics

essential to understanding their dynamics. We therefore use Kuramoto oscillations to model these interactions.

Unlike theories that assume variations in the features of these oscillations, in particular frequency, are due solely to noise endemic to the complexity of biological systems, we treat much of these observable variations as deterministic. Our modelling approach to these systems is to represent them as non-autonomous Kuramoto phase oscillators.

3.2.1 Cell energy metabolism

The biological system as considered in this model is summarised in Fig. 3.1(A). It is constituted by four key processes: glycolysis, converting glucose, ATP and ADP into NADH, pyruvate and ATP, OXPHOS, converting oxygen, NADH and pyruvate into ATP, and the supplies of glucose and oxygen. The main purpose of this mechanism is the creation of ATP, which is primarily used to fuel ion pumps. Ion pumps actively transport ions across the cell's boundary against the electrochemical gradient, without which the cell would be forced to maintain an ionic equilibrium with its surroundings. Instead, the cell is able to accept the ions it needs for survival, and prevent itself from being flooded with an unhealthy quantity. Neuronal firing also relies on the ability of ion pumps to dramatically and rapidly change the balance of ions between the cell interior and exterior: the process is triggered only once the cell's membrane potential crosses the action potential threshold, typically requiring a change of some 100mV [155].

Communication between the metabolic processes is also well established [112, 120, 121, 123]. Glycolysis enzymes exist all around the cytosol, each facilitating an element of the wider glycolytic reaction. Not only do these distributed enzymes rely on regulation and supply common to them all, but the exchange of acetaldehyde molecules has been observed to drive coherence between glycolytic processes. Mitochondria, housing the OXPHOS process, exist in a more fixed state than the glycolysis enzymes of the cytosol, but are similarly thought to mutually organise their processes for the efficient running of the cell. Mapping precisely the exact positions and connections of these processes however would be challenging, if not impossible. In our model we therefore focus on the importance of molecular

exchanges in their communication, and the diffusive nature of these exchanges making distance a key consideration. Hence, we have assumed all-to-all coupled networks, but weighted these connections such that if were they considered around a ring, coupling strength would decrease the further apart any two given oscillators were.
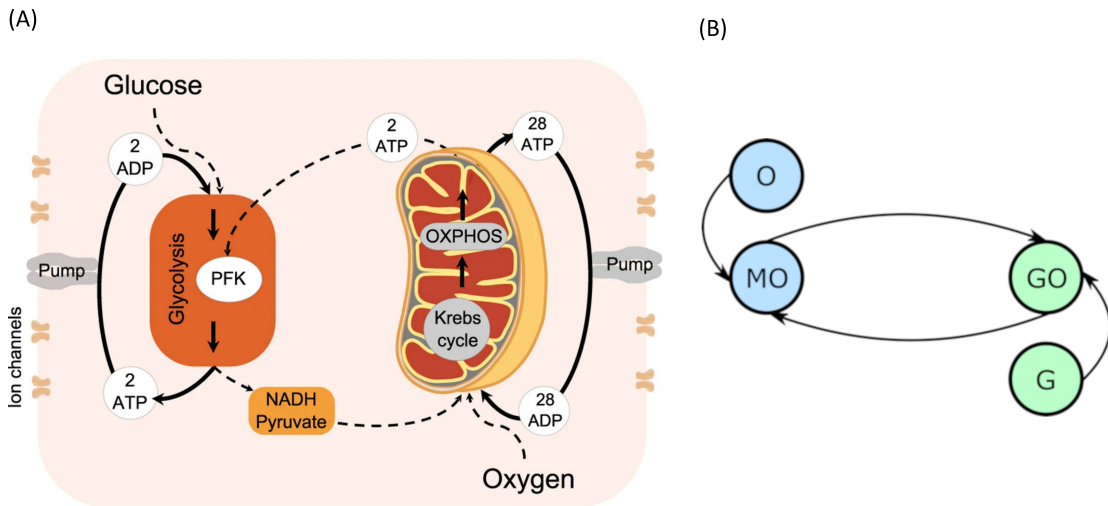
Figure 3.1: (A) The cellular energy metabolism considered in the Lancaster et al. model, reprinted with permission from [138]. (B) An oscillator model diagram of A, where each circle represents an oscillator, and each line a coupling. MO denotes the mitochondrial oscillator, GO the glycolysis, G the glucose driving and O the oxygen.

3.2.2 Defining the model

Each of these four metabolic processes is represented by a Kuramoto oscillator. Kuramoto oscillators are a type of nonlinearly interacting phase oscillators, which are a reduction of ordinary differential equations featuring self-sustaining oscillations from many degrees of freedom to just one: the phase of the oscillation. The phase of an oscillator is defined as its position along its cycle at a given time. This cycle can be represented in phase space, as shown in Fig. 3.2(A), where the meaning of any particular phase value can easily be seen.

Here phase has only been defined on the cycle of the oscillator equation. However, when oscillators interact or are driven by external forces, they will be perturbed away from this cycle. The phase in the vicinity of the cycle must therefore also be defined, which can
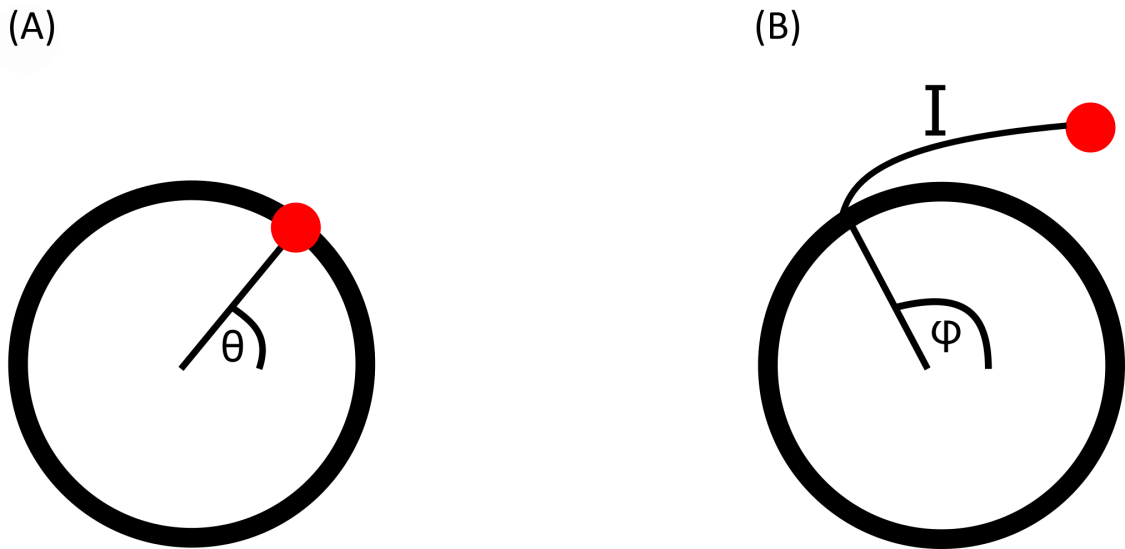
Figure 3.2: (A) An oscillatory cycle in phase space, at a phase value of θ. (B) A point perturbed from an oscillatory cycle, returning along isochron I to the cycle at a point with phase φ. The perturbed point is therefore also assigned the phase φ.

be done for stable oscillators using isochrons. When a stable oscillator is perturbed its phase will initially leave its cycle, but will return to it over time if not further perturbed. Isochrons connect the point to which a phase is perturbed to the point on the cycle it will first return to after the decay of the perturbation, assigning both the same phase value. This is demonstrated in Fig. 3.2(B). In order to remain in this region of attraction of the cycle, where isochrons can be used, the perturbations must be sufficiently weak, placing constraints on the strength of couplings between oscillators and drivers [4, 5].

This definition requires further extension to allow for the phases of non-autonomous oscillators. As the frequency, also known as the velocity of the phase, of the oscillator changes at each moment in time the system is transformed from one autonomous system to another. To maintain a consistent definition of phase across these systems, we must require that each system resides in the region of attraction of the one proceeding it, in order to use the same reasoning as the isochrons of perturbations. As with the weak coupling requirements of interactions, this definition constrains the system to only small changes in the frequency of oscillation from second to second [8].

This theory was applied to the biology of cellular ATP production by Lancaster et al. [138] in the following equations for the oscillators' phases

$$\dot{\theta}_{GO} = \omega_{GO} + \epsilon_1 \sin\left(\theta_{GO} - \theta_{MO}\right) - \epsilon_4 \sin\left(\theta_{GO} - \omega_G t\right) + \sigma\eta(t)$$

$$\dot{\theta}_{MO} = \omega_{MO} - \epsilon_2 \sin\left(\theta_{MO} - \theta_{GO}\right) - \epsilon_3 \sin\left(\theta_{MO} - \omega_O t\right) + \sigma\eta(t), \qquad (3.1)$$

where the subscript GO represents the glycolytic oscillator, MO the OXPHOS, G the glucose driving and O the oxygen. ω_X is the frequency of oscillator X, ϵ the relevant oscillator coupling strength, θ_X the phase, t time, $\eta(t)$ a noise term and σ the scaling parameter of the noise. These are hence two oscillators as described above, coupled to one another and their respective metabolic drivers, with their frequency rendered non-autonomous by the addition of a time-dependent noise parameter.

We convert this model to now consist of networks of oscillators, weighted such that neighbours around a ring interact with a maximal coupling strength, and those opposite with a minimal strength. This is shown diagrammatically in Fig. 3.3.
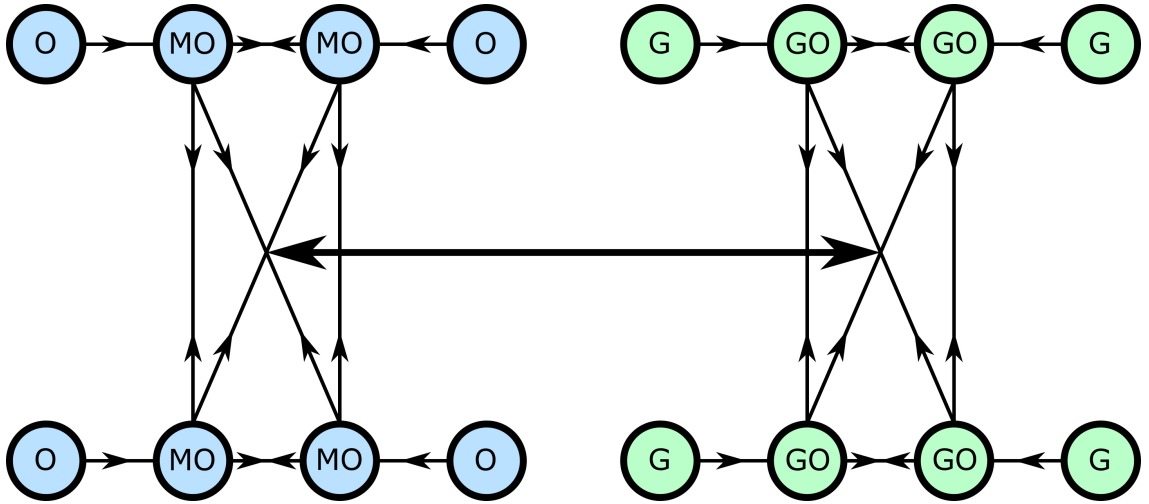
Figure 3.3: The network cellular metabolism model, with each circle representing an oscillator and each line a coupling.

We also consider, instead of the stochastic non-autonomicity in Lancaster et al. [138], a deterministic variation of the oscillation frequencies. This gives the glycolysis and OXPHOS phase equations as

$$\dot{\theta}_{GOni} = \frac{K_{GO}}{N} \sum_{j=1}^{N} W_{ij} \sin\left(\theta_{GOj} - \theta_{GOi}\right)$$

$$\dot{\theta}_{MOni} = \frac{K_{MO}}{M} \sum_{j=1}^{M} W_{ij} \sin\left(\theta_{MOj} - \theta_{MOi}\right), \tag{3.2}$$

respectively, where θ_{GOni} is the phase of the oscillator i due to network interactions, N is the number of glycolytic oscillators, M the number of OXPHOS oscillators, K_X the relevant network coupling strength and W_{ij} the weighting function between oscillators i and j.

The oscillators are organised into all-to-all couple networks, with a certain weight applied to each coupling. Each oscillator is further assigned an index, to create a ring structure where oscillator i and $i + 1$ are considered neighbours, as are the first oscillator, index 1, and the final, index N. The weight of the coupling between these oscillators is determined by their indices, such that the larger the difference between the indices, the smaller the weighting of their coupling. This weighting function is defined, for $i \leq \frac{N}{2}$, as

$$W_{ij} = \begin{cases} \dfrac{W}{|i - j|}, & \text{for } j \in \left[1, i + \frac{N}{2} - 1\right] \\[2em] \dfrac{W}{|j - N - i|}, & \text{for } j \in \left[i + \frac{N}{2}, N\right], \end{cases} \tag{3.3}$$

and for $N \geq i > \frac{N}{2}$ as

$$W_{ij} = \begin{cases} \dfrac{W}{|i - j|}, & \text{for } j \in \left[i - \frac{N}{2} + 1, N\right] \\[2em] \dfrac{W}{|j + N - i|}, & \text{for } j \in \left[1, i - \frac{N}{2}\right], \end{cases} \tag{3.4}$$

where W is a constant to be chosen.

The glucose and oxygen drivers are

$$\dot{\theta}_{GOGi} = \epsilon_G \sin\left(\theta_{GOi} - \theta_{Gi}\right)$$

$$\dot{\theta}_{MOOi} = \epsilon_O \sin\left(\theta_{MOi} - \theta_{Oi}\right), \tag{3.5}$$

where θ_{GOGi} is the phase of glycolysis oscillator i due to glucose coupling. The inter-network interactions arise through coupling each network to the mean field of the other [140, 153, 154]. This mean field arises as the average of each individual oscillation, characterising their collective state. It can be defined through the Kuramoto order parameter, $r_X e^{i\Psi} = \frac{1}{N}\sum_{k=1}^{N} e^{i\theta_{Xk}}$, where Ψ is the phase of the mean field. $r_X = 1$ hence indicates a totally ordered network with all oscillators at the same phase of their cycle, while $r_X = 0$ represents a totally disordered network. The inter-network equations therefore are

$$\dot{\theta}_{GOMOi} = F_{GO} r_{MO} \sin\left(\Psi_{MO} - \theta_{GOi}\right)$$

$$\dot{\theta}_{MOGOi} = F_{MO} r_{GO} \sin\left(\Psi_{GO} - \theta_{MOi}\right), \tag{3.6}$$

where F_X is the inter-network coupling strength and the average phase of network X is $\Psi_X = \frac{1}{N}\sum_{i=1}^{N} \theta_{Xi}$.

The four governing differential phase equations are hence

$$\dot{\theta}_{Gi} = \omega_{Gi}(t)$$

$$\dot{\theta}_{Oi} = \omega_{Oi}(t)$$

$$\dot{\theta}_{GOi} = \omega_{GOi}(t) + \dot{\theta}_{GOni} - \dot{\theta}_{GOGi} + \dot{\theta}_{GOMOi}$$

$$\dot{\theta}_{MOi} = \omega_{MOi}(t) + \dot{\theta}_{MOni} - \dot{\theta}_{MOOi} - \dot{\theta}_{MOGOi}, \tag{3.7}$$

where $\omega_{Gi}(t) = \omega_G + A_G \sin\left(\omega_{Gm}t + t_i\right)$, and $\omega_O(t)$, $\omega_{GO}(t)$ and $\omega_{MO}(t)$ have equivalent expressions for their respective elements, is the time-varying natural frequency of each oscillator i. In this paper we use the deterministic variation formulation for these frequencies, but any other time varying formulation, such as random noise, are

also valid methods provided that the variation is slow. ω_G is the mean frequency around which the non-autonomous frequency is modulated, A_G is the amplitude of modulation of the frequency, ω_{Gm} is the frequency of modulation and t_i is a perturbation of the modulation in time, taking a random number between 0s and $\frac{1}{\omega_{Gm}}$s. This perturbation ensures a distribution of frequencies within each element, while assigning the oscillators the same mean frequency and deterministic cycle of modulation.

3.2.3   Analysing synchronisation

The phenomenon of synchronisation between oscillators is a key part of understanding their dynamics. Oscillators can be considered synchronised when the difference between their phases remains constant. This is well established in the context of permanent synchronisation, where the phase difference between two oscillators does not ever change unless the parameters of the system change or a new influence is introduced [4,5]. Lucas et al. [2, 96] however found a different form of synchronisation, intermittent, where a pair of oscillators can transition repeatedly between synchronised and unsynchronised states without the system being changed. This phenomenon has only been observed for non-autonomous oscillators, and only when examined over finite time periods. When observed in an asymptotic, averaging time scale, it can easily be mistaken for complete desynchronisation.

For living systems, synchronisation between oscillators represents a state of stability and cooperative working between oscillators. Synchronised oscillators are, to an extent, able to resist perturbation away from this state and coordinate their oscillations for a variety of ends, including temporally compartmentalising conflicting processes [129, 156]. As in, for example, Lancaster et al. [138], certain combinations of synchronisation can be considered as the 'healthy' state of a cell, and the parameters at which they do and do not exist can therefore inform us about the mechanisms of pathological transitions. We will apply these methods of synchronisation analysis to our cellular metabolism model.

3.2.4 Numerical simulations

We conducted analysis of the model to determine the impacts on the dynamics made by the additions of weighted networks and deterministic non-autonomicity to the Lancaster et al. model [138]. These simulations involved numerical integration of the differential phase equations, defined in Eq. 3.7. This was conducted using the inbuilt Matlab ode15s algorithm, which is a partially implicit numerical integration scheme using a variable integration step and evaluates errors through interpolated backwards differences [62]. The equations were integrated for a period of 10,000 seconds at a sampling frequency of 0.1 seconds. The first 5,000 seconds were discarded, assuming they were dominated by transient dynamics, and then the final 5,000 seconds analysed to determine what, if any, modes of synchronisation were present.

This analysis involved calculating the phase coherence, as defined in [157, 158], between the glycolysis and OXPHOS oscillators and their glucose and oxygen drivers, respectively, and between the network oscillators and the mean field driving of the other network. The phase difference between these components was also calculated, as was the Kuramoto order parameter of each network.

For autonomous systems, time series are defined as coherent at a phase coherence value of or close to 1. However in non-autonomous systems, series may be coherent yet exhibit a time-averaged phase coherence of significantly less than 1 due to their modulation in time away from their coherent mean. Additionally, slight numerical simulation errors and noise can make it impossible to attain a numerical phase coherence of precisely 1. Through observations of numerical simulations, we have therefore defined coherence greater than 0.9 and phase difference within a bounded 2π region for the entire 5,000 seconds as indicative of permanently synchronised oscillators. If the coherence value was greater than 0.9 but the phase difference unbounded, we instead categorised the oscillators as intermittently synchronised. Networks were considered synchronised when their time-averaged Kuramoto order parameter exceeded 0.5, the threshold at which a network is more ordered than disordered. This was considered permanent if the parameter varied by less than 0.2 over the entire 5,000 seconds, and intermittently if it varied by more than this. Similarly to phase coherence, the Kuramoto order parameter of non-autonomous oscillations will naturally vary in time

due to frequency modulation, even in highly ordered networks, and so simulations indicated that only variations of greater than 0.2 are due solely to intermittency or disorder.

3.2.5 Experimental comparison

We have also analysed data collected by Amemiya et al. on glycolytic oscillations of starved HeLa cells [132]. In this experiment, the optical NADH fluorescence of numerous cells was measured over time after glucose was added to their environment. We calculated the group phase coherence, as defined by Sheppard et al. [159], of groups of cells around the culture. This coherence was further tested against 19 WIAAFT surrogates, as defined in [64], such that any non-zero coherence is considered significant. We analysed both groups near to one another and far from one another, to identify any significant differences between the two. These groups were constructed using hierarchical agglomerative clustering with the 'complete' linkage method, which considers the furthest Euclidean distance between groups of cells when defining the clusters. The culture was $1400\mu m$ by $1200\mu m$ in area, and near groups were defined as having $300\mu m$–$400\mu m$ between their average positions, while the average positions of far groups were $900\mu m$–$1200\mu m$ apart.

Simulations of this experiment were also conducted, using some of the results of the group coherence analysis and the general numerical simulations. This was done by numerically integrating a realisation of the system at a certain parameter set using a four step Runge-Kutta algorithm. The results of this and all the above methods are presented in the following section.

3.3 Results

There are six possible modes of synchronisation within our cellular metabolism model: glycolysis to glucose, glycolysis network, glycolysis to OXPHOS, OXPHOS network and OXPHOS to oxygen. While it would not be possible for glycolysis to be synchronised to OXPHOS, but OXPHOS to not synchronise to glycolysis in an individual oscillator model, it is possible for a network to become synchronised to a mean field driving,

without the network from which that mean field arises becoming synchronised to the network it is driving.

We examined whether each of these synchronisations occurred, and whether they were permanent or intermittent, at 2,500 different combinations of the parameters F_{GO} and F_{MO}, as defined in Eq. 3.2. This is similar to the analysis conducted in Lancaster et al. [138], and hence provides some understanding of the impact of each of the changes we have made in this model.

The parameters for which these simulations were conducted are given in Table 3.2. Most of these parameters, ϵ_G, ϵ_O, F_{GO}, F_{MO}, ω_G, ω_{GO}, ω_{MO}, ω_O, are identical to those used in Lancaster et al. [138] to allow a direct comparison, revealing the effects of the changes from that model. K_{GO} and K_{MO} did not exist in the Lancaster et al. model, and they have been set to be equal to the other non-varied coupling parameters. The frequencies and amplitudes of modulation were determined by their ratio to the mean frequencies, as studied by Lucas et al. [2]. W may be set to 1 as the relevance of the weighted coupling is in the relative weightings between different oscillator pairs. N and M cannot be determined purely biologically: the glycolysis oscillators represent a collection of often-distributed glycolytic enzymes that are not realistically quantifiable, while the number of a mitochondria in a cell type can vary significantly [134, 135]. Instead, the network sizes are chosen such that there a sufficiently many oscillators to validate the mean field approximation [140], and not so many as to make computational simulation infeasible.

We present first the analysis of the individual oscillator model of Lancaster et al. [138] in Fig. 3.4(A), for parameters ϵ_2 and ϵ_1 as defined in Eq. 3.1.

Table 3.2: Parameters of the non-autonomous weighted network simulations.

Parameter	Value(s)
ϵ_G	0.025
ϵ_O	0.025
K_{GO}	0.025
K_{MO}	0.025
F_{GO}	[0, 0.3]
F_{MO}	[0, 0.3]
ω_G	$\frac{2\pi}{200}$ Hz
ω_{GO}	$\frac{2\pi}{200}$ Hz
ω_{MO}	$\frac{2\pi}{100}$ Hz
ω_O	$\frac{2\pi}{100}$ Hz
ω_{Gm}	$\frac{2\pi}{2000}$ Hz
ω_{GOm}	$\frac{2\pi}{2000}$ Hz
ω_{MOm}	$\frac{2\pi}{1000}$ Hz
ω_{Om}	$\frac{2\pi}{1000}$ Hz
A_G	$\frac{2\pi}{600}$ Hz
A_{GO}	$\frac{2\pi}{600}$ Hz
A_{MO}	$\frac{2\pi}{300}$ Hz
A_O	$\frac{2\pi}{300}$ Hz
N	100
M	100
W	1
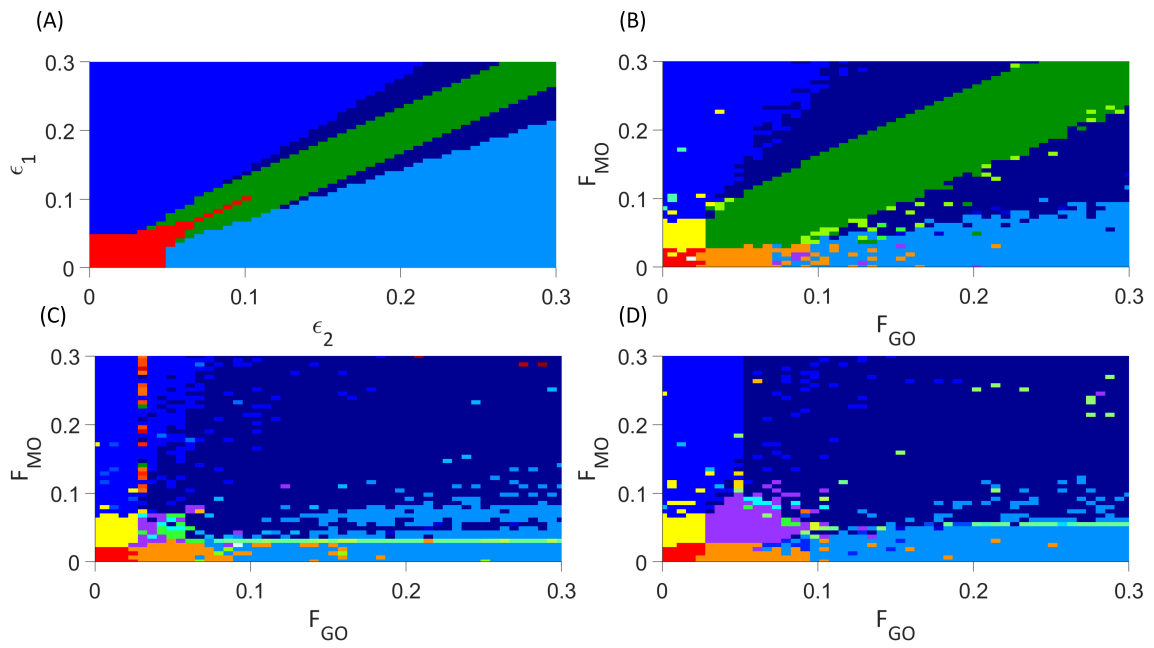
Figure 3.4: Analysis of the synchronisation regimes at different parameter values, at parameter steps of 0.006 between each simulation, (A) for the modified Lancaster et al. model [138]. (B) for the Lancaster et al. individual oscillator model with added deterministic non-autonomous frequencies and intermittent synchronisation analysis. (C) for the unweighted network model. (D) for the weighted network model. Regimes are defined in Table 3.3 and 3.3.

Table 3.3: Synchronisation regimes for each simulated model.

Model	Colour	GO-G	GO	GO-MO	MO-GO	MO	MO-O
Non-network models	Red	Permanent	N/A	No	No	N/A	Permanent
	Yellow	Permanent	N/A	No	No	N/A	No
	Blue	Permanent	N/A	Permanent	Permanent	N/A	No
	Orange	No	N/A	No	No	N/A	Permanent
	Dark green	No	N/A	No	No	N/A	No
	Dark blue	No	N/A	Permanent	Permanent	N/A	No
	Light blue	No	N/A	Permanent	Permanent	N/A	Permanent
Network models	Red	Permanent	Permanent	No	No	Permanent	Permanent
	Orange	No	Permanent	No	No	Permanent	Permanent
	Light blue	No	Permanent	Permanent	Permanent	Permanent	Permanent
	Yellow	Permanent	Permanent	No	No	Permanent	No
	Blue	Permanent	Permanent	Permanent	Permanent	Permanent	No
	Purple	No	Permanent	No	No	Permanent	No
	Green	No	Permanent	No	No	Intermittent	No
	Cyan	No	Intermittent	No	No	Permanent	No
	Dark blue	No	Permanent	Permanent	Permanent	Permanent	No

Introducing each new element of our model in turn to examine this same parameter space, we first include our deterministic variation of the frequency and analyse for intermittent synchronisation, as well as permanent, but otherwise maintain the Lancaster et al. model [138]. The results are in Fig. 3.4(B), and the main regimes described in Table 3.3. This results in the splitting of the red region in the Lancaster et al. analysis [138] into three regimes, two new: permanent synchronisation between glycolysis and glucose only, and oxygen and OXPHOS only. The dark blue region, where only glycolysis and OXPHOS are synchronised, is also made significantly larger, and there are spots of intermittently synchronised regimes that appear only briefly throughout the parameter space.

The next step is to introduce unweighted networks of glycolysis and OXPHOS oscillators. The result is in Fig. 3.4(C). This introduces a new regime, where only the networks are internally synchronised, and converts the dark green regime, where there is no synchronisation, into the even further increased dark blue regime. Once again, intermittent regimes are spotted briefly throughout the parameter space.

The final step in constructing our full model, is to weight the glycolysis and OXPHOS networks according to Eq. 3.3 and 3.4. Fig. 3.4(D) shows the results of this final simulation. This splits the new regime observed in the previous simulation into the purple, green and cyan regimes: the purple representing the same permanent synchronisation within each network, the green a new intermittent synchronisation of the OXPHOS network, and the cyan a new intermittent synchronisation of the glycolysis network. The weighting reduces the size of the dark blue region, giving more space to the blue and light blue, and as in the previous simulations produces small regimes of intermittent synchronisation.

3.3.1 Experimental comparison

In 2019 Amemiya et al. constructed a model of cellular glycolysis to explain the glycolytic oscillations they had observed in HeLa cells [160]. This model adopted an approach more similar to the mainstream discussed in the previous section. We therefore offer a comparison between this model and the one we have presented here, to help illuminate

further the differences between our approach and ones more characteristic of the cellular modelling mainstream, applied in the context of this experiment.

The Amemiya et al. model [160] constructs glycolysis as two main processes: the phosphofructokinase 1 (PFK) reaction and the pyruvate kinase (PK) reaction. The former is modelled as the first step, converting glucose and ATP into intermediaries, while the second is the last reaction, converting these intermediaries into ATP and pools of NADH and other products. The model focuses on the masses of the metabolites required for these reactions, from their entry into the cell to their consumption in the metabolic process. This technique consists of seven autonomous linear differential equations and twenty two parameters to model the glycolysis metabolic branch only, which contrasts to the four non-autonomous nonlinear oscillator equations of Eq. 3.7 and the thirteen parameters of Table 3.2 to model both the glycolysis and OXPHOS branches.

In addition to a measure of coherence within a network, the order parameter may also be considered the amplitude of the network's mean field. We can therefore consider it both an indication of the amplitude of our system, and the degree to which the glycolysis and OXPHOS networks are operating effectively. We introduce a modified Kuramoto order parameter s, where

$$se^{i\Psi_{GOMO}} = \frac{1}{(N+M)} \left(\sum_{i=1}^{N} e^{i\theta_{GOi}} + \sum_{j=1}^{M} e^{i\theta_{MOj}} \right),$$

which takes into account both networks. This parameter can be compared to the time series of NADH fluorescence from a single cell in the Amemiya et al. experiment [132], as NADH production in the cellular metabolic system is maximised when glycolysis and OXPHOS are able to act coherently. We provide this comparison in Fig. 3.6, and this can be further compared to an equivalent output of the Amemiya et al. model in Fig. 2 of [160]. The Amemiya et al. model considers just glycolysis, and is built on 7 autonomous differential equations tracking the change in quantities of a range of metabolites, relying on 22 parameters [160]. In contrast, the model we have presented here accounts for both glycolysis and OXPHOS through two types of non-autonomous differential phase equations, using 21 parameters.

The parameters used in this simulation are given in Table 3.4, where $A = 9.511 \times 10^{-7}$ and $B = 1.931 \times 10^{-3}$ are the coefficients of the quadratic and linear terms, respectively,

of the curve in Fig. 3.6(B), as found by quadratic curve fitting. The modulation frequency of the glycolysis oscillations was extracted from group coherence analysis of the Amemiya et al. data, which found that for both cell groups close to and far from one another there was significantly coherent oscillations in the range 0.1–0.2Hz. This analysis is presented in Fig. 3.5. The other frequencies were selected to maintain the same ratio with the extracted glycolysis modulation as discussed in Lancaster et al. [138]. The coupling parameters were chosen to reflect the dynamics shown in the experimental time series and identified in Fig. 3.4: the simulation begins with $F_{GO} = F_{MO} = 0.6$, and all other parameters at 0.025 to re-create the dark blue regime of synchrony between the networks found in Fig. 3.4(D), resulting in the initial amplitude spike as glucose is first introduced to the environment. Over the next 355.9s these couplings decrease according to the gradient of Fig. 3.6(B) and ϵ_{GO} equivalently increases, as the damage the cells sustained during their starvation period inhibits their processes and reducing metabolite supplies leaves the system less stable to fluctuations in these quantities. This results in a trending decrease in the networks' amplitude and the emergence of oscillations. After 382.9s the supply of glucose is almost entirely exhausted, flat-lining ϵ_{GO} at 0.7 and causing the oscillations to begin to degrade into more noise-like behaviour. For the final 517s of the simulation F_{GO} and F_{MO} have reached 0 as the cells begin to die, their oscillations continue to diminish, and their NADH production dries up.

While the curve presented in Fig. 3.6(A) depends on the initial phases of each oscillator, which are randomised, and therefore will not be identical from simulation to simulation, its oscillator features and overall trend are indicative of the parameters in Table 3.4. And while this simulation is not an identical reflection of the experiment in every feature, it is an indication of the capacity of our model to reproduce the oscillating nature of biological processes, and the ease with which it can be adapted to a plethora of different cells and circumstances.

3.4   Discussion

The conversion of established metabolic models, such as that of Lancaster et al. [138], to consider networks of processes offers both greater biological realism and a resulting transformation of the dynamics we expect to see from such models. The step from

Table 3.4: Parameters of the HeLa experiment simulation.

Parameter	Value(s)		
	0–355.9s	**356s–382.9s**	**383s–800s**
ϵ_G	$-At^2 + Bt + 0.025$	0.7	0.7
ϵ_O	0.025	0.025	0.025
K_{GO}	0.025	0.025	0.025
K_{MO}	0.025	0.025	0.025
F_{GO}	$At^2 - Bt + 0.6$	$At^2 - Bt + 0.6$	0
F_{MO}	$At^2 - Bt + 0.6$	$At^2 - Bt + 0.6$	0
ω_G	$\frac{40\pi}{3}$ Hz	$\frac{40\pi}{3}$ Hz	$\frac{40\pi}{3}$ Hz
ω_{GO}	$\frac{40\pi}{3}$ Hz	$\frac{40\pi}{3}$ Hz	$\frac{40\pi}{3}$ Hz
ω_{MO}	$\frac{80\pi}{3}$ Hz	$\frac{80\pi}{3}$ Hz	$\frac{40\pi}{3}$ Hz
ω_O	$\frac{80\pi}{3}$ Hz	$\frac{80\pi}{3}$ Hz	$\frac{40\pi}{3}$ Hz
ω_{Gm}	$\frac{4\pi}{3}$ Hz	$\frac{4\pi}{3}$ Hz	$\frac{4\pi}{3}$ Hz
ω_{GOm}	$\frac{4\pi}{3}$ Hz	$\frac{4\pi}{3}$ Hz	$\frac{4\pi}{3}$ Hz
ω_{MOm}	$\frac{8\pi}{3}$ Hz	$\frac{8\pi}{3}$ Hz	$\frac{8\pi}{3}$ Hz
ω_{Om}	$\frac{8\pi}{3}$ Hz	$\frac{8\pi}{3}$ Hz	$\frac{8\pi}{3}$ Hz
A_G	$\frac{2\pi}{9}$ Hz	$\frac{2\pi}{9}$ Hz	$\frac{2\pi}{9}$ Hz
A_{GO}	$\frac{2\pi}{9}$ Hz	$\frac{2\pi}{9}$ Hz	$\frac{2\pi}{9}$ Hz
A_{MO}	$\frac{4\pi}{9}$ Hz	$\frac{4\pi}{9}$ Hz	$\frac{4\pi}{9}$ Hz
A_O	$\frac{4\pi}{9}$ Hz	$\frac{4\pi}{9}$ Hz	$\frac{4\pi}{9}$ Hz
N	100	100	100
M	100	100	100
W	1	1	1
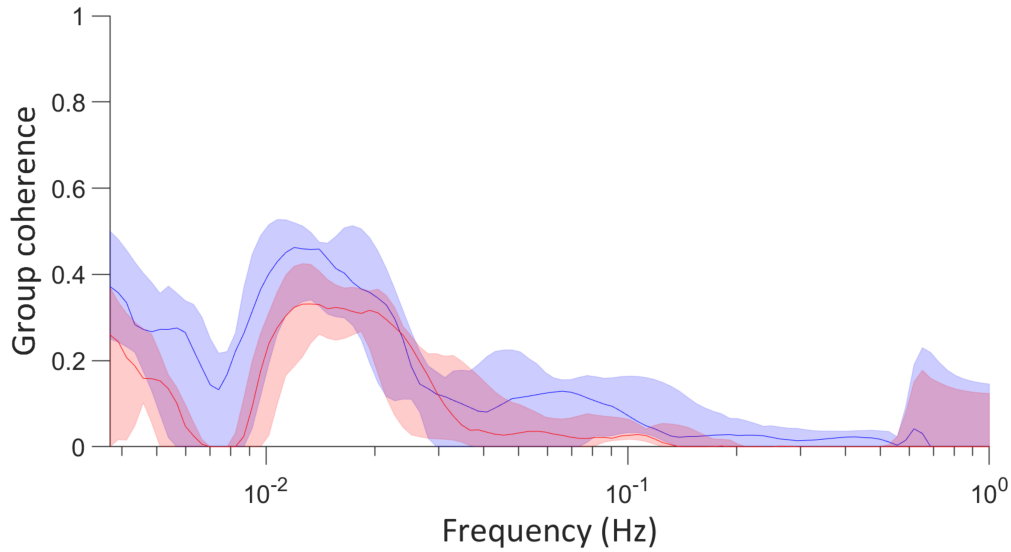
Figure 3.5: Surrogate tested coherence between groups of cells examined in [132], calculated with the coherence algorithm presented in [159]. Red colouring indicates groups of cells far from one another, $900\mu m$–$1200\mu m$ distance between their average positions, and blue close to one another, $300\mu m$–$400\mu m$ distance between their average positions. The dimensions of the culture were $1400\mu m$ by $1200\mu m$. The solid coloured lines are the median coherence of each pair of groups, and the shaded regions the range from the minimum to maximum coherence. The cell groups were constructed using hierarchical agglomerative clustering with the 'complete' linkage method.
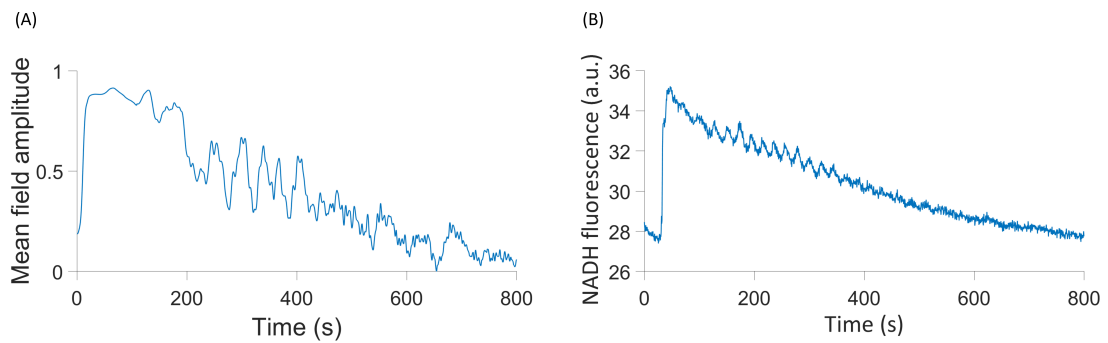
Figure 3.6: (A) Simulation of the HeLa experiment using a modified order parameter. (B) The time series of NADH fluorescence in a single cell in the Amemiya et al. experiment [132].

Fig. 3.4(B) to 3.4(C) for example overhauls the parameter space, introducing entirely new regimes and destroying once-firm fixtures of the non-network model. It is clear from all of these results that networks result in an even greater area of the parameter space

featuring synchronisation, with the only regime of total desynchronisation disappearing once networks are introduced, and the networks themselves never being desynchronised. This aligns well with the imperative of such biological processes to remain robust against significant external perturbations, and the expectation that these parameter values do not represent catastrophic departure from the healthy state of the system. More significant perturbations of the coupling parameters, to both higher values and the entire elimination of more coupling modes, are likely required to completely desynchronise the networks, which would represent even further departures from the healthy parameter states of the cell.

In healthy human cells, ATP is produced primarily through OXPHOS, with support from glycolysis. In our model, this may be represented by synchronisation between the networks, and between the OXPHOS network and its oxygen driving [138]. Internal synchronisation of both networks is also required to characterise a healthy condition: disregulation within the metabolic processes is a key indicator of a malfunctioning cell. This state is represented in the bottom right of each graph in Fig. 3.4, but is significantly diminished in area with the addition of deterministic frequency modulation from Fig. 3.4(A) to 3.4(B). A cancerous state, may be indicated by an opposite state: a mode switch to the dominance of glycolysis, known as the Warburg effect, is reflected by synchronisation between the networks and between glycolysis and glucose, but not OXPHOS and oxygen [138]. Due to the decreased relevance of OXPHOS to the metabolic process in cancer, it may be represented by either ordered or disordered OXPHOS networks. This regime is found in the top left of each of Fig. 3.4, similarly decreasing in area between Fig. 3.4(A) and 3.4(B) as with the bottom right regime.

Network models also offer greater potential for oscillator systems: while reducing oscillating differential equations to just their phase provides a much simpler system that still contains the key dynamics, only at the mesoscopic level of networks of many oscillators can the system amplitude be rebuilt. Further work on this model could therefore provide not just an order parameter of the network indicative of its activity, but an amplitude of its production.

The turn to deterministic non-autonomous frequencies and finite time synchronisation analysis similarly promises a significant change to the dynamics of metabolic models.

89

Intermittent synchronisation allows greater nuance between the states of 'healthy' and 'pathological', more reflective of the complexity of living systems, yet further ways for the processes to stabilise in spite of significant perturbation and ever more complex and effective ways for them to compartmentalise. However, with the introduction of this non-autonomicity comes greater challenges for numerical simulations: the numerical integration of nonlinear oscillating differential equations is an already delicate task, and the addition of another dimension of time sensitivity requires alternative methods.

Further work with more sensitive numerical integration algorithms and more sophisticated methods for identifying intermittent synchronisation would be likely to find a far greater role of the phenomenon in the model's parameter spaces, and further clarify exactly which dynamic we can expect to find at each parameter combination. The integration scheme used in this work has resulted in multiple 'islands' of synchronisation regimes, which are unrelated to the regimes at all neighbouring parameter values, and yet are reproduced under the same simulation conditions. Non-autonomous oscillations pose a particular challenge to numerical integration schemes due to their two highly distinct frequency modes. Schemes designed to adapt to this situation may be able to provide greater clarity on our model, with which we may be able to further identify parameters leading to pathological states and more complex dynamics within the model.

3.5   Acknowledgements

3.6 Data Availability Statement

The data collected in [132], analysed in this paper, can be found at 10.17635/lancaster/researchdata/406. The Matlab codes used for the numerical and experimental analyses in this paper will be made available by the final version.

3.7 Appendix

In this section we discuss the additional analysis of the experimental data in [132] that underpins the comparison of the cell energy metabolism model analysed in this chapter to the aforementioned experimental data.

In the experiment of [132], three different cell cultures were grown. All were cultivated under the same conditions of 72 hours of access to plentiful glucose and the application of fetal bovine serum. The latter promoted the growth of the cells, and the former ensured they had sufficient metabolites to conduct their ordinary functions. After this, each were starved of one or both of these supplies for a period of 24 hours. The first was starved of only glucose, and will hereafter be referred to as Glc–1. The second, Glc–2 underwent the same procedure to provide a repeat experiment. The third was starved of both glucose and fetal bovine serum, and will be referred to as FBS–. After this period of starvation, glucose was injected around the cell culture, at which point the cells once again began to conduct significant amounts of glycolytic processes, and the results of this were observed.

Our primary aim in this analysis was to investigate the extent to which the gylcolytic oscillations of these cells are similar to one another, and whether any similarity has any spatial dependence.

To do so by analysing cells pair by pair is not particularly feasible, given that each of the three cultures consisted of hundreds of cells. Such analysis would therefore be either unnecessarily time consuming, or not be robust against any unrepresentative dynamics of individual cells due to only considering a few pairs. Instead of this therefore, we used the generalised group coherence presented in [158], which calculates the wavelet phase coherence between different spatial groups of data.

This procedure defines a power-normalised wavelet transform in a group as

$$w_{n,\sigma}(t) = \frac{W_{n,\sigma}}{\frac{1}{NT}\sum_{n=1}^{N}\sum_{t=1}^{T}W_{n,\sigma}(t)\overline{W_{n,\sigma}(t)}}, \qquad (3.8)$$

for each time-series n and timescale σ, where $W_{n,\sigma}$ is the conventional wavelet transform of the time-series. The generalised group wavelet phase coherence between a group A and a group B is then defined as

$$\left|\Pi_\sigma^{(AB)}\right| = \left|\frac{1}{NT}\sum_{n=1}^{N}\sum_{t=1}^{T}w_{n,\sigma}^{(A)}(t)\overline{w_{n,\sigma}^{(B)}(t)}\right|. \qquad (3.9)$$

In a sense therefore, this quantity is the average pairwise wavelet phase coherence between each pair of time-series which have been collected into two groups. The phase coherence itself tracks to what extent the phases of the two groups are coherence with one another over their frequency spectra and time. This is most commonly interpreted in either a time-averaged or frequency-averaged fashion (with Fig. 3.5 being an example of time-averaged phase coherence). In the time-averaged representation, for a given frequency in their combined spectrum, their phase coherence will be 1 if their time-series of that decomposed frequency mode were perfectly coherent at all time. If at any points they were not coherent, it will be less than 1, and if they were always totally incoherent it will be 0. For the frequency-averaged form, the coherence of every decomposed frequency mode is averaged at every time point, to produce a phase coherence time-series.

The first task to enable this analysis therefore was to construct each cell culture into groups of cells. To do this, we applied a hierarchical agglomerative clustering algorithm. This algorithm starts by viewing each cell in each culture as its own group of size one, then calculates the 'linkage' between each group and every other one. This linkage quantifies the degree of similarity between groups, usually using a notion of distance between them, but can be defined in various ways. The pair of the groups with the smallest linkage are then combined into a new group, and this procedure continues until some pre-defined end point, or until all cells have been joined into a single group. For this analysis, the 'complete' linkage was used, which is defined as

$$d(a, b) = \mathsf{max}\left(\mathsf{dist}\left(x, y\right)\right) \quad \forall\ x \in a\ \&\ y \in b, \tag{3.10}$$

for any two groups a and b, and where dist is the Euclidean distance function. In other words, the linkage between two groups is the greatest distance between each pair of their cells.

Making the determination on how many groups in which to organise the cells for the purpose of this analysis rests on three considerations: having sufficiently many groups that the categories of 'near' and 'far' group coherence calculations consist of a sufficient number of group comparisons, having sufficiently few groups that each group consists of sufficiently many cells, and ensuring that while both these conditions are met, the groups constructed are not evidently 'unnatural'. The process of applying these considerations to deriving groups in each cell culture is a matter of trial and error of different numbers of groups, judged by inspection. Due to the pairwise nature of the group coherence calculation, the final part of this algorithm is to reduce each group to contain the same number of cells as the one which contains the fewest. To do this, the cell with the greatest of distances between each cell and the average position of the group is removed repeatedly until the desired size is reached.

The Glc–1 cell culture was divided into 10 groups, each consisting of 31 cells, shown in Fig. 3.7. This ensured plenty of cells in each group, and that there are multiple groups on the edges of the culture, that can be used to calculate the group coherence at larger distances.

Glc–2, in Fig. 3.8 was similarly divided into 10 groups, this time each consisting of 30 cells. The similarity between this and Glc–1 is unsurprising, given that they were cultivated with an identical procedure, leading to only minor differences between the two cultures.

FBS–, on the other hand, had far fewer cells survive its starvation process than Glc–1 and 2, given that it was starved of fetal bovine serum in addition to glucose. As a result the cells are positioned even more heterogenously than in the other cultures, and more attention was required to ensure that the groups were not excessively spatially incoherent, or 'unnatural'. This was mainly achieved by increasing the number of groups
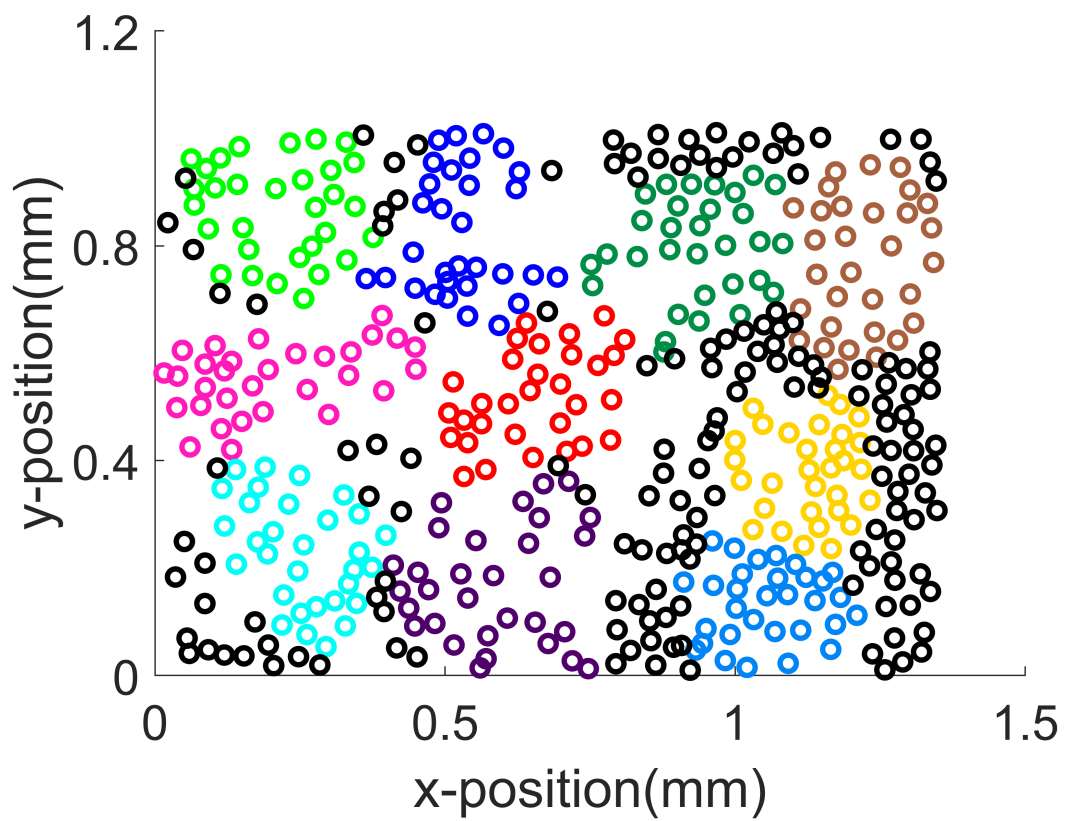
Figure 3.7: The Glc–1 cell culture, with the groups constructed by the hierarchical agglomerative clustering algorithm coloured, and the cells not assigned to a group left in black.
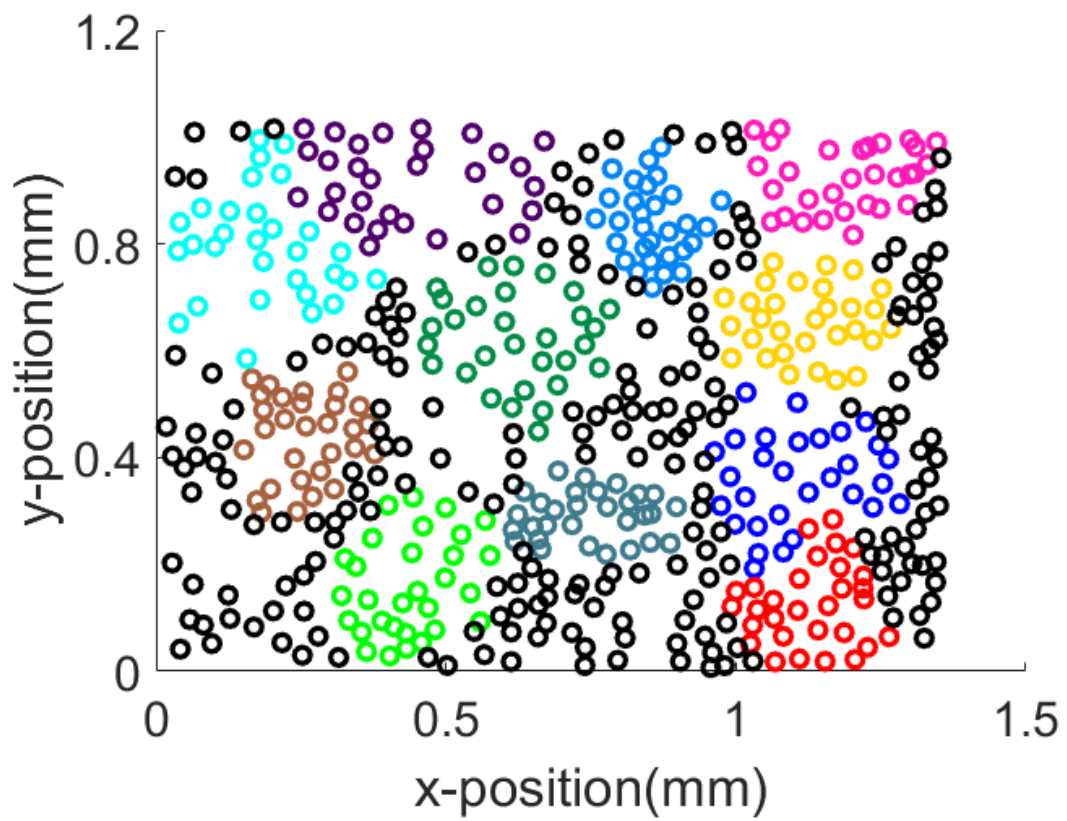
Figure 3.8: The Glc–2 cell culture, with the groups constructed by the hierarchical agglomerative clustering algorithm coloured, and the cells not assigned to a group left in black.
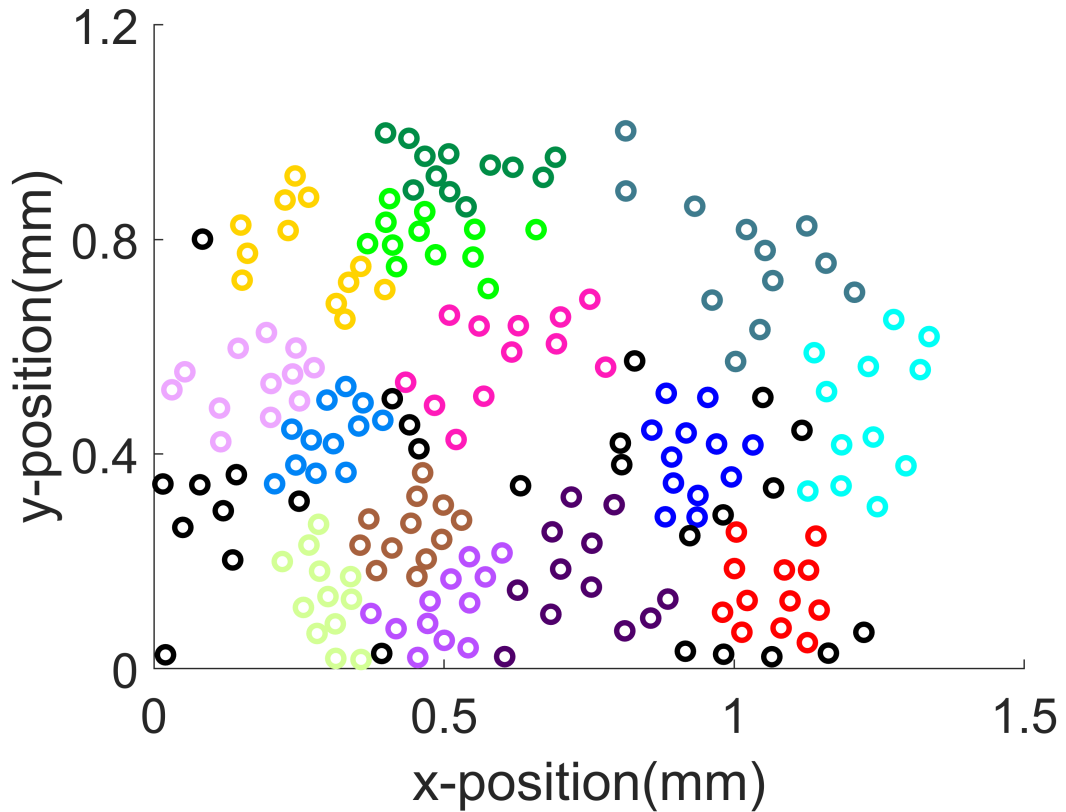
Figure 3.9: The FBS– cell culture, with the groups constructed by the hierarchical agglomerative clustering algorithm coloured, and the cells not assigned to a group left in black.

compared to the other cultures to 14. This is not to say that these resulting groups are the most coherent possible, but these 14 groups already consisted of much fewer cells than in Glc–1 and 2, specifically, 12, and to decrease this further by increasing the number of the groups risks making on any peculiarities of individual cells too impactful on the overall dynamics of the group. These groups are shown in Fig. 3.9.

Next, the definition of 'far' and 'near' groups, which will determine whether coherence between groups has spatial dependence, is made for each culture. These definitions, certain distances between the average position of two groups, and which group falls into which are summarised in Table 3.5.

The wavelet phase coherence between each of these groups can then be calculated and compared to one another, after being tested against 19 WIAAFT surrogates, so that any non-zero coherence can be considered to be statistically significant. This analysis

Table 3.5: The 'near' and 'far' groups of cells in each of the three cultures.

Analysis	Groups
Glc–1 0.3–0.4 mm	Dark blue–red, Dark blue–green, Red–dark green, Red–indigo, Green–pink, Pink–cyan, Gold–brown, Indigo–cyan
Glc–1 0.9–1.2 mm	Green–gold, Green–blue, Green–brown, Pink–gold, Pink–blue, Pink–brown, Brown–cyan
Glc–2 0.3–0.4 mm	Dark blue–teal, Green–brown, Green–teal, Pink–blue, Gold–blue, Blue–dark green, Dark green–indigo, Dark green–teal, Brown–cyan
Glc–2 0.9–1.2 mm	Dark blue–cyan, Red–brown, Red–indigo, Red–cyan, Green–pink, Pink–brown, Pink–cyan, Gold–cyan
FBS– 0.3–0.4 mm	Dark blue–pink, Dark blue–cyan, Red–indigo, Red–cyan, Pink–gold, Pink–blue, Pink–dark green, Pink–brown, Gold–blue, Gold–dark green, Blue–purple, Brown–indigo, Brown–light pink, Cyan–teal
FBS– 0.8–1.2 mm	Red–green, Red–gold, Red–blue, Red–dark green, Green–cyan, Gold–cyan, Blue–cyan, Dark green–cyan, Cyan–light pink, Dark green–light green, Dark green–purple, Brown–cyan, Cyan–purple, Teal–light pink, Teal–purple
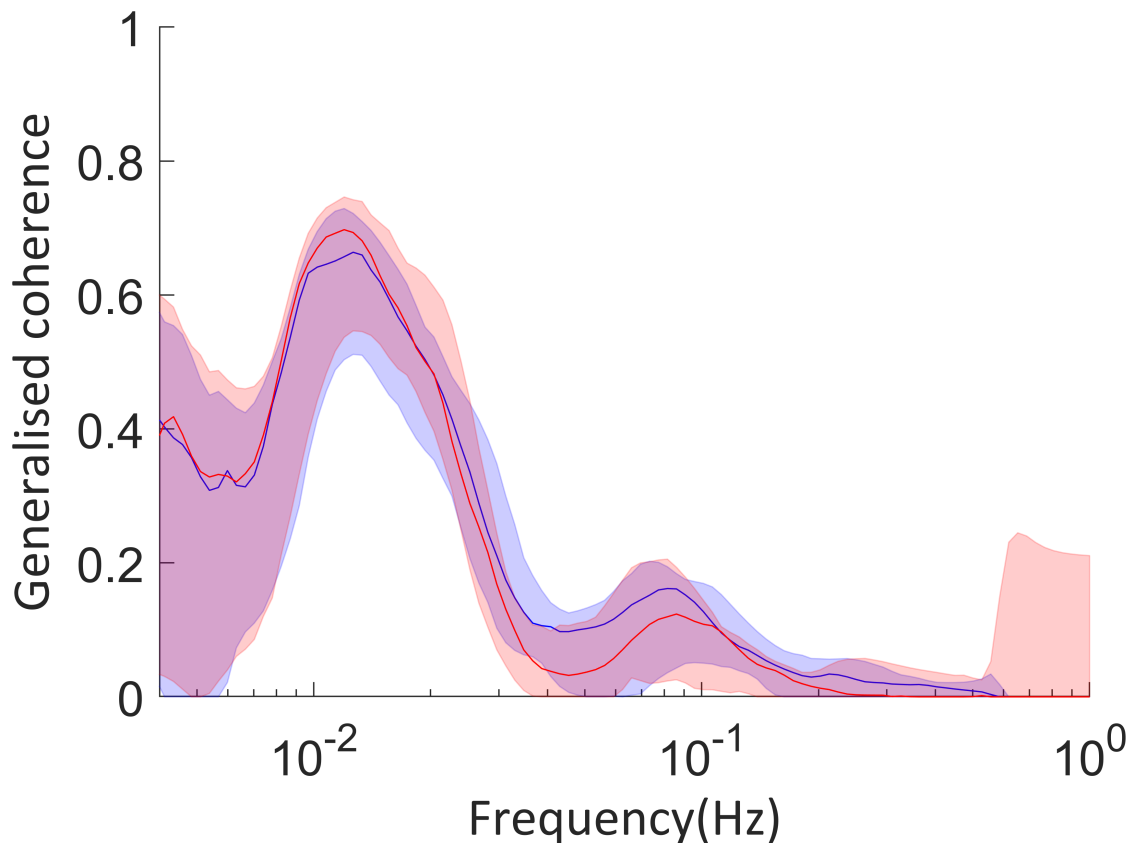
Figure 3.10: Surrogate tested coherence between groups of cells in the Glc–2 culture. Red colouring indicates groups of cells far from one another, 0.9 mm–1.2 mm distance between their average positions, and blue close to one another, 0.3 mm–0.4 mm distance between their average positions, as listed in Table 3.5. The solid coloured lines are the median coherence of each pair of groups, and the shaded regions the range from the minimum to maximum coherence.

was already presented for Glc–1 in Fig. 3.5, and Glc–2 is shown in Fig. 3.10 and FBS– in 3.11. In these figures, the mean of the coherence between all the groups in that category at that frequency is shown by the solid lines, and the shaded regions show the range from the smallest to largest coherence of these groups. The 'near' groups analysis is represented by the blue lines and regions, and the 'far' groups by the red.

These results show no evidence of significant differences in the coherent frequencies between near groups and far groups. There are however coherence peaks at frequencies common to all three cultures. The largest of these occur in the range $0.01 - 0.02$ Hz, and a smaller one between $0.07 - 0.1$ Hz. That these peaks are recurrent between all three cultures, but does not appear to depend on the distance between the cells,
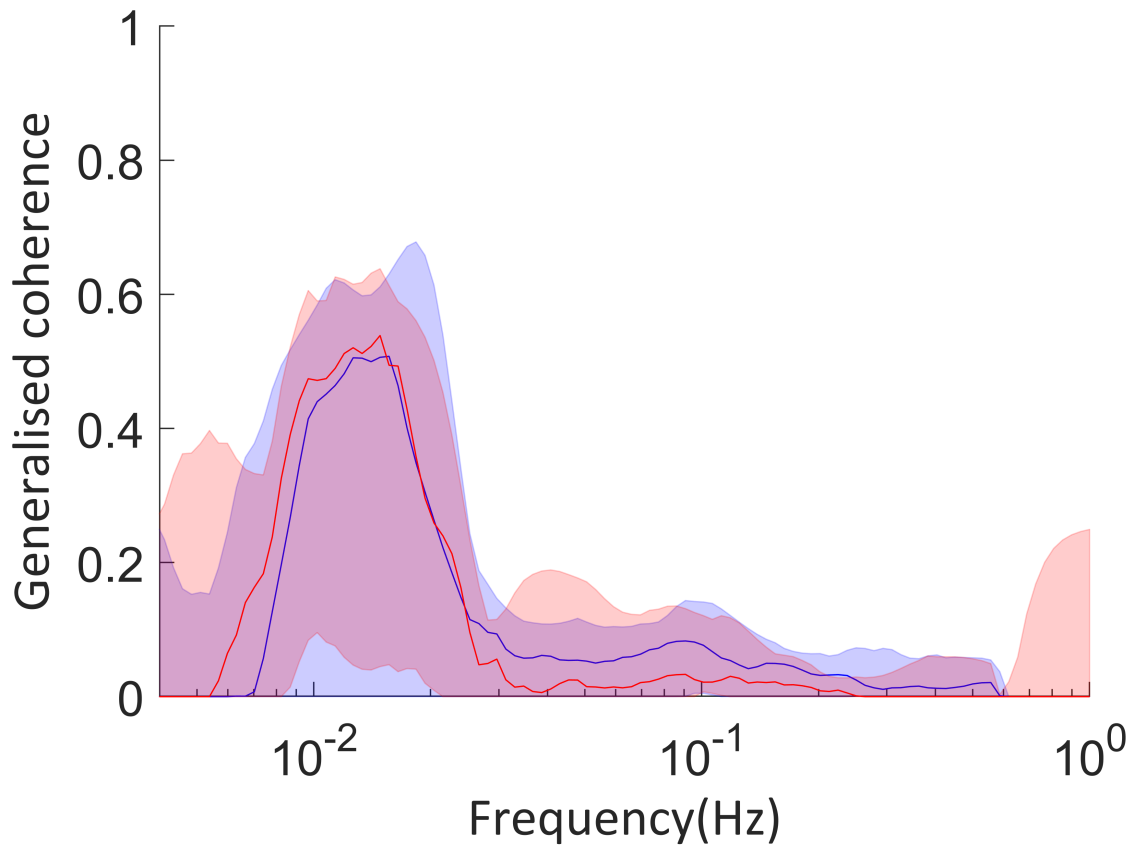
Figure 3.11: Surrogate tested coherence between groups of cells in the FBS– culture. Red colouring indicates groups of cells far from one another, 0.8 mm–1.2 mm distance between their average positions, and blue close to one another, 0.3 mm–0.4 mm distance between their average positions, as listed in Table 3.5. The solid coloured lines are the median coherence of each pair of groups, and the shaded regions the range from the minimum to maximum coherence.

suggests that they are not arising due to communication between the cells. Or at least, the unlikely possibility that the cells are communicating just as effectively with their immediate neighbours as with cells at the opposite end of the culture, or from a non-symmetrical external driver. Instead, the most likely cause is that these oscillatory modes are fundamental to the biology of the cells. The fact that the lower frequency, higher coherence, peak is consistent with other experimental measurements of glycolysis also strengthens this theory [111,161], and hence this value was used as the natural frequency of the glycolytical oscillations in the modelling in this chapter. It is less obvious however what causes the higher frequency peaks, warranting further investigation.

To ensure that these coherence peaks are fundamental dynamics arising from the cells' biology, we next check that they are not harmonically related to one another, or any other frequency mode present in the time-series using the algorithm presented in [162], developed from the work in [163,164]. If there were a harmonic relationship, this would suggest that the concerned frequency mode is not biologically generated, but a super-position of lower frequencies. To do this, the phase time-series produced by the wavelet transform are partitioned into 24 bins. The phase time-series are then compared pair-wise, calculating the phase distribution of the higher frequency series, $p(\phi_1)$, and the conditional phase distribution of the higher frequency series given the lower frequency series, $p(\phi_1 \parallel \phi_2)$. From the former, the Shannon entropy can be calculated as

$$H\left(\Phi_1\right) = -\sum_{\phi_1=1}^{24} p\left(\phi_1\right) \log_2 p\left(\phi_1\right). \tag{3.11}$$

Then, from the latter, the mean entropy is calculated as

$$H\left(\Phi_1 \parallel \Phi_2\right) = -\sum_{\phi_2=1}^{24} p\left(\phi_2\right) \sum_{\phi_1=1}^{24} p\left(\phi_1 \parallel \phi_2\right) \log_2 p\left(\phi_1 \parallel \phi_2\right). \tag{3.12}$$

Finally, the mutual information between the two phase time-series is

$$M\left(\Phi_1, \Phi_2\right) = H\left(\Phi_1\right) - H\left(\Phi_1 \parallel \Phi_2\right). \tag{3.13}$$

It is this quantity that is used to ascertain whether there is a harmonic relationship between the two modes. If the higher mode shares a significant amount of information with the lower one, then the conclusion drawn is that the higher mode must be a higher harmonic of the lower one, and not an independent dynamic. This has been applied to study, for example, interactions between the brain and the cardio-respiratory system [165].

This can hence be numerically calculated from the cellular time-series data, to investigate whether the previously identified peaks are a product of harmonic relations. The mutual information quantity described in Eq. 3.13 is compared against the standard deviation of the same quantity calculated for 19 WIAAFT surrogates. Where the mutual information is multiples of the standard deviation higher than the mutual information calculated at that frequency from the surrogates, then this non-zero mutual information in the signal is considered to be statistically significant.

It is not, however, as simple to do so for many time-series as it was for the coherence, due to the lack of a group analogue. Instead, all the cells of the culture were checked individually. In Fig. 3.12 and 3.13 we present this analysis for two randomly selected cells from the Glc–1 and Glc–2 cultures, respectively, that are also reflective of the dynamics seen in the other cells.

In both cases, we see mutual information peaks four to five times higher than the standard deviation of the surrogates at many of the frequencies between 0.01 and 0.02 Hz. This is hence strongly suggestive that the higher frequency, 0.02 Hz, is a harmonic produce of the lower, 0.01 Hz, and that the latter is the biologically generated mode. There is no similar harmonic relationship to the other coherence peak at 0.07 to 0.1 Hz, suggesting that this is also a 'real' mode.

3.7.1 Non-autonomous phase

In this and the previous chapter we have discussed adapting the notion of isochrons used to define autonomous phase for a range of initial conditions to non-autonomous phase. The method we have adpoted here is to consider the non-autonomous system to consist of a sequence of autonomous systems, with each subsequent autonomous system being a modulation of the previous with respect to the given time-dependence rule [8].
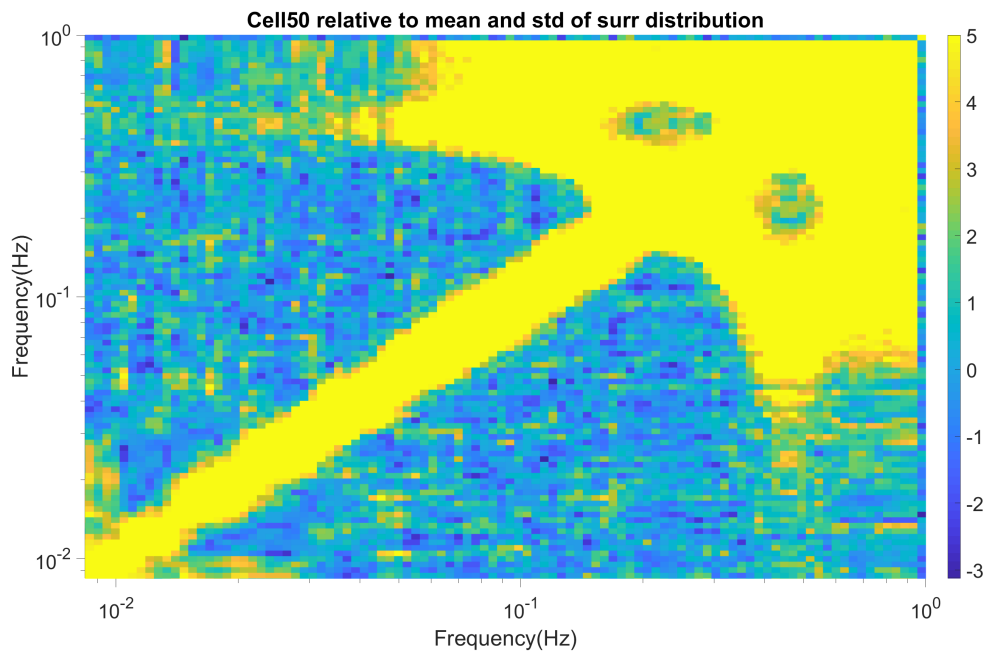
Figure 3.12: The mutual information between frequency modes in the 50th cell of the Glc–1 culture, relative to the standard deviation in the mutual information of 19 numerically generated WIAAFT surrogates.
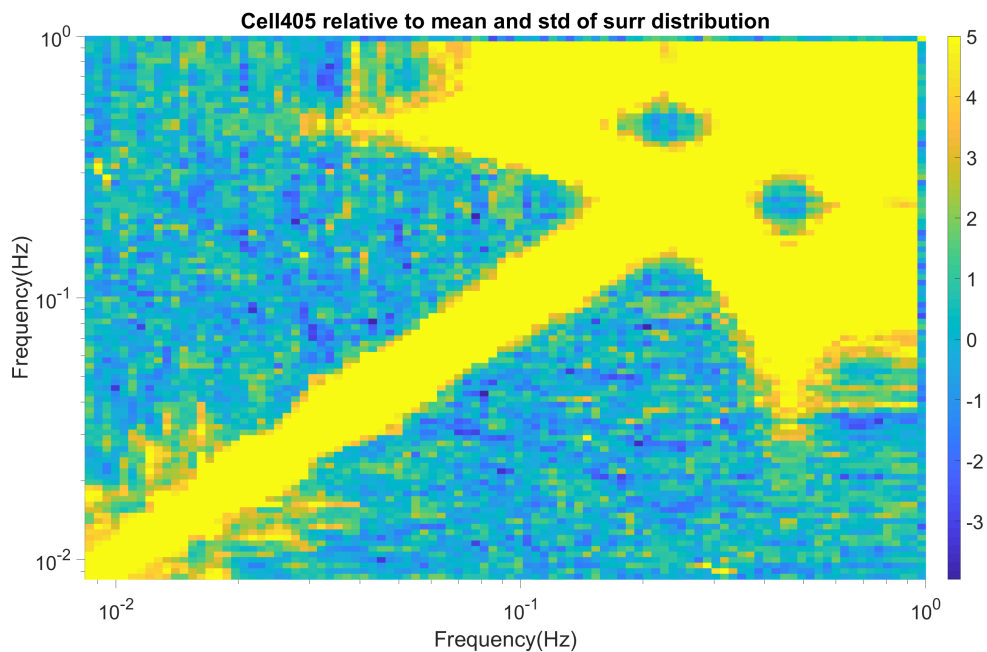
Figure 3.13: The mutual information between frequency modes in the 405th cell of the Glc–2 culture, relative to the standard deviation in the mutual information of 19 numerically generated WIAAFT surrogates.

Then, at each time, the phase may be defined in the usual manner for an autonomous system via isochrons. However, it should be noted that isochrons are defined under the assumption of an asymptotic convergence of an off-cycle trajectory back to the cycle, which is not inherently compatible with a non-autonomous system, which may have changed significantly over this asymptotic time frame such that the same phase definition may no longer be valid. To account for this, the slow-fast requirement states that the non-autonomous dynamics, the frequency of the time-dependence through which each autonomous system is connected, must be slow with respect to the dynamics of the autonomous systems. If this is met, the phase as defined by the isochrons of an autonomous system remains within the basin of attraction of the cycle of the next autonomous system, and so is still defined. This can be continued on through an asymptotic time frame, thereby ensuring each initial phase remains defined throughout the entire evolution of the non-autonomous system.

An alternative perspective is to define strictly non-autonomous isochrons, rather than a series of autonomous ones, by considering an attractive cylinder in the system's extended state space. In essence, the autonomous cycle is extended to a cylinder through the inclusion of the time dimension [85, 87]. An isochron can be connected to each point on this cylinder through the set of points that converge to this point on the cylinder as they are evolved forwards in time. However, this redefines the phase of such trajectories to be constant till their point of convergence, as opposed to the modulating phase produced by the approach we used in this thesis.

3.7.2 HeLa cells, glucose starvation and modelling the HeLa experiment

The HeLa cells analysed to support the modelling efforts in this and previous chapter are an immortal cell line originally harvested from a cervical cancer tumour. It must be noted that this harvesting was not done with the permission of the patient, Henrietta Lacks, and that her estate is currently suing for compensation from the sale of these cells. This provenance was not known to the author until the completion of this research, and they had no involvement with the experiment conducted in [132], which was completed before the start of this project. However, this demonstrates the importance of researching the

history of such cell cultures before conducting or benefiting from experiments involving them, and the disturbing commonality with which modern science continues to directly benefit from historic unethical practices.

It has also been discussed in this and the previous chapter, and more extensively in this appendix, that these cells underwent a variety of starvation procedures, particularly of glucose, before their glycolysis was measured. It is the opinion of the authors of [132] that this starvation is necessary in order for the cells to produce glycolytic oscillations, and that without it they would not do so. If so, this would hence limit any wider conclusions from the experiment to just the context of cells similarly starved of glucose. However, no equivalent data without starvation conditions has been available for analysis to verify this claim. It is one of the hypotheses of this thesis that such oscillations are easy to misidentify without application of the specialist methods discussed in Chapter 4, which are not currently common in biological physics, as has been discussed more extensively in the beginning of Chapter 2. Further investigation of the question of glycolytic oscillations in healthy cells under 'typical' conditions is therefore needed in order to expand the conclusions of the frequency and existence of glycolytic oscillations beyond the glycolysis of pathological cells in starvation conditions.

In the modelling approach to the HeLa cell data in this chapter this starvation procedure was accounted for by initialising the simulation with a relatively low glucose coupling strength, and then increasing it for the first 355.9 s of the total 800 s simulation. This promotes the transition from a disordered to ordered system that mirrors the initial spike of glycolysis seen in the experimental data once glucose is added. The coupling strengths between the glycolytic and OXPHOS networks are conversely initiated at a relatively high value, and decrease over the first 382.9 s of the simulation along the same, but inverted, gradient as the increase in the glucose coupling. This is intended to represent a breakdown of the relationship between glycolysis and OXPHOS resulting from damage caused by the starvation procedure, and cancerous cells' unhealthy favouring of glycolysis. This has the effect, along with the increase in glucose coupling, of facilitating a transition from an ordered to disordered system, which produces a downward trend of the order parameter, as is seen in the experimental data. The parameters of quadratic gradient of these three coupling strengths were determined through estimating the gradient of

the experimental data, and adjusted through trial and error. All other parameters in the simulation remain fixed, and are derived with reference to [138].

The simulation in Chapter 2 is of an earlier stage of the modelling process. Similarly, the glucose is increased over the course of the simulation, but the values are selected for visual similarity rather than estimated from the experimental data. The glycolysis and OXPHOS network coupling strengths are also initialised at a relatively high value, but unlike in the Chapter 3 simulation, kept constant throughout the simulation. The reduction in their value was not required to generate a downward trend because of the much sharper gradient of the glucose coupling strength variation in this simulation.

This results in simulations that match some, but not all, of the features of the experimental data. The sharp increase and downward trend is reflected, but the gradient of the trend does not precisely match. The existence of oscillations is the same in both, as is their declining amplitude over the course of the simulation/experiment. However, the absolute amplitude and frequencies of these oscillations do not match. The mismatches are largely a result of the difficulty of manipulating the simulation to produce an upward and then downward trend. In the simulation of this chapter in particular, the oscillations and overall simulation behaves much more unstably than the experimental data as a result of the simultaneous transitions of increasing glucose strength and decreasing inter-network strength. A simulation of the same experiment using a similar model in [166] was more successful at replicating the oscillation frequency using a simpler parameter set by considering only the detrended experimental data.

3.7.3 Numerical integration and non-autonomicity

In this chapter we have utilised two different numerical integration methods; a fixed step explicit four step Runge-Kutta algorithm, and a variable step, variable order implicit ode15s algorithm. The latter is intended to be more accurate and computationally efficient for stiff differential equations, such as interacting oscillations we have considered here. However, in the simulations shown in Fig. 3.4, it resulted in many single parameter combinations in which the dynamical regime is different to all those at surrounding parameter combinations, a.k.a. 'islands'. The quantity of these also increases as the complexity of the simulations are increased from autonomous individual oscillators, to

non-autonomous individual oscillators, to non-autonomous networks. When these simulations are re-conducted using the Runge-Kutta algorithm instead, these islands are significantly reduced in number, albeit not entirely eliminated. This hence implies that there is a strong chance that these islands are not a 'real' reflection of the dynamics of the system, but a product of numerical integration inaccuracy of the ode15s algorithm. The most significant difference between this and the Runge-Kutta algorithm is the variable step and order of the former vs the fixed of the latter. As discussed in Section 4.3, this variation is determined by the algorithm's estimation of its error, and can be used to increase the step size/reduce the order, as well as the inverse. Perhaps the most likely explanation for the apparent error in this algorithm is that it is not well suited to multiscale oscillations in particular. Because the non-autonomous modulation we have introduced is at a much slower scale than the dynamics of the modulated oscillations, the ode15s algorithm may be determining that the dynamics of one of these scales is at a certain time allowing an increase of step size/decrease of order, without identifying that doing so will introduce unacceptable error in the regime of the other scale. However, much more testing and comparison would be required before any such conclusion could be asserted.

3.7.4   Synchronisation and oscillations in cellular metabolism

As is discussed at the beginning of Chapter 2, this and the previous chapter approach cell energy metabolism from the perspective that its constituent processes are oscillatory. In this framework, glycolysis and OXPHOS must co-operate effectively to be able to produce sufficient ATP for the healthy functioning of the cell over a sustained period. This is because of their interlinked nature; OXPHOS requires pyruvate and NADH to be produced by glycolysis, and glycolysis requires ATP to be produced by OXPHOS. Therefore, if the processes are not cooperating synchronously, they are not reliably able to meet the demands of the cell. Hence, in this chapter we refer to this synchronised state as being a healthy one, and disruptions of it as being indicative of pathological states.

3.7.5 Corrections

The units of the angular frequencies in Tables 3.2 and 3.4 are listed as Hz, but should be rad/s.

4. Distinguishing between deterministic oscillations and noise

Thus far we have been primarily concerned with deterministic dynamics. In the previous two chapters, we have developed a model for the energy metabolism of cells entirely based in determinism, compared it to similarly deterministic models, and analysed experimental cellular data to find their deterministic components. However, determinism forms only a part of how the dynamics of the physical world, and living systems in particular, are understood. In this chapter, we will consider another significant part of this picture, random noise, and how it connects to the deterministic framework we have previously outlined and developed further.

The application of probabilistic rules to understand dynamical behaviour is extremely widespread. In this framework, the evolution of the system cannot be uniquely and precisely predicted at each time, as this evolution, or the evolution of sum subsystem, attains each of its possible values only with some probability. This is applied in the main when the physical system is believed to have many degrees of freedom that cannot each be examined and recombined to reveal the macroscopic picture. Instead, it is thought that the change in the macroscopic variables of the system may be able to be predicted with a sufficient quantity of sufficiently high quality data.

This approach is particularly common when modelling living systems, and other physical systems that cannot be effectively isolated from their environment. This is in large part because the influence of this environment is assumed to lead to the addition of such complexity, of such difficulty to measure, that it could not be understood deterministically. In this case, it can be common to attempt to remove this influence so as to isolate

the 'true' dynamics of the system, for example by filtering the time-series. This is not the only case in which a probabilistic framework is applied, however. Living systems are also highly likely to exhibit the complex dynamics, and the impossibility of isolating their microscopic components, that motivate such a description. In other words, thermodynamic openness often leads to an assumption of the existence of useless noise in the system that should be removed, and the complex far from equilibrium behaviour it leads to is often consigned to a probabilistic description.

We have already developed in the previous chapters a simple deterministic non-autonomous model that can generate complex dynamics, and demonstrated that these dynamics can be comparable to those of a real physical system. In this chapter we will more directly contrast similar models, and the fundamental framework from which they are derived, to the traditional statistical framework. We will develop this comparison in order to further explore the advantages and disadvantages of a variety of approaches to understanding far from equilibrium behaviour in thermodynamically open systems.

Joe Rowland Adams, Julian Newman and Aneta Stefanovska, European Physical Journal Special Topics (in submission)

Julian Newman author contribution statement — "I provided the necessary mathematical background for formulating and contrasting the two frameworks described in Section II. Accordingly, in terms of the actual writing, I wrote almost all of Section II (as well as much of Sections I and V); and I produced the model equations in Section IV. I proposed some minor changes to some of the numerical experiments in Section III, and contributed some aspects of the discussion of results in Sections III and IV. I engaged in proof-editing of the whole manuscript, particularly to ensure consistency of nomenclature and clarity of the unifying message across the manuscript."

Joe Rowland Adams author contribution statement — "I wrote the majority of the abstract and Sections I, III, IV and V, provided some edits and the initial draft of the analogy represented in Fig. 4.1 to Section II, conducted all numerical simulations and analyses and produced all figures, and was involved in proof-editing the whole manuscript."

Abstract

Time-dependent dynamics is ubiquitous in the natural world and beyond. Effectively analysing its presence in data is essential to our ability to understand the systems from which it is recorded. However, the traditional framework for dynamics analysis in terms of asymptotic dynamics does not consider the time dimension explicitly. We contrast commonly used analysis techniques based on this traditional framework—such as the autocorrelation function, power-spectral density and multiscale sample entropy—with an alternative framework in terms of finite-time dynamics of networks of time-dependent cyclic processes. In time-independent systems, the net effect of a large number of individually intractable contributions may be considered as noise; we show that time-dependent systems with only a small number of contributions may appear noise-like when analysed within the traditional framework using power-spectral density estimation. However, methods characteristic of the time-dependent finite-time-dynamics framework, such as the wavelet transform and wavelet bispectrum, are able to identify the determinism and provide crucial information about the analysed system. Finally, we compare these two frameworks for three sets of experimental data. We demonstrate that while traditional techniques are unable to

reliably detect and understand underlying time-dependent dynamics, the alternative framework identifies deterministic oscillations and interactions.

4.1 Introduction

A fundamental problem in the analysis of experimental time-series data is the identification and filtering of "noise", which is considered to obscure the real underlying dominant mechanisms responsible for the functioning of the particular system from which the time-series was recorded [167–169]. This is therefore relevant to a huge range of scientific fields and physical problems, including, to name a few: engineering [29], quantum and particle physics [170, 171], geophysics [37], biology and medicine [34, 42, 45, 172], power grids [173], and economics [174]. Although it is well-known that there are some dynamical phenomena in which the randomness of "noise" actually itself plays an integral part in the functioning of the system [44, 175, 176], generally speaking one seeks to separate deterministic functioning from the fog of background processes that simply impede the visibility of the deterministic functioning ("observational noise"), or even the actual efficiency of the deterministic functioning ("dynamical noise"). Indeed, in general, it is precisely this connotation of being "present but not positively functional" that is generally conjured in the usage of the word "noise" [30–33, 35, 36, 38–41, 43].

Despite the wide relevance and significant impact of this problem, there is neither a unified mathematical characterisation nor consensus physical explanation for the existence of noise. In this paper, we propose an alternative physical mechanism through which so-called "1/f noise" can be generated and a corresponding mathematical framework through which it can be understood.

Noise in its most common definition is a phenomenon whose constituent frequencies each contribute significant power, with no single frequency contributing far more than every other, and with contributions from a broad range of frequencies. We now outline the origin and development of this definition.

- In the 1920s, Johnson and Schottky observe broad-frequency current fluctuations in a vacuum tube. Many explanations for this were proposed, including atomic impurities [177, 178]

- In 1905 and 1906, Einstein and Smolochowski characterise Brownian motion, a paradigmatic example of noise, as due to the impact of intractably many water molecules on pollen grains [46, 179]. This is emblematic of one of the dominant understandings of the physics of noise as a very high-dimensional process

- In the 1960s, Mandelbrot suggested that '1/f' noise and multifractals are related to the same physical phenomena, characterised by an extension of correlations globally throughout the system ('wildness') and by obeying some law or symmetry that holds across scales ('self-affinity') [180]. It was more recently shown that '1/f' noise and fractals can be unified in a self-similar hierarchy [181].

- In 1987, the field of dynamics is applied to try and explain the origin of noise [182]. In this framework, noise is thought to arise in high-spatial-dimensional dissipative systems with self-organised critical states. Such systems form minimally stable states on a range of length scales. It was argued that small perturbations to the system propagate exclusively within these differently scaled states, produced a response on a range of temporal scales, i.e. noise

In all of these physical explanations for noise, the systems are considered to be in general closed to exchanges of matter, and to hence exhibit time-independent dynamics. To generate such broad frequency spectrum dynamics therefore, they therefore rely on the superposition of many time-independent components, i.e. *high-dimensionality*.

As a result of its inscrutability under traditional analysis techniques, noise is commonly associated with a random evolution, where there is little correlation between its subsequent values in time. Hence, rather than constructing a high-dimensional time-independent deterministic model, noise is often represented by (stationary) stochastic processes.

Our alternative explanation is instead based on the observation that the vast majority of real physical systems are *open* to matter and energy exchanges, and as a result exhibit *time-dependent* dynamics. We will demonstrate that models based in this principle generate a noise-like spread of frequency power contribution while being both *low-dimensional* and consisting of an entirely deterministic, highly correlative, evolution rule.

This method for generating 'noise' is both computationally less demanding to generate and more easily analysed than the high-dimensional alternatives, and its deterministic

rules provide much more useful information about a system than assuming it to be a stochastic process. Hence, in systems where this mechanism is possible, which we will outline further in Section 4.2.5, accounting for it may lead to much more informative data analysis and modelling approaches.

Due to the time-dependence of this mechanism, traditional and widely used analysis techniques that are based in the assumption of time-independence, such as the power-spectral density, can produce misleading results in this context. This will be demonstrated in Sections 4.3 and 4.4. We will hence outline the theoretical (in Section 4.2) and practical (in Sections 4.3 and 4.4) need for an alternative analysis framework based in time-dependence, in addition to demonstrating its aforementioned advantages.

4.2 Two frameworks for describing physical systems and their output time-series

As we will outline further, the traditional framework of theoretical dynamical systems analysis is in terms of *autonomous* or *time-independent* dynamical systems, and the resulting natural framework for experimental time-series analysis is that of *stationary stochastic processes*, i.e. random processes whose probability distributions do not change in time. The natural consequence of this is that methods such as computation of *estimated power-spectral density* are used to distinguish "deterministic oscillatory behaviour within the signal" (identified as isolated high peaks) from "noise within the signal" (often identified by inverse power laws).

Although time-series analysis methodologies ultimately rooted in the mathematical theory of stationary stochastic processes remain the predominant framework for analysing experimental time-series, there are several contexts in which assumptions of time-independence are considered unrealistic or insufficiently accurate. In such cases, a typical approach is to regard the time-series as a *nonstationary* process for which one can seek to estimate time-dependent parameters describing the approximately "time-locally stationary" probability distribution of the process [183, 184].

However, in this paper, by going back to the link between physical concepts and their mathematical implications for modelling in terms of dynamical systems, we arrive at an alternative framework for the mathematical description of systems subject to time-dependent external influences. Our main points in the paper are as follows.

1. For analysing time-series recorded from systems open to influence from their environment, our framework is physically motivated in a way that both the classical "stationary" framework and its "nonstationary" generalisations are not.

2. Both the traditional framework and our framework include a distinction between deterministic oscillatory processes and "noise"; but—as seen through numerically generated data—our framework's model for how deterministic oscillatory processes manifest in experimentally measurable time-series gives rise to results that in many cases would likely be characterised by typical traditional spectral analysis as noise. Specifically, low-dimensional deterministic non-chaotic phase-oscillator networks can easily give "noise-like" signals, if such a network is not constrained to being an autonomous dynamical system but is instead allowed to have time-dependent parameters.

3. While the mathematics of the traditional framework naturally leads to time-series analysis methods such as estimation of classical power spectra, the mathematics of our framework naturally leads to time-series analysis methods based on *deterministic time-frequency representation*. In particular, in trying to decipher the content of a signal that looks complex in the time-domain, classical power-spectral density estimation gives a time-independent representation of the entire signal in the frequency domain, thus "blurring all of time together", whereas time-frequency analysis enables a decomposition of the signal over a two-dimensional *time-frequency space*. From the same numerically generated data as in point (2), now analysed with the continuous wavelet transform, we see that indeed this "two-dimensional resolvability" reveals the determinism which appeared "noise-like" under typical traditional "one-dimensional" spectral analysis.

4. It logically follows from point (3) that if our framework is physically appropriate, then such deterministic time-frequency analysis methods will in practice avoid the

mischaracterisation of physical oscillatory processes as noise described in point (2); we evidence the reality of this conclusion using experimental data.

5. More generally, the full "toolbox" of stationarity-based statistical time-series analysis techniques that scientists apply in order to gain various kinds of insight about the system (e.g. entropy for measuring "complexity", and autocorrelation for measuring statistical memory) does not provide any further help towards elucidating a most basic understanding of those systems where the time-dependent characteristics are seen to cause classical time-independent spectral density estimation to be deficient. In other words, explicitly time-resolved time-series analysis techniques really are necessary to gain an understanding of the system from which the signal is recorded, if the system is open to significant, freely time-variable external influence.

Throughout various disciplines in the natural and social sciences, when one records a time-series $(X(t) : t \in [0, T])$, it is common to investigate the presence of deterministic oscillations and/or noise through computation of the squared magnitude of the Fourier transform,

$$E_X(f) = \left| \int e^{2\pi i f t} \tilde{X}(t) \, dt \right|^2 \tag{4.1}$$

where $\tilde{X}$ is obtained from the original X through some combination of detrending and padding. Then:

- Peaks that stand out at a set of isolated frequencies are regarded as representing deterministic oscillatory processes either at those frequencies or at fundamental frequencies of which those frequencies appear as harmonics due to non-linearities.

- In a log-log plot of $E_X(f)$ against f, roughly linear trends across a large range of frequencies are taken as representing noise of a "colour" determined by the gradient of the trend.

We will now review the mathematical framework that underlies this approach; then, we will review the physical assumptions behind this framework, consider the implications of when those physical assumptions are not met, and accordingly develop an alternative mathematical framework.

4.2.1 The classical framework: autonomous dynamics and stationary processes

The simplest kind of quantitative model of a deterministic continuous-time system is an *autonomous differential equation*,

$$\dot{x}(t) = F(x(t)), \tag{4.2}$$

where F is a deterministic vector field with no dependence on t. A time-series $X(t)$ recorded from such a system can then be expected to take the form

$$X(t) = H(x(t)), \tag{4.3}$$

where H is some observable function and $x(t)$ is a solution of Eq. (4.2). Now if we define the time "$t = 0$" to be the start of the recording, then this time is typically random relative to the actual functioning of the physical system itself. Accordingly, if the solution $x(t)$ being observed is modelled as having its long-time-asymptotic statistics as being given by some ergodic invariant probability measure μ of the system (4.2)—i.e. μ represents the probability distribution of where $x(t)$ will be at a very large random time t [1]—then one may regard the initial condition $x(0)$ as itself a random variable of distribution μ, in which case the recorded time-series $X(t)$ then becomes *a sample realisation of an ergodic stationary stochastic process*. The "stationarity" here means that the probabilistic law of the process is invariant under time-translations, while the "ergodicity" means that parameters of the probabilistic law of the process can be estimated just from the statistics of an individual sample realisation provided that the duration of the recorded segment of the sample is sufficiently long. In the case that $x(t)$ is simply a stable periodic orbit, representing a *fixed-frequency deterministic oscillatory process*, the invariant measure μ is just the temporally uniform distribution along the orbit.

Now one may assume that there is *noise* in either the behaviour of the system itself ("dynamical noise") or the time-series measuring equipment ("observational noise") or indeed both, so that the time-series $X(t)$ takes a form such as (in the case of "additive

---

[1] This can be expressed rigorously as saying that for every bounded continuous observable function h, $\frac{1}{t} \int_0^t h(x(s))\, ds \to \mathbb{E}_\mu[h]$ as $t \to \infty$; this property is invariant under translation of the time-axis, i.e. under recalibration of "$t = 0$".

noise")

$$X(t) = H(x(t)) + \xi_{\text{obs}}, \tag{4.4}$$

$$\dot{x}(t) = F(x(t)) + \xi_{\text{dyn}}. \tag{4.5}$$

The deterministic component F in (4.5) still represents the *functional* component in the progress of the system, while both ξ_{obs} and ξ_{dyn} are the pseudorandom net result of background processes that affect the system or its recording. The observational noise can, once identified, simply be filtered out of the signal through linear filtering; by contrast, the dynamical noise is inseparable from the actual progression of the state of the system, leading to the branch of science and mathematics known as *stochastic filtering* [185]. Nevertheless, if the vector field F simply represents an oscillatory process (i.e. has a stable limit cycle) and the noise is not too strong, one can expect a basic linear frequency decomposition of $X(t)$ to yield a clear distinction between background noise (whether observational or dynamical or both) and a relatively narrow peak representing the approximate natural frequency of the oscillatory process.

Now if one assumes that there is noise, then one can usually expect little further harm to be done by assuming, as a reasonable approximation, that this noise is a *stationary noise* process (again, meaning that its law is invariant under time-translations). Hence, if the time-series $X(t)$ is assumed to arise from a model such as (4.4)–(4.5), then it will often be natural to treat this time-series as a finite-time segment of a sample realisation of an ergodic stationary stochastic process.

Accordingly, the traditional framework of time-series analysis—upon which a vast range of time-series analysis methods is based—is indeed to

- regard the time-series as a finite-time segment of a sample realisation of an ergodic stationary stochastic process,

- and view the aim of time-series analysis as being to estimate parameters of the probabilistic law of this underlying stochastic process.

(Such parameters can be single numbers, such as mean and standard deviation, but can also include functions of one or more variables, such as power-spectral density, which is a function of frequency.)

4.2.2 Noise in the classical framework

The theory of stationary stochastic processes gives rise to the defining of various kinds of stationary noise—in particular, of various "colours" as defined by their *power-spectral density* (PSD). Roughly speaking, the PSD of a stationary stochastic process $(X(t) : t \in \mathbb{R})$ is the function $\mathcal{P}_X$ defined on the frequency axis by

$$\mathcal{P}_X = \lim_{T \to \infty} \mathcal{P}_X^{(T)} \tag{4.6}$$

$$\mathcal{P}_X^{(T)}(f) = \mathbb{E}\left[\frac{1}{T}\left|\int_0^T e^{2\pi i f t} X(t)\, dt\right|^2\right]. \tag{4.7}$$

The process X is considered "white noise" if $\mathcal{P}_X$ is constant, while it is considered "pink noise" if $\mathcal{P}_X(f) \propto 1/f^\beta$ for some $\beta \in (0,2)$, and "blue noise" for some $\beta \in (-2,0)$. Such "$1/f$" behaviour has been observed in diverse processes [186–191], especially biological and electronic, and questions regarding the origin of this behaviour have been much-researched [182]. Assuming sufficient ergodicity properties, one can estimate the PSD from a single time-series recording, provided the recording is of sufficiently long duration. In practice, a typical procedure is to compute the quantity inside the expectation in the definition of $\mathcal{P}_X^{(T)}$—namely

$$\frac{1}{T}\left|\int_0^T e^{2\pi i f t} X(t)\, dt\right|^2, \tag{4.8}$$

where $(X(t) : t \in [0,T])$ is the actual time-series recording, with T the total duration of the recording (or one can first detrend and add some padding for the sake of more effective Fast Fourier Transform computation). In other words, up to a constant time-normalisation, the function E_X as defined in Eq. (4.1) is taken as the PSD estimate; noise in the signal is then investigated by looking for a roughly linear trend in the graph of E_X plotted on a log-log plot, with the β-value for the $1/f^\beta$ law of the noise being estimated by the negated gradient of a best-fit straight line.

An expert statistician may prefer somewhat more advanced PSD estimators than simply taking the time-normalised deterministic energy-spectral density E_X of the entire signal recording $(X(t) : t \in [0,T])$. Nonetheless, this simple approach is already perfectly reasonable as a PSD estimator: second-order spectra and second-order correlations are Fourier-transform pairs (up to normalisation), and ergodicity implies that the sample autocorrelation function for the recorded time-series is a good approximation of the

underlying "population" autocorrelation function for the stochastic process from which the recording is sampled.

There also exist other methods for experimental analysis of noise besides PSD estimation, such as autocorrelation functions (the Fourier counterpart to PSD) and detrended fluctuation analysis [192]. But in this paper, we apply PSD estimation for the analysis of 'noise', as it is generally the most standard and widely applied method for this purpose.

4.2.3 Emergence of noise

Having discussed how, in the classical framework, the noise terms in Eqs. (4.4) and (4.5) may be considered analytically and numerically, let us now briefly discuss classical mechanisms for how such noise terms arise *physically*.

Two of the main classical mechanisms of emergence of noise from ultimately deterministic fundamental laws of physics are:

- as the net effect of many individually intractable small influences (e.g. Brownian motion of pollen particles [46, 179]);

- as an ergodic chaotic process (e.g. turbulent "subgrid" processes in climate models [193, 194]).

Both mechanisms represent behaviour that, on the one hand, is too "complicated" to be able to form a deterministic model from time-series data, and yet on the other hand can be approximated with high quantitative accuracy at the level of statistics and probability theory. As we have already indicated, one usually does not expect such pseudorandom behaviour to play an important role in the functioning of the system, but rather to obscure the real mechanisms behind the functioning of the system.

4.2.4 Non-isolated systems and our finite-time framework

The mathematical modelling assumption that a system can be described by an autonomous differential equation represents a physical assumption that the system can be treated either as (a) entirely isolated from the rest of the universe, or at least as (b) unable to have any interaction with its environment besides dissipation of energy

into its environment (according to a time-independent dissipation law). In other words, generically speaking, an autonomous differential equation can only describe an *unforced* physical system. If one wishes to incorporate time-dependent external forcing into a dynamical model, then this model cannot be an autonomous differential equation (at least, not without extending the phase space of the differential equation, but we will come back to this point shortly).

As above, a "classical" way to incorporate such external forcing is to model it as dynamical noise with a stationary probability distribution, and another approach is to model it as periodic or quasiperiodic. However, one cannot typically expect that a system open to influence from an ever-changing environment will exhibit characteristics that are time-independent or that follow some indefinite-time pattern such as quasiperiodicity. One approach towards overcoming this issue when analysing time-series is to generalise concepts from the theory of stationary stochastic processes and estimation of their time-independent statistical parameters to the broader theory of *nonstationary* stochastic processes and estimation of their time-dependent statistical parameters. However, a difficulty with this approach is that, to be logically sound, unless one either assumes *a priori* a very specific form of time-dependence (again, unlikely to be appropriate for systems freely open to influence from their environment) or assumes that the variance is so low as to make the process approximately deterministic, one must assume that there is a time scale on which the stochastic process is approximately an ergodic stationary process, with this time scale being sufficiently slow that the approximate ergodicity is manifested in individual sample realisations (i.e. the statistics of a typical sample realisation in a time-window whose duration is of this time scale approximates the time-localised "population" statistics) and the nonstationarity itself must then take place on an even slower time scale. In short, the framework of parameter-estimation for generic nonstationary processes really assumes that the process represents an adiabatically slow parameter-drift through a parameter-dependent ergodic stationary stochastic process. An illustrative example of how this framework may be applied is in the use of methods such as *moving-window autocorrelation* for early warning of a bifurcation-induced critical transition, when a parameter of an autonomous dynamical system subject to stationary noise is being slowly forced (e.g. anthropogenic forcing of climate tipping elements, when the unforced tipping element is modelled as an autonomous system subject to stationary

noise) [195]. Once again, this kind of approach does not deal with the kind of temporal variation of external forcing that is typically bound to be present in systems that are freely open to general influences from the surrounding world.

In addressing the problem of how to analyse non-isolated systems and time-series recorded from them, rather than seeking to solve the problem at the level of mathematical adaptation of the classical framework (e.g. nonstationary stochastic processes), here we instead seek to solve the problem by "re-deriving from scratch" how physical concepts that seem reasonable for thermodynamically non-isolated processes should translate into a mathematical dynamical systems framework. We first build our framework at the "physical concepts" level, as follows.

P1. Physical systems in the real world subject to ongoing external forcing will generally exhibit *bounded, non-static behaviour*.

P2. Very often, in a bounded non-static system, an important role will be played by *cyclic* or *oscillatory* processes within the system; by this we mean, processes whose functioning is of such a nature that it is reasonable to describe the "instantaneous state" of the process simply in terms of "*what point along the cycle the process is at*".

P3. However, in contrast to the classical model of cyclic processes as a stable periodic orbit of an autonomous dynamical system, these processes do not necessarily possess any internal strict periodicity, but instead progress through the cycle in a way that is inextricably linked to their ever-changing environment. Perhaps the clearest examples of this kind of oscillatory process are *biological* oscillatory processes, such as the beating of the heart: on the one hand, one can provide a detailed physical description of the cycle, and yet on the other hand there is no fixed rate of progression through the cycle (in the case of the beating of the heart, no constant "resting heart rate" [196]), as all biological processes in an organism need to be able to very freely adapt to the continual changes in their environment, otherwise the organism will quickly die.

P4. In many situations, an important role in the functioning of a system is played by *interactions* between oscillatory processes within the system. Furthermore, these

interactions may themselves be of a time-dependent nature, due to ever-changing external influences.

P5. As in the classical framework, we may consider there also to be noise in the system and/or in the measuring of time-series. (And of course, there may also be deterministic behaviour besides "oscillatory processes", but in this paper we will focus on the same problem as we have been discussing for the classical case, namely the separation of oscillations from noise.)

The fact that the oscillatory processes are "cyclic but not strictly periodic" implies that it is often appropriate to speak of "time-localised frequency" but *only as an approximate-valued quantity*. The conceptual impossibility of having an arbitrarily high-precision quantification of time-localised frequency for the behaviour in an arbitrarily small time-interval around a specified moment in time is an important manifestation of the *Heisenberg uncertainty principle*. (This will play an important role in the analysis of time-series under our framework.) The notion of an analytic "instantaneous frequency" can arise through the Hilbert transform [197]. There are still restrictions in these contexts however, for instance that the real part of the Fourier transform has only positive frequency. But importantly, this concept in application to measured data, despite being analytic, is still an approximation of the time-localised frequency operating in practice, which is still restricted by the Heisenberg uncertainty principle.

Assuming the system's evolution can be modelled by a finite-dimensional differential equation, we can express our above physical description in mathematical language as follows:

$$X(t) = H(\theta_1(t), \ldots, \theta_n(t), t) \tag{4.9}$$

$$[\text{maybe} + \text{noise, maybe} + \text{other components}]$$

$$\dot{\theta}_i(t) = F_i(2\pi f_i(t), \theta_1(t), \ldots, \theta_n(t), t) \tag{4.10}$$

$$[\text{maybe} + \text{noise}], \quad i = 1, \ldots, n,$$

where $\theta_1(t), \ldots, \theta_n(t)$ are angles between 0 and 2π each representing the phase of a cyclic process, and $f_1(t), \ldots, f_n(t)$ are these cyclic processes' "time-localised internal frequency". Note that the angular velocity $\dot{\theta}_i(t)$ is not the same concept as time-localised frequency. (Indeed, this may even be seen in the classical framework of autonomous

dynamics. In an autonomous coupled pair of oscillators, each oscillator may progress strictly periodically with some time-independent frequency different from the oscillator's time-independent internal frequency, but the effect of the coupling is not only to alter the oscillators' frequencies: it will also change the proportions of how much time each oscillator spends in the different parts of the cycle, resulting in *time-dependent* instantaneous angular velocities even though the frequencies are constant in time.)

Perhaps the simplest example of a concrete model within this abstract framework is to take

$$H(\theta_1, \ldots, \theta_n, t) = \frac{1}{n} \sum_{i=1}^{n} A_i(t) h_i(\theta_i) \tag{4.11}$$

$$F_i(\omega, \theta_1, \ldots, \theta_n, t) = \omega + C_i(\theta_1, \ldots, \theta_n, t), \tag{4.12}$$

where A_i is a potentially time-dependent amplitude measuring how strongly the i-th cyclic process influences the time-series, h_i represents the shape of how the phase of the i-th cyclic process appears in the time series, and C_i is a potentially time-dependent phase coupling function, which we take as 0 if there is no coupling; so the model becomes

$$X(t) = \frac{1}{n} \sum_{i=1}^{n} A_i(t) h_i(\theta_i(t)) \; [\text{maybe} + \text{noise}] \tag{4.13}$$

$$\dot{\theta}_i(t) = 2\pi f_i(t) + C_i(\theta_1(t), \ldots, \theta_n(t), t) \tag{4.14}$$

$$[\text{maybe} + \text{noise}].$$

A standard example of the observable function H is the *mean field*, where $A_i = 1$ and $h_i = \sin$, i.e.

$$H(\theta_1, \ldots, \theta_n, t) = \frac{1}{n} \sum_{i=1}^{n} \sin(\theta_i); \tag{4.15}$$

and a standard example of a phase coupling function is *Kuramoto* coupling,

$$C_i(\theta_1, \ldots, \theta_n, t) = \sum_{j \in \{1, \ldots, n\} \setminus \{i\}} a_{ij}(t) \sin(\theta_j - \theta_i). \tag{4.16}$$

The first important point to make is that in our framework, the cyclic processes $\theta_1, \ldots, \theta_n$ are governed by a *non-autonomous* differential equation. Some clarifications are worth making immediately.

- If the system being modelled is open to freely time-varying influence from its environment, then there is no reason at all to expect the t-dependence in $f_i(t)$

or $F_i(\omega, \theta_1, \ldots, \theta_n, t)$ to follow any indefinite-time pattern such as periodicity or almost-periodicity. Thus, our framework is to be understood as a framework for studying dynamics on explicitly finite time scales, in contrast to the classical theory of autonomous dynamical systems where "qualitative analysis of dynamics" is understood in terms of coordinate-invariant long-time-asymptotic properties. Indeed, in our framework, the differential equations describing the cyclic processes $\theta_1, \ldots, \theta_n$ need not be well-defined on infinite time at all: outside the assumption of a specified form of time-dependence, a non-autonomous dynamical system can perfectly well be defined to exist only on a bounded time-interval [58, 88], just as real physical systems often only exist and operate on bounded time-intervals. Such dynamical systems are called *finite-time dynamical systems*.

- If the time-dependence does strictly follow some indefinite-time pattern such as periodicity or almost-periodicity, then one can extend the phase space to incorporate the forcing (physically corresponding to "taking the system and its external forcing as one larger system"), so as to give an autonomous dynamical system. A common misconception is that even outside such assumptions on the time-dependence, simply adding time itself as a new dimension in the phase space enables non-autonomous dynamical systems to be reduced to the domain of applicability of autonomous dynamical systems theory. But the problem with this is that the theory of autonomous dynamical systems concerns *bounded* invariant objects (e.g. fixed points, periodic orbits, compact attractors and their natural invariant measures, etc.) rather than being concerned with systems whose state grows unboundedly; obviously, if time itself is regarded as part of the state of the system, then this "state" will grow unboundedly [8, Remark 2.5].

- We have explained that for autonomous dynamical systems, the time-independence naturally gives rise to the applicability of stationary stochastic processes theory for the analysis of a time-series, even in the complete absence of noise. However, for a non-autonomous dynamical system, changing the time of recording will change the actual law of the system relative to the time of recording, and so there would generally be no analogous logic justifying the use of nonstationary stochastic processes theory to describe a time-series taken from a deterministic non-autonomous

dynamical system. When there is also noise present, then stochastic processes theory may be appropriate for studying an isolated noise component; but as we have already said, seeking to apply a framework of time-dependent parameter estimation for nonstationary stochastic processes to the actual time-series recording $X(t)$ would be problematic.

The theory of finite-time dynamical systems has been growing in popularity in recent decades [58, 86, 88, 91, 198–200]. Our framework above is particularly concerned with *oscillatory* dynamics on finite time scales. A model for cell energy metabolism that already serves to exemplify our above general framework has been developed in [201]; our present paper illustrates how this framework can, in fact, serve as a general overarching framework for the study of complex systems in terms of interacting oscillatory components. Let us also mention that a finite-time framework for qualitative analysis of dynamical stability of oscillatory processes subject to slow-time-scale external influences has been developed in [58].

4.2.5 Reconsideration of apparent "noise" via our framework

In Sec. 4.2.3, we mentioned two classical mechanisms for the emergence of noise from determinstic fundamental laws of physics. Considering these mechanisms in the context of autonomous networks of oscillators, expressed in the same way as in our framework above except without the time-dependence in F_i and f_i, a signal $X(t) = H(\theta_1(t), \ldots, \theta_n(t))$ could produce noise-like results if

- n is extremely large (i.e. the system is very high-dimensional), or

- the system of equations

$$\dot{\theta}_i(t) = F_i(2\pi f_i, \theta_1(t), \ldots, \theta_n(t)) \tag{4.17}$$

  is chaotic.

In both cases, even though the original equation is deterministic, one cannot practically obtain a deterministic description from time-series analysis, and so probabilistic modelling is chosen instead.

The central point of this paper is the observation that *without* the need either for very large n [46–48], or for chaotic behaviour [49–52, 202], or for fast time scales, the incorporation of time-dependence into the model (again, *not* necessarily of a fast time scale) can lead to results that a typical PSD approach will characterise as noise; and thus, for analysis of experimental time-series data arising from a system where our framework is appropriate (i.e. fulfilling at least the description in P1–P3), a different methodology is needed to distinguish prominent, functionally important oscillatory components from noise.

Specifically, methodology that tracks time-dependent characteristics of a signal over time is needed in order to understand the behaviour of the system from which the signal is recorded. This is, in fact, not just unique to the problem of avoiding mischaracterisation of functionally important components as noise; it is a general principle relevant to all of time-series analysis. To help illustrate this general point, we will also briefly look at a couple of other time-series analysis techniques based on the traditional framework besides PSD estimation—namely, entropy (for describing the "level of complexity" of a system) and autocorrelation (which concerns the nature of "statistical memory" in a process)—to see that they do not actually help to provide any real insight into the nature of a system when the more fundamental question of time-dependent versus time-independent characteristics is ignored.

This observation is similar to one already made in [203], that of "harmonic noise". Where we consider a deterministic oscillator with deterministic frequency modulation, there a deterministic oscillator is modulated in frequency and amplitude by a Wiener process. This results in the similar conclusion that a noise-like profile is produced, despite deterministic elements. Albeit in that case, the use of a Wiener process means some degree of stochastic behaviour may be expected, while we see noise-like dynamics from pure determinism. Nevertheless, this further demonstrates that this phenomenon is potentially pervasive.

We now illustrate in Fig. 4.1 the difference between the classical mechanism of noise-emergence in terms of a net effect of individually intractible influences and our mechanism
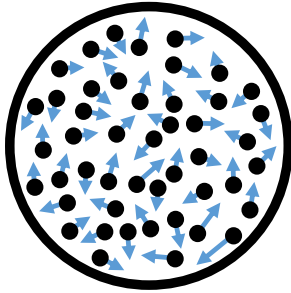
Classical framework **Our framework**
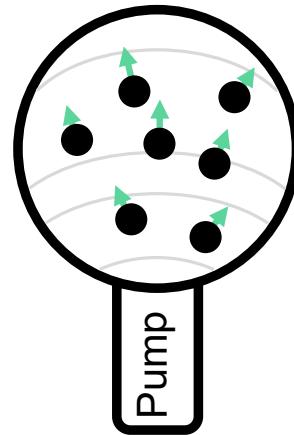
Figure 4.1: A physical analogy for the difference between two mechanisms for the generation of signal components that may be identified as noise by a typical PSD analysis as described in Sec. 4.2.2. On the left, representing a classical mechanism of noise emergence as in Sec. 4.2.3, we have the classical Brownian motion experiment of pollen grains on undisturbed water, performing highly complex motion due to the large number of small mesoscopic-scale interactions with water molecules. On the right, metaphorically representing the framework described in Sec. 4.2.4, we have a less complex motion arising from water currents induced by an external pump whose strength has the freedom to modulate according to external factors. In the latter case, an entirely macroscopic-level deterministic description of the origin of the motion in terms of the time-dependent behaviour of the pump would be obtainable by suitable time-resolved time-series analysis of the motion.

for apparent "noise", by making an analogy to Brownian motion. Einstein and Smoluchowski originated the view of Brownian motion as caused by intractably many small contributions [46, 179], which became the characteristic view of how "noise" components in a dynamical model under the classical framework arise physically. On the left of Fig. 4.1, we depict the classical Brownian motion experiment: we have a very high-dimensional system of interacting water molecules and pollen particles (not necessarily subject to any perturbations coming from outside this system), such that the velocity vector of an individual pollen grain, as a function of time, may be approximated probabilistically as a two-dimensional stationary Gaussian white noise process. On the right of Fig. 4.1, the main driver of the motion of an object on the water is not complex interactions with water molecules whose determinism is only resolvable at the microscopic level, but rather is macroscopic water currents induced by an external pump applying a force that is not constant but free to vary over time according to relevant external factors. If the water currents are sufficiently simple, then merely observing the motion of the object may clearly show the determinism; but if the water currents are not quite so simple (but still much simpler than the mesoscopic-scale interactions with water molecules in the classical Brownian motion experiment), one may wish to record the motion and apply more advanced analysis methods to separate out macroscopically resolvable deterministic components from pseudorandom contributions to the motion. However, if the methods applied ignore the reality that the system has time-dependent characteristics due to the temporally varying pump, the conclusions will not be reliable: in particular, the dominant time-dependent determinism may be mischaracterised as pseudorandomness. The point of the analogy is that where the classical framework regards the determinism underlying the origin of an apparently noise-like process (as identified by stationarity-based tools such as classical PSD analysis) to be too complex for deterministic description and hence best treated probabilistically as a stationary stochastic process, our framework instead considers the possibility of entirely tractable deterministic dynamics involving time-variability that arises from the system's not being isolated from its environment.

Such time-dependent oscillatory behaviour resulting from external forcing is, as we have said, characteristic of thermodynamically open systems, which are found throughout nature. Cells regularly exchange molecules with their surroundings through active ion channels [204], colloidal particles can be driven to new collective behaviours by external

128

fields [205], and Josephson-junction arrays show complex properties when driven by a magnetic field [206], to name just a few examples of driven physical systems.

We have said that for analysis of experimental time-series data arising from a system where our framework is appropriate, a different methodology from the typical PSD approach is needed to distinguish prominent oscillatory components from noise. We now explain how *time-frequency analysis* naturally arises as such a methodology.

4.2.6 Deterministic time-frequency analysis

Just as there is a plethora of well-known time-series analysis methods based on the traditional framework of stationarity, so there also exist many—currently not-quite-as-widely used (due to the ongoing prominence of the traditional framework in the sciences)—time-series analysis tools designed for gaining an understanding of time-dependent oscillatory dynamics; see [207] for an overview of several such methods. At the heart of many of these methods lies *deterministic time-frequency analysis*, which we now go on to describe.

We have explained how the classical framework naturally leads to the use of PSD estimation as the means of separating oscillatory processes from noise; for our model in its above-mentioned "simplest form", namely Eqs. (4.13)–(4.14), the analogous natural tool to use is deterministic linear time-frequency analysis. In our phrase "deterministic linear time-frequency analysis":

- "Time-frequency analysis" refers to time-evolving time-localised description of the frequency content of the signal. There are many different time-frequency analysers, such as the windowed Fourier transform and the continuous wavelet transform [208].

- By "deterministic", we mean a time-frequency analyser that can be applied to an individual signal, as opposed to a time-frequency analyser defined theoretically in terms of the probabilistic law of a stochastic process from which the recorded signal is assumed to arise as a sample realisation.

- By "linear", we mean that for signals $X_1, \ldots, X_n$ linearly superposed to form a new signal $Y = c_1 X_1 + \ldots + c_n X_n$, we have

$$\mathrm{Ampl}_Y(f, t) e^{i.\mathrm{Phase}_Y(f,t)} = \sum_{i=1}^{n} c_i \mathrm{Ampl}_{X_i}(f, t) e^{i.\mathrm{Phase}_{X_i}(f,t)}, \qquad (4.18)$$

where $\mathrm{Ampl}_X(f, t)$ and $\mathrm{Phase}_X(f, t)$ denote respectively the amplitude and the phase assigned by the time-frequency analyser to the frequency f around time t for a signal X.

The key difference between classical time-independent frequency-domain representations of a signal (such as the Fourier transform and PSD estimators derived therefrom) and representations given by time-frequency analysis is that

- the former representations do not resolve in time but, in a sense, blur all time together;

- the latter representations enable a "two-dimensional resolving of the frequency content" in which the frequency-decomposition is itself resolved in the time dimension.

It is precisely this distinction that plays the key role in the phenomenon that we will present in this paper, where the apparent time-domain complexity of a signal is concluded to be deterministically intractable noise by a frequency-domain representation, but is resolved into clear deterministic components by a time-frequency-domain representation.

Let us expound more precisely the link between our framework in the form of Eqs. (4.13)–(4.14) and deterministic linear time-frequency analysis. The linearity implies that, firstly in the absence of coupling (i.e. $C_i = 0$) and with h_i being sinusoidal, the individual oscillations

$$A_i(t) \sin\left(\theta_i(0) + 2\pi \int_0^t f_i(s)\,ds\right) \qquad (4.19)$$

will appear as single modes of time-dependent frequency. Then,

- if h_i is non-sinusoidal, the i-th oscillator will contribute a "non-linear" oscillatory component

$$A_i(t) h\left(\theta_i(0) + 2\pi \int_0^t f_i(s)\,ds\right) \qquad (4.20)$$

to the time-series, appearing in the linear time-frequency analysis as a fundamental mode plus harmonics that are multiples of the fundamental mode;

- if there is coupling, then as we have described, the presence of this coupling not only affects the frequency with which the individual oscillators complete their cycles, but also distorts the relative rates at which different parts of the cycle are progressed through—this makes the oscillations "non-linear", again resulting in the presence of harmonics in the linear time-frequency analysis.

Consequently, the presence of coupling can be investigated through *higher-order spectral analysis* such as bispectral analysis (which will also detect individual non-linear oscillatory components even without coupling). But once again, under our framework one should not use the classical definitions defined for stationary stochastic processes (nor even generalised versions for time-locally stationary stochastic processes), but should use higher-order spectra derived from deterministic time-frequency analysis [63,209]. In order to infer more about the causality and origins of couplings identified by bispectral analysis, additional analysis techniques such as dynamical Bayesian inference (see e.g. [210] and the references therein) can also be used.

The previously-mentioned *Heisenberg uncertainty principle* plays an important role in time-frequency analysis: in the time-frequency analyser one must decide upon a suitable trade-off between precision of the frequency axis and precision of the time axis; an arbitrarily high-precision description in time-frequency space of the time-localised frequency content of a signal is conceptually impossible.

Let us return to our earlier point that in generic deterministic non-autonomous dynamical systems, there is no basis for describing solutions in terms of nonstationary stochastic processes. Traditional time-series analysis is essentially centred around the concept of *estimation of parameters from sample data*, either time-independent if the time-series is assumed to come from a stationary process or time-dependent if the time-series is assumed to come from a nonstationary process. However, time-series analysis methodologies suited to our framework such as deterministic time-frequency analysis *do not seek to "estimate" any quantities associated with some "population" of which the time-series is considered a "sample"*. In the mathematics of deterministic time-frequency analysis, *time itself* plays a somewhat mathematically analogous role to "the underlying probability space" in traditional stochastic processes theory. In other words, in deterministic time-frequency analysis, the actual recorded time-series is its own popula-

tion. (Deterministic time-frequency analysers can also be used to define time-dependent parameters of nonstationary stochastic processes, e.g. "wavelet power" defined as the expected squared magnitude of the continuous wavelet transform at a given frequency. But as we have already indicated, in the absence of an assumption on the specific form that the nonstationarity takes or an assumption of extremely low variance, the ability to estimate such time-dependent parameters from a single sample realisation would require such slow variation in the time-localised frequency content that one could simply instead apply classical estimation of time-independent parameters to large-duration segments of the signal.)

4.3   Numerical comparisons of the two frameworks

In this section, we

- illustrate numerically how signals arising from not-very-high-dimensional oscillator networks according to our framework can be identified as $1/f^\beta$ noise when analysed by the typical procedure of computing its PSD and looking for a roughly linear downward trend in a log-log plot;

- show that applying the continuous wavelet transform resolves the true "determinism"—i.e., that the signal has a relatively small number of individually tractable components, as opposed to a large number of individually intractable components for which only statistical rather than deterministic analysis is possible;

- illustrate how the continuous wavelet transform, and higher-order spectral analysis based thereon, can reveal further features of the underlying deterministic behaviour, such as the presence of coupling between oscillators.

We consider signals of the form

$$X(t) = \frac{1}{n} \sum_{i=1}^{n} \sin\left(\theta_i(t)\right) \tag{4.21}$$

where the system of oscillators θ_i evolves according to the non-autonomous differential equation

$$\frac{1}{2\pi}\dot{\theta}_i = f_i(t) + \left[\frac{A}{n} \sum_{j=1}^{n} \sin\left(\theta_j - \theta_i\right)\right], \tag{4.22}$$

where $A > 0$ corresponds to the presence of coupling, and $A = 0$ to the absence of coupling. We take the time-dependence of $f_i(t)$ itself to be relatively slow compared to the internal time-periods $\frac{1}{f_i(t)}$ of the oscillations themselves. Note that it is precisely the addition of this new relatively *slow* time scale, without the need of any fast time scale, that will be responsible for causing the signal to become "noise-like" when analysed by typical traditional spectral analysis. As discussed in Section 4.2.4, time-dependence arises physically from the system being subject to influence from its ever-changing environment.

In several of our simulations, for the sake of simplicity we take $f_i(t)$ to be a relatively low-frequency periodic function

$$f_i(t) = f_{0i} + f_{0i} A_{\omega i} \sin \left(2\pi t f_{\omega i} \right) ; \tag{4.23}$$

but (as we will see) the periodicity itself is not at all a requirement for our results.

For the simulations in this section, we numerically integrate Eq. (4.22) with various parameter values of the model, using a 4th order Runge-Kutta algorithm and an integration step of 0.001 s, and with the initial phase values $\theta_1(0), \dots, \theta_n(0)$ of the oscillators evenly distributed in the range $[0, 2\pi]$. The models are simulated up to different times generally corresponding to around the longest time computationally feasible. For the PSD computations, zero padding is then added symmetrically at the start and end of the signal such that the total number of points in the resulting time series is the nearest power of two above the original number of points before the zero padding was added. This zero padding is added to stabilise the computations. The gradient of the PSDs are estimated by fitting to 1 degree polynomial using Matlab's polyfit function. The wavelet transform and wavelet bispectrum computations were carried out in MODA, for which formulae can be found in [211].
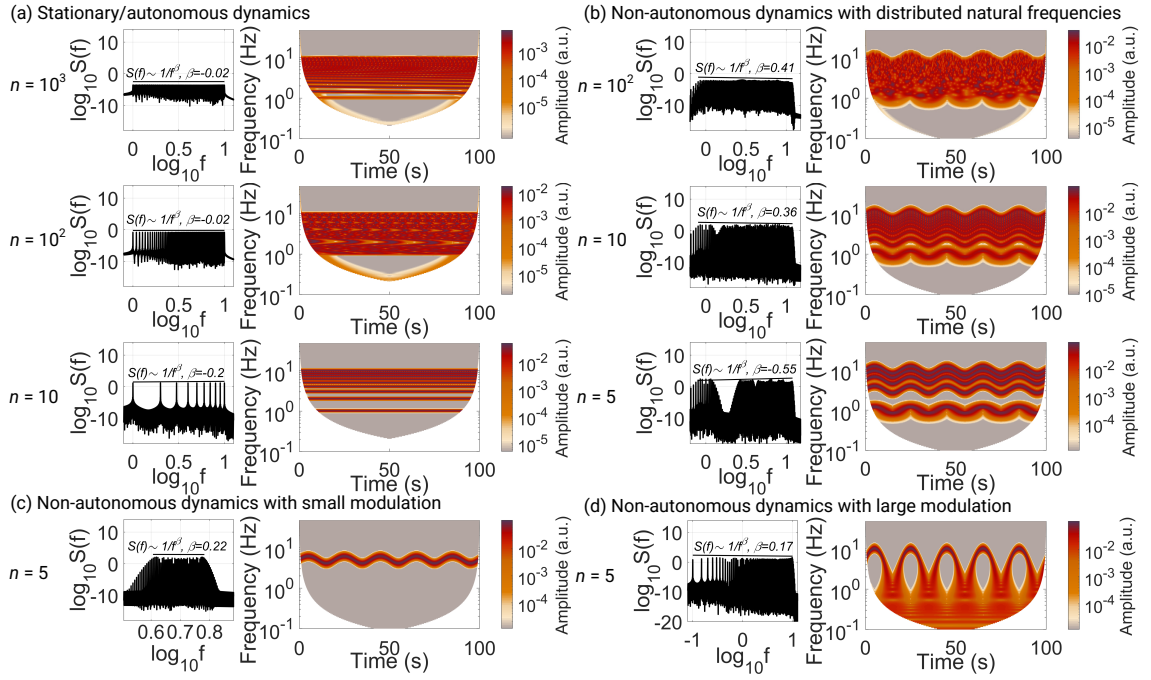
Figure 4.2: Power-spectral densities and wavelet transforms of autonomous and non-autonomous oscillator models. The PSD $S(f)$ and the magnitude $|W(t, f)|$ of the wavelet transform $W(t, f)$ are computed for different time series $X(t)$ as given by Eqs. (4.21)–(4.23) for different parameter values, all without coupling (i.e. $A = 0$). All wavelet transforms are computed using the lognormal wavelet. (a) Ensembles of $n = 10$, 10^2 and 10^3 autonomous oscillators (i.e. $A_{\omega i} = 0$ for all i). The frequencies f_{0i} are linearly distributed in the range $[1, 10]$ Hz. The log-log PSDs of the mean fields of the oscillator ensembles are calculated, with the exponent β of their linear best fit indicated, where $S(f) \sim 1/f^\beta$. The wavelet transforms are calculated with a frequency resolution of 5. The $n = 10$ and $n = 10^2$ ensembles are simulated for 10000 s, and the $n = 10^3$ for 1000 s. (b) The same analyses as in (a) applied to non-autonomous ensembles of varying sizes, with centre frequencies f_{0i} linearly distributed in the range $[1, 10]$ Hz, modulation amplitude factor $A_{\omega i} = 0.2$ and modulation frequency $f_{\omega i} = 0.05$ Hz. The $n = 10^2$ ensemble is simulated for 20000 s, and the $n = 10$ and $n = 5$ for 200000 s. The wavelet transform is calculated with a frequency resolution of 2. (c) $n = 5$ non-autonomous oscillators, with $f_{0i} = 5.05$ Hz for each $i = 1, \ldots, 5$, and otherwise identical parameters to (b). (d) $n = 5$ non-autonomous oscillators with identical parameters to (c), but with larger modulation amplitude $f_{0i} A_{\omega i} = 4.95$ Hz.

134
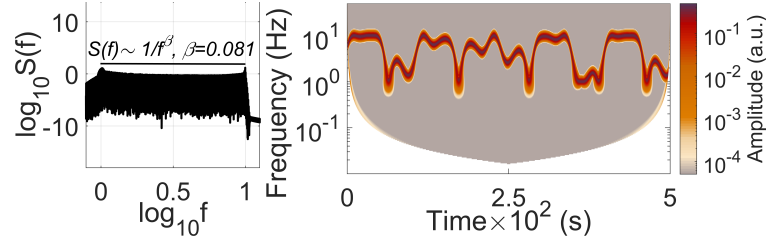
Figure 4.3: The production of noise-like behaviour by aperiodic deterministic oscillations. One non-autonomous oscillator with an aperiodically modulated natural frequency, simulated over a 200000 s period, is analysed in its power-spectral density and wavelet transform. The wavelet transform is constructed using the lognormal wavelet with frequency resolution 2. The analysed signal is $X(t) = \sin(\theta(t))$ where $\theta(t)$ evolves according to the equation $\frac{1}{2\pi}\dot{\theta}(t) = f(t)$ with $f(t) = 5.5$ Hz $+4.51$ Hz $\sin\left(2\pi 10^{-2}t + \sin(0.13t)\right)$.
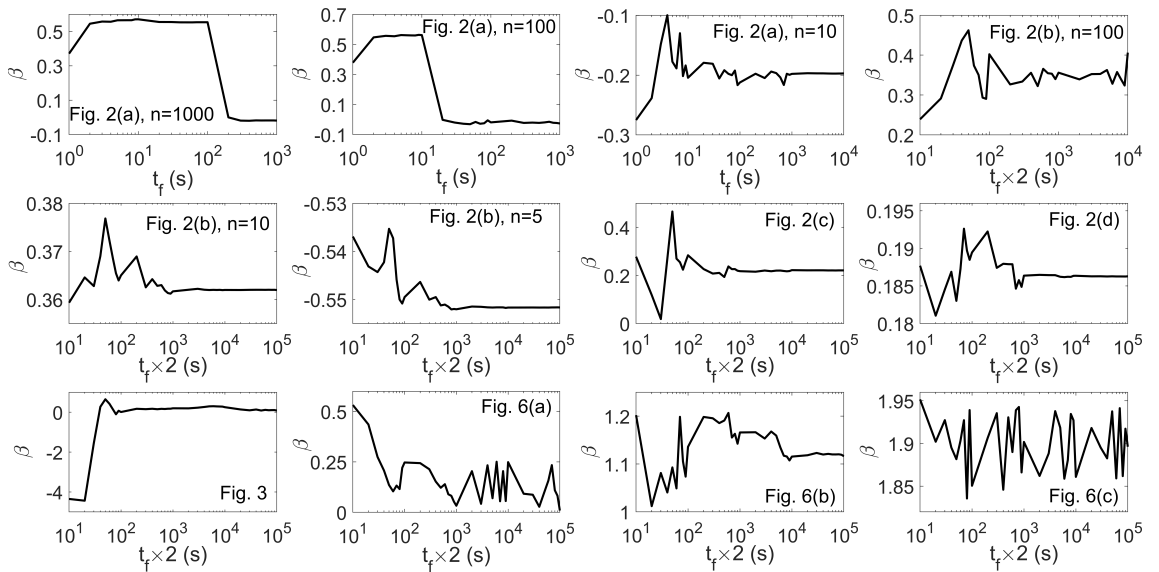
Figure 4.4: The amount of time each model requires to obtain convergence of the gradient of the PSD. The β factor of the $1/f^\beta$ gradient of the PSD of a model is calculated from time-series of a range of lengths, t_f. The model to which each plot refers is indicated by the legend specifying the figure in which that model was first introduced.
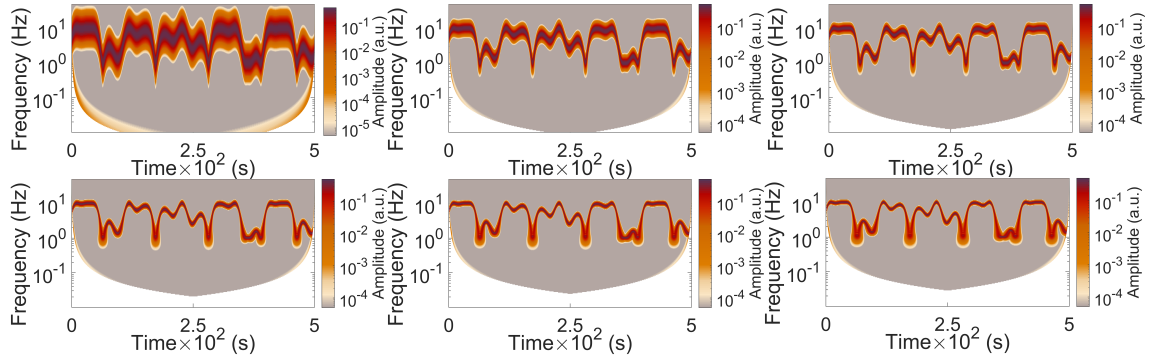
Figure 4.5: The role of the frequency resolution in the wavelet transform, using the lognormal wavelet. Considered for the aperiodic model of Fig. 4.3. In order, from left to right along the upper row and then left to right along the lower row, a frequency resolution of $R = 0.5, 1, 1.5, 2.5, 3, 3.5$ was used, rather than $R = 2$ as in Fig. 4.3.

4.3.1 Autonomous vs non-autonomous noise

First, in the absence of coupling (i.e. $A = 0$), we consider the dependence of "noise-like" behaviour in a signal on the number of oscillatory components n and their range of frequencies, in the autonomous case (i.e. without time-dependence) versus the non-autonomous case, as defined by Eqs. (4.21)–(4.23) with $A_{\omega i} = 0$ in the autonomous case and $A_{\omega i} > 0$ in the non-autonomous case. This is examined in Fig. 4.2. We will first consider the PSD plots and then the wavelet transform plots. (In Fig. 4.2 and everywhere else in this paper, all wavelet transform plots show the magnitude $|W(t,f)|$ of the wavelet transform $W(t,f)$ plotted over time-frequency space.)

In Fig. 4.2(a), from top to bottom, we consider 10^3, 10^2 and 10 autonomous oscillators, respectively. For $n = 10$ there are 10 clear peaks in the power-spectral density, indicating determinism, while these become less clear and more numerous for $n = 10^2$ and $n = 10^3$ oscillators. This is as expected for time-independent systems within the classical framework: a few processes are identifiable, but the more there are, the more noise-like their mean dynamics appears.

Fig. 4.2(b) analyses non-autonomous ensembles with the same parameters as in (a), except for the addition of a time-dependent modulation. In contrast to the autonomous ensembles, with this time-dependent modulation only a small number of oscillators is

required to produce a noise-like PSD distribution. While the relationship between the increase in n and the reduction of identifiable peaks as the PSD becomes increasingly smooth, indicating noisy dynamics, is preserved, this begins at a much smaller n. Even for $n = 5$, where the small number of centre frequencies f_{0i} does not very well fill out the frequency range being analysed, resulting in a frequency gap and a negative β, we do not see clear isolated peaks corresponding to the 5 oscillators.

In Fig. 4.2(c) non-autonomous oscillators with common centre frequency and a relatively small modulation amplitude ($f_{0i}A_{\omega i} = 1.01$ Hz) are analysed. (So the only difference between the five oscillatory components is their initial phase $\theta_i(0)$.) The PSD again shows no isolated peaks and appears noise-like.

Finally, in Fig. 4.2(d) we examine a non-autonomous ensemble with identical parameters to (c) except for a larger modulation amplitude ($f_{0i}A_{\omega i} = 4.95$ Hz). Predictably, this spreads the power spectrum over a larger frequency range than in (b), and while there are as a result more clearly identifiable peaks at lower frequencies (namely, the natural frequency plus integer multiples of the modulation frequency [212, p53], which become more clearly distinct at lower frequencies due to the logarithmic frequency axis), higher frequencies remain noise-like, and the noise-like dynamics predictably occurs over a larger range of frequencies.

In these latter two cases, (c) and (d), as the frequency $f_i(t)$ of these oscillators is the same across all i, there is functionally no difference made by the value of n. In other words, this indicates that even a single non-autonomous oscillator can be sufficient to generate dynamics whose PSD representation appears noise-like. We see in Fig. 4.2 that it is the introduction of time-dependent modulation that leads to noise-like PSDs, and that it is not contingent on any other particular parameter.

In accordance with Sec. 4.2.6, we now analyse the time-series produced from the above models using time-frequency analysis; specifically, we use the continuous wavelet transform because of its logarithmic frequency resolution that enables the simultaneous resolving of oscillatory components of a wide range of time scales. (We use the lognormal wavelet as the mother wavelet for the wavelet transform, since this provides particularly good time-frequency resolution [63, 213].)

In Fig. 4.2, the wavelet transforms identify deterministic time-dependence in (b)–(d), and suggest that there is no time-dependence in (a). In (a) and (b), where the centre frequencies of the individual oscillatory contributions are linearly distributed in the range $[1, 10]$ Hz, for $n \leq 10$ many of the individual oscillatory contributions are clearly resolved, but the inidividual oscillatory contributions become harder to identify as n is increased. Accordingly, at higher values of n, separate analyses that consider narrower frequency ranges may be required to identify each contribution (although in the non-autonomous setup in (b), if one were to take n sufficiently large, the Heisenberg uncertainty principle would make it impossible to resolve any of the n individual contributions under any choice of frequency range and parameters of the wavelet transform).

In summary, in the autonomous case, very large n (such that individual contributions would be intractable from a time-series) gives an approximation to white noise as expected under classical notions of emergence of noise; but not so large n is required in the non-autonomous case to produce pink noise—indeed, sufficiently small n that the continuous wavelet transform can detect individual contributing oscillators θ_i.

Next, we demonstrate that this phenomenon is not exclusive to periodic time-dependence of the oscillators' internal frequencies, but can readily occur for aperiodic forms of time-dependence. In Fig. 4.3 we analyse a single ($n = 1$) aperiodically frequency-modulated oscillator, demonstrating that the power-spectral density is still noise-like. Once again, the wavelet transform resolves the true nature of the signal as being not at all like "noise" but rather a simple oscillation whose frequency is gradually modulated, with the form of frequency modulation also clearly seen in the wavelet transform.

As discussed in Section 4.2.2, the theoretical power-spectral density is defined over an infinite time span. Thus, an approximation of the "true" PSD must be calculated over finite time, but this approximation becomes less accurate the shorter the finite time interval. In Fig. 4.4 we examine the length of time required to reach a convergent gradient of the power-spectral density for every model considered in this section; the largest value shown on the time axis in each of the plots in Fig. 4.4 is equal to the simulation time that was used for the PSD estimation in the corresponding figure in this section where the model was analysed (which, as we have said, corresponds to around the longest time computationally feasible). We see in Fig. 4.4 that for most cases, this

time is sufficient to reach convergence. So the mischaracterisation of relatively simple deterministic but time-dependent dynamics as noise-like is not based on insufficient accuracy of empirical PSD estimators, but is based truly on the concept itself of using a linear trend in a log-log plot of PSD as an indicator of noise when the signal comes from a system subject to time-dependent influences in a manner that makes the framework of stationary stochastic processes inappropriate. Rather than seeking to gain a better understanding of the system by improving the supposed precision or accuracy of PSD estimation, instead, in order to gain even a basic correct understanding of the system, one must incorporate the time dimension explicitly into the analysis, as exemplified in the wavelet transform.

Finally in this subsection, we demonstrate the practical implications of the Heisenberg uncertainty principle, as discussed in Section 4.2.6, for the wavelet transform. Specifically, for this analysis method the frequency resolution parameter determines the trade-off between precision in the time domain and the frequency domain. In Fig. 4.5, we see that for the highest frequency resolution considered, the higher frequencies are finely resolved in time-frequency space, while the lower frequencies have a more blurry representation in the time-domain; then, as the frequency resolution is decreased, the lower frequencies become less blurry in the time domain, but the higher frequencies start to become more blurry in the frequency domain; and at the lowest frequency resolution values, all frequencies are very poorly resolved in the frequency domain. This illustrates how, in time-frequency analysis, the parameter controlling the trade-off between time localisation and frequency resolution needs to be carefully optimised, on a case-by-case basis, to the combination of how quickly the time-dependent characteristics of oscillations change and how large the distance in frequency is between different oscillatory contributions that one seeks to resolve; otherwise, the number and the nature (e.g. noise versus oscillation) of the components present in the signal may be unnecessarily misidentified.

4.3.2 Coupling

While the uncoupled ensemble models that we have discussed thus far have already been instructive in illustrating the problem with applying the classical PSD-approach of noise
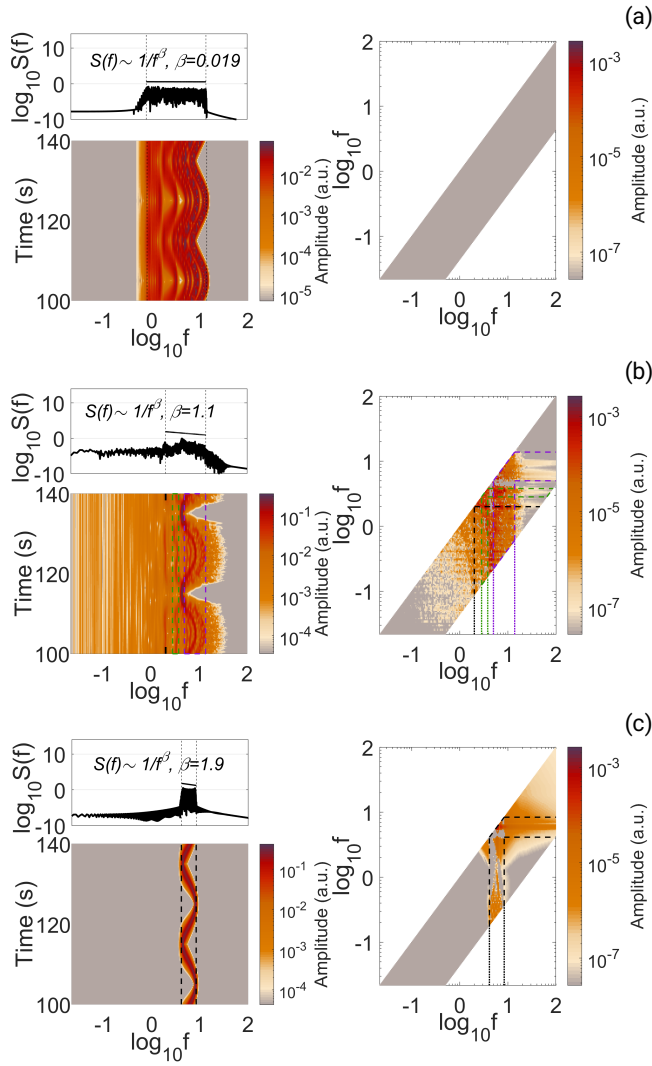
Figure 4.6: PSDs, wavelet transforms and wavelet bispectra of non-autonomous oscillator networks with varying coupling strengths. PSDs (top left), wavelet transforms (bottom left) and wavelet bispectra (right) of the mean field of networks of $n = 10$ non-autonomous oscillators are plotted. Specifically, the wavelet bispectra results show the wavelet biamplitude associated to each point in frequency-frequency space after subtraction of the 95% significance critical threshold given by a surrogate test involving 59 numerically generated surrogate signals. The wavelet transforms and wavelet bispectra are calculated using a lognormal wavelet with frequency resolution 5. Centre frequencies f_{0i} of the oscillators are distributed equidistantly over the range $[1, 10]$ Hz, with an addition of a random number between 0 and 1 Hz to reduce harmonic relationships between the frequencies. The modulation amplitude factor is $A_{\omega i} = 0.3$ and the modulation frequency is $f_{\omega i} = 0.05$ Hz. The network coupling strengths A are (a) 0 s^{-1}, (b) 5 s^{-1} and (c) 10 s^{-1}. The models are simulated for 200000 s.

characterisation to systems with time-dependent characteristics, systems with multiple oscillatory components will far more often have some coupling between oscillatory components. Detection of coupling between components of a signal serves as a particularly strong indicator that these components are not "noise" to be discarded, but rather represent functionally significant deterministic processes. Understanding a system's coupling relationships can also reveal much about its physical behaviour, representing the means by which systems exchange energy, as occurs throughout the physical world [204–206]. In our framework we consider phase-phase coupling between oscillatory components; specifically, here we will consider phase-phase coupling in which oscillators attract each other's phases to their own, as in Eq. (4.22).

We analyse non-autonomous networks consisting of $n = 10$ oscillators of distinct time-dependent internal frequency, with all-to-all coupling of Kuramoto form, according to Eq. (4.22). In Fig. 4.6 we analyse such a network with three coupling strengths A: $A = 0$ in (a), reducing back to the uncoupled ensemble case; $A = 5$ s^{-1} in (b), providing an intermediate-strength coupling; and $A = 10$ s^{-1} in (c), representing strong coupling.

In order to detect and analyse the coupling present in these models, after calculating the wavelet transform we additionally consider the wavelet bispectrum [209, 211], which is designed to detect non-linearities, such as coupling, within or between signals [63, 211]. Bispectra are defined over frequency-frequency space, such that the presence of a bispectral peak around a frequency pair (f_1, f_2) may indicate a coupling between two oscillatory components of frequencies in the vicinity of f_1 and f_2. (However, on the diagonal, i.e. $f_1 = f_2$, or more generally for rationally dependent f_1 and f_2, bispectral peaks may indicate just a single non-sinusoidal oscillatory component, with the bispectral peaks arising from harmonics of this non-sinusoidal component.) Here in Fig. 4.6, and in all other bispectra plots in this paper, we calculate a biamplitude value (i.e. modulus of the time-averaged instantaneous wavelet bispectrum) at each point in frequency-frequency space as in [211], and apply a statistical significance test to decide at which points in the frequency-frequency space we deem the biamplitude value to be "significant". More specifically, at each point in frequency-frequency space we subtract from the wavelet biamplitude value a critical threshold (at 95% significance) calculated from the bispectra of wavelet iterative amplitude adjusted Fourier transform (WIAAFT) surrogates gen-

erated from the time-series under investigation, according to the procedure described in [64]; hence, the strictly positive (i.e. non-grey) values shown in these bispectra plots correspond to where the bispectrum value is considered "significant". (The point is that this "significance" potentially indicates that the level of time-localised phase bicoherence around the given frequency-pair is, at least for some of the time, higher than one would expect if the oscillatory components seen in the wavelet transform around these two frequencies had no kind of direct or indirect coupling between them.)

Let us now discuss both the wavelet transform results and the wavelet bispectrum results. In Fig. 4.6(a), where we have reduced back to the uncoupled ensemble case, the results we expect based on the previous subsection are confirmed: the PSD is noise-like and the wavelet transform appears to indicate non-noise-like frequency modes with a deterministic time-dependence. When medium-strength coupling is introduced in (b), the PSD continues to be noise-like. The wavelet transform shows periods of asynchrony where the oscillations cluster around three dominant modes, and shorter periods of synchrony where the oscillations cluster around just one dominant mode. One of the three modes in the asynchronous case lies roughly at the frequency value indicated by the black ticks; another lies within the green-marked frequency band; and the third lies within the purple-marked frequency band (where we see the fundamental frequency of this mode and also harmonics arising from different combinations of the three frequency modes. In the periods of synchrony, the one frequency mode appears to represent the coinciding of the upper two of the three previous frequency modes while the lowest of the three previous frequency modes vanishes in amplitude. This alternation between three dominant modes and one dominant mode is indicative of the intermittent synchronisation phenomenon of non-autonomous systems [2]. In (c), the wavelet transform shows that the network has become highly synchronised around a single frequency mode, and yet despite this coherent behaviour the PSD of this mode still appears noise-like. So we see in all these cases that non-autonomous networks of a small number of interacting oscillators can also appear to be noise-like when analysed by the classical PSD approach, even when synchronised.

Now we discuss the wavelet bispectrum results, especially with a view to considering what we can learn from this analysis tool that would be difficult or impossible to learn

from classical spectral analysis under the traditional framework. As expected, no significant bispectral content is found in (a), where there is no coupling. In (c), the full synchronisation of the system into a single mode masks the underlying coupling, leading to only one significant bispectral amplitude peak (indicated by the black-marked frequency band), which occurs on the diagonal and thus cannot indicate coupling between different frequency modes. (More precisely, much of the peak—which is inherently spread out rather than pointlike due to the Heisenberg Uncertainty Principle—is found to be significant against surrogates, while parts of it, particularly near the "summit" on the diagonal, do not exceed the corresponding surrogate threshold. This peak likely arises because of how wide the frequency modulation over time is. As we will explain shortly, the time-averaged wavelet bispectra as shown in this paper, though certainly better suited to time-dependent systems than classical bispectrum estimates defined for stationary stochastic processes, are still only the first step in a thorough approach to applying wavelet bispectral analysis.) With non-synchronising coupling in (b), however, we detect large areas of significant biamplitude, which are mostly contained within the frequency regions of the dominant modes identified in the wavelet transform. Significant biamplitude values in areas of the frequency-frequency space corresponding to two distinct such frequency regions indicate coupling between the modes represented by those frequency regions.

We have used wavelet bispectral analysis to investigate coupling between frequency modes. Results indicative of coupling or the absence thereof between frequency modes would have been obtainable from classical bispectral analysis if the network were an autonomous dynamical system (i.e. if there were no frequency modulation or other form of time-dependent characteristics); but as seen in the various PSD computations shown in this section, the presence of frequency modulation drastically alters the classical spectral properties to the point that individual oscillators look like pink noise.

The bispectral results shown here (and also later for experimental data) are the most basic wavelet bispectral analysis computations, which do not explicitly show the time-evolution of bispectral properties. Having performed such computations and identified significant biamplitude peaks, one can further examine the genuineness of the apparent presence of

coupling, as well as further properties of such coupling and its time-dependence, using methods described in [63, 211].

4.3.3   Entropy and autocorrelation

What we call the "traditional framework of time-series analysis", as described in Sec. 4.2, can be summarised as the approach in which one regards a recorded time-series as being a finite-duration segment of a sample realisation of an ergodic stationary stochastic process, and uses this recording to seek to estimate statistical parameters or properties of the underlying stochastic process so as to help learn more about the physical system from which the time-series was measured. PSD analysis is a common tool for understanding noise that is based on the traditional framework; but as we have said, the full "toolbox" of time-series analysis methods based on the traditional framework is vast. Here, we now illustrate how including more of these methods in the analysis of a time-series does not help to gain an understanding of the underlying behaviour of the system if there is significant time-dependence in the properties of oscillatory components of the time-series, and hence time-resolved methods such as the wavelet transform and other methods described in [207] are still needed. Specifically, as two examples of well-known analysis tools that are intended to gain certain types of information about a time-series—and yet which are ultimately based on the traditional framework and do not resolve in time—we will consider firstly *multiscale sample entropy* [214] and secondly *autocorrelation* (the Fourier counterpart to PSD).

Entropy measures are intended to give a quantification of the "complexity" of a time-series. Multiscale sample entropy is particularly designed to avoid characterising randomness as inherently a behaviour of high complexity, such that, for example, stationary white noise will appear as being of relatively low "complexity" compared to other forms of complex-looking behaviour [55, 57, 214]. Multiscale sample entropy generalises the established sample entropy calculation to multiple time scales, identifying over which of these the time-series may be more or less complex.

144
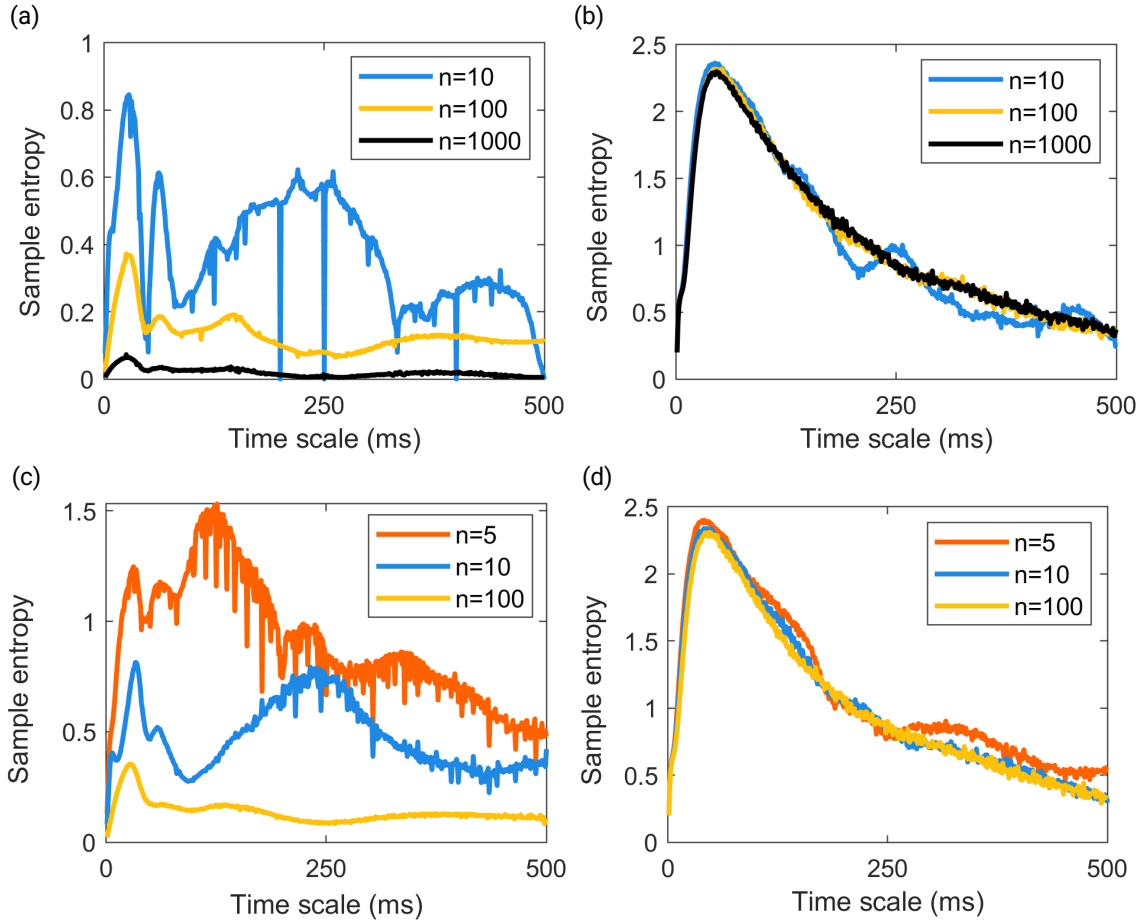
Figure 4.7: Multiscale sample entropy of autonomous and non-autonomous oscillator ensembles. In (a) the autonomous models in Fig. 4.2 (a); in (b) the same models as in (a) but with the addition of a random number between 0 and 1 Hz to each frequency f_{0i}; in (c) the non-autonomous models in Fig 4.2 (b); and in (d) the same models as in (c) but with the addition of a random number between 0 and 1 Hz to each centre frequency f_{0i}. In each case, the multiscale sample entropy is calculated for the time-series simulated up to a duration of $T = 200$ s. The parameters of the multiscale sample entropy are $m = 2$ and $r = 0.15$.
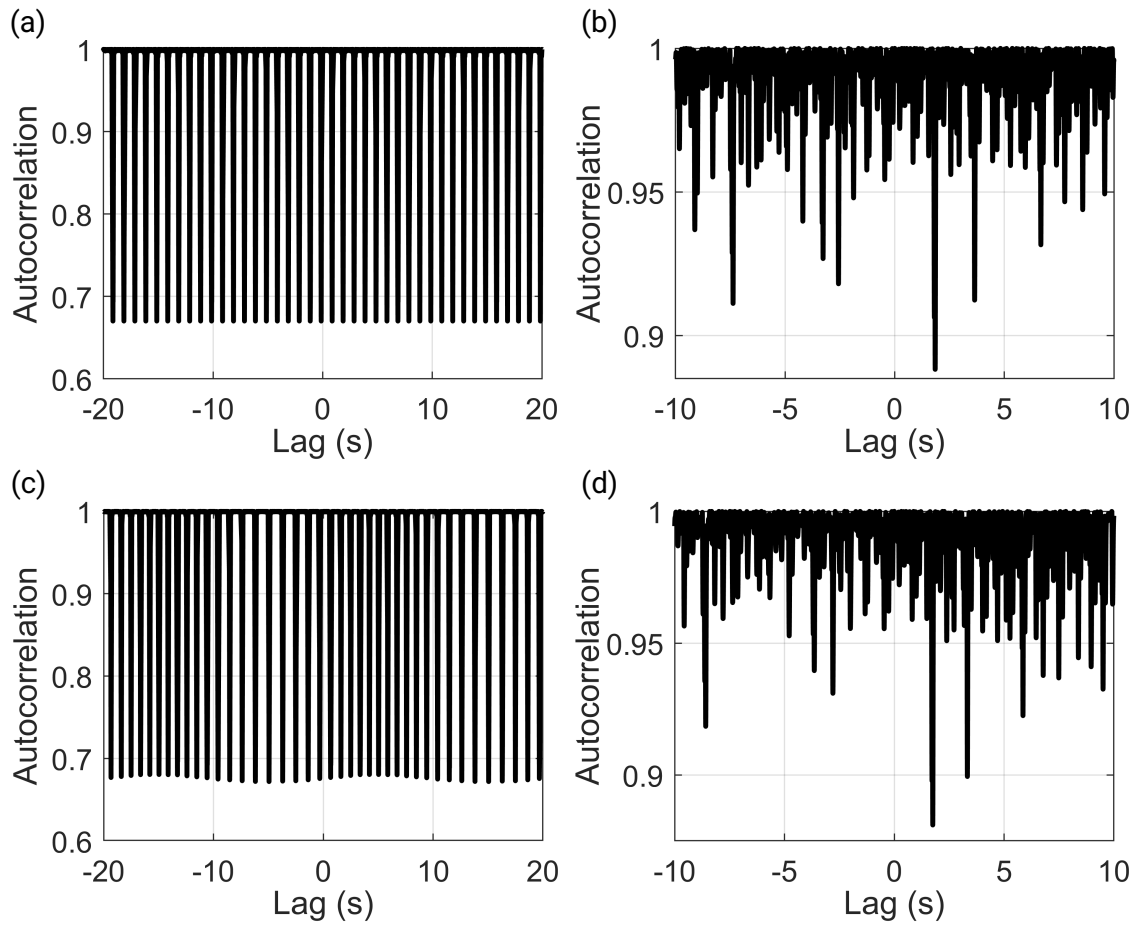
Figure 4.8: Autocorrelation of autonomous and non-autonomous oscillator ensembles analysed in Fig. 4.7 with $n = 10$. Each plot corresponds to the same model as that of the same letter in Fig. 4.7. The window size is (a) 0.028 s, (b) 0.044 s, (c) 0.034 s and (d) 0.044 s, in each case equal to the greatest entropy peak in the corresponding model in Fig. 4.7.

To define multiscale sample entropy, we first need to define sample entropy [215], which is defined for discrete-time signals $(x_n)_{n=1,\ldots,N}$. Heuristically, for a fixed positive-integer parameter m, the sample entropy is the negative of the natural logarithm of the probability that two randomly selected distinct length-$(m+1)$ segments of the signal will share approximately the same $(m+1)$-th entry conditional on the event that they share approximately the same first m entries; thus, a larger value of the sample entropy corresponds to the time-series being "less predictable" and thus "more complex". To be more precise: given a signal length N, an integer $m \in \{1, \ldots, N-1\}$ (often chosen as $m = 2$) and a "tolerance" parameter $\rho > 0$, letting C_{N-m} be the set of all pairs (i,j) of integers i and j with $1 \leq i < j \leq N-m$, the sample entropy of a signal $(x_n)_{n=1,\ldots,N}$ is defined as

$$\mathrm{SampEn}(m, \rho, N, (x_n)_{n=1,\ldots,N}) :=$$
$$\log \frac{\#\{(i,j) \in C_{N-m} : d[\,(x_i, \ldots, x_{i+m-1}),\, (x_j, \ldots, x_{j+m-1})\,] < \rho\}}{\#\{(i,j) \in C_{N-m} : d[\,(x_i, \ldots, x_{i+m})\quad,\quad (x_j, \ldots, x_{j+m})\,] < \rho\}} \quad (4.24)$$

where d is a function for measuring distances between vectors (in the calculation of Fig. 4.7 we use Euclidean distance). From a statistical point of view within the above-described traditional framework of time-series analysis, as in [215] the quantity $\mathrm{SampEn}(m, \rho, N, (x_n)_{n=1,\ldots,N})$ is a statistic seeking to estimate—for the underlying ergodic stationary stochastic process $(X_n)_{n\in\mathbb{Z}}$ from which the time-series $(x_n)_{n=1,\ldots,N}$ is assumed to arise as a sample—the value of the parameter

$$\lim_{N\to\infty} \mathbb{E}[\mathrm{SampEn}(m, \rho, N, (X_n)_{n=1,\ldots,N})]. \quad (4.25)$$

Whereas the sample entropy of a discrete-time signal is a single number, the *multiscale sample entropy* of a discretely sampled signal is a function whose input variable is the "time scale" s under consideration; the corresponding output is the sample entropy of the *sequence of mean averages* of consecutive time windows of duration s. To be precise: for a discretely sampled signal $(x_t)_{t=\frac{1}{f_s}, \frac{2}{f_s}, \ldots, \frac{f_s T - 1}{f_s}, T}$ of duration T and sampling frequency f_s, fixing a positive-integer parameter m and a parameter $r > 0$ and setting $\rho = r\sigma$ where σ is the standard deviation of the set of all points $x_{\frac{1}{f_s}}, x_{\frac{2}{f_s}} \ldots, x_T$ in the signal, the multiscale sample entropy associates to each "time scale" $s > 0$ (where s is a multiple of $\frac{1}{f_s}$ that is much smaller than T) the sample entropy of the signal $(y_n)_{n=1,2,\ldots,\lfloor \frac{T}{s} \rfloor}$ where

y_n is the mean over the n-th time window of length s, i.e.

$$y_n = \frac{f_{\mathrm{s}}}{s} \sum_{i=1}^{\frac{s}{f_{\mathrm{s}}}} x_{(n-1)s+\frac{i}{f_{\mathrm{s}}}}, \qquad (4.26)$$

and $\lfloor \cdot \rfloor$ is the rounding-down operation.

Now for sample entropy, it is advised that one ensure a signal length N of at least 10^m. For multiscale sample entropy, since a larger scale s corresponds to a smaller number of points $\lfloor \frac{T}{s} \rfloor$ in the downsampled signal for which the sample entropy is calculated, it is necessary to limit the scale s to achieve the above advice. Accordingly, in this paper, we present the multiscale sample entropy up to the maximum such permissible scale.

In Fig. 4.7 we present the multiscale sample entropy of models considered in the previous sections, and modifications thereof. Fig. 4.7(a) shows results for the autonomous cases analysed in Fig. 4.2(a), and Fig. 4.7(c) shows results for the non-autonomous cases analysed in Fig. 4.2(b). The results in plot (a) are of a qualitatively fairly similar nature to those in plot (b), apart from the relatively sharp drops in entropy as a function of scale seen at certain scale values in the $n = 10$ case. There is no indication from these plots that multiscale sample entropy can be used to help distinguish time-independent (i.e. autonomous) from time-dependent (i.e. non-autonomous) dynamics.

However, perhaps not too much should be deduced from plots (a) and (c) due to the rational ratios between the frequencies $f_i(t)$ of the different oscillators present in the model, which could significantly affect the entropy analysis. Accordingly, just as we added random numbers to the centre frequencies to reduce rational relationships when considering bispectra, so likewise now in plots (b) and (d) of Fig. 4.7, we show results for the same models as in plots (a) and (c) respectively except with the addition of random numbers between 0 and 1 Hz to the centre frequencies f_{0i} of the oscillators. This is for the same purpose as in the bispectra examination; rational relationships between the frequencies introduce further higher harmonics which will reduce the estimated entropy, and are not representative of the vast majority of real physical processes. Now, in this more generically representative scenario, we actually see results indicating similar conclusions to what we saw in Fig. 4.2 when considering power-spectral density: The sample entropy as a function of scale shows a similar picture to that seen for white noise in Fig. 3 of [214] and Fig. 1 of [57]; but,

- in the autonomous case shown in plot (b), for the relatively low-dimensional case $n = 10$, the deviations away from the monotonically decaying "noise-like" curve are fairly clear, while for larger n the result more closely follows a monotonically decaying curve resemblant of "noise-like" behaviour;

- however, in the non-autonomous case shown in plot (d), $n = 10$ is already sufficient to follow remarkably closely the "noise-like" picture.

So whereas the cases shown in plots (a) and (c) merely indicate the *insufficiency* of multiscale sample entropy to be able to distinguish autonomous from non-autonomous dynamics, the more generically representative results shown in plots (b) and (d) indicate not only the insufficiency of multiscale sample entropy in this regard (since the results in (b) and (d) are quite similar to each other) but furthermore the potential for positive mischaracterisation of relatively low-dimensional deterministic behaviour as noise, just as has been seen for power-spectral density.

Autocorrelation analysis is also a widely applied time-series analysis method, that describes the "statistical memory" of a signal across different time scales. The sample auto-correlation function (which seeks to estimate the "population" autocorrelation function of the ergodic stationary stochastic process from which the time-series is assumed to be a sample) calculates the correlation between values in the time-series separated in time by a given "lag" (the input variable of the autocorrelation function). Here, we work with a slight adaptation of the standard definition of sample autocorrelation, that sometimes gives more suitable results that the standard definition: for a discretely sampled signal $(x_t)_{t=\frac{1}{f_\mathrm{s}}, \frac{2}{f_\mathrm{s}}, \dots, \frac{f_\mathrm{s}T-1}{f_\mathrm{s}}, T}$ of duration T and sampling frequency f_s, we fix a window-length $L \in (0, T)$ independent of the lag under investigation, and then associate to each lag $k \in [-\frac{T-L}{2}, \frac{T-L}{2}]$ (where k is a multiple of $\frac{1}{f_\mathrm{s}}$) the cosine of the angle between the vector $\left(x_{\frac{i}{f_\mathrm{s}}}\right)_{\frac{i}{f_\mathrm{s}} \in [\frac{T-L}{2}, \frac{T+L}{2}]}$ and the vector $\left(x_{\frac{i}{f_\mathrm{s}}+k}\right)_{\frac{i}{f_\mathrm{s}} \in [\frac{T-L}{2}, \frac{T+L}{2}]}$, as calculated by the normalised dot product. (The difference from the usual definition of the sample autocorrelation function is as follows: in the usual definition, for each lag k one considers correlation between the time-windows $[0, T - |k|]$ and $[|k|, T]$, whereas in our approach one considers the correlation between the time-windows $[\frac{T-L}{2}, \frac{T+L}{2}]$ and $[\frac{T-L}{2} + k, \frac{T+L}{2} + k]$.)

In Fig. 4.8 we calculate the autocorrelation of the models in Fig. 4.7 with $n = 10$, using a window size L equal to the time scale at their greatest entropy peak. We see that plots (a) and (c) slightly reveal a qualitative difference, namely a constant lower envelope in the autonomous case and a slightly variable lower envelope in the non-autonomous case, but these observations are peculiar to the precise setup considered in (a) and (c) where the frequencies $f_i(t)$ have rational ratios; once we move to the much more generically representative cases in plots (b) and (d), we see no clear qualitative difference between plots (b) and (d) that might indicate that one is generated by time-independent dynamics and the other by time-dependent dynamics. In conclusion, as is to be expected, there is no clear way in which non-time-resolved autocorrelation functions can be used to help distinguish between time-independent and time-dependent dynamics.

Just like power-spectral density, the two analysis methods that we have considered in this subsection do not resolve the time dimension: just as classical power spectra are defined over the frequency axis without an axis for the progression of time, so likewise the multiscale sample entropy and the autocorrelation are defined as a function of a variable representing a "width of time-gap", while still effectively treating the actual progression of time as of no more significance than an atemporal set of statistical re-trials (the essence of ergodicity). Accordingly, as we have evidenced, they cannot be expected to provide a suitable methodology for gaining even a basic understanding of the behaviour of systems subject to temporal modulation of characteristics (such as frequency of oscillatory components)—nor indeed can any other tools based on the classical framework of time-series analysis. Instead, time-resolved methodologies such as deterministic time-frequency analysis are truly necessary for successfully analysing signals recorded from such systems.

4.4 Experimental comparisons of the two frameworks

We now investigate the physical appropriateness of our framework as contrasted with the classical framework for three physical systems from which experimental data has been recorded; specifically, we will see how deterministic time-frequency analysis reveals important information not yielded by methods within the classical framework's approach to time-series analysis. In particular,

(a)

(b)

$S(f) \sim 1/f^\beta$, β=1.9

(c)

(d)

(e)
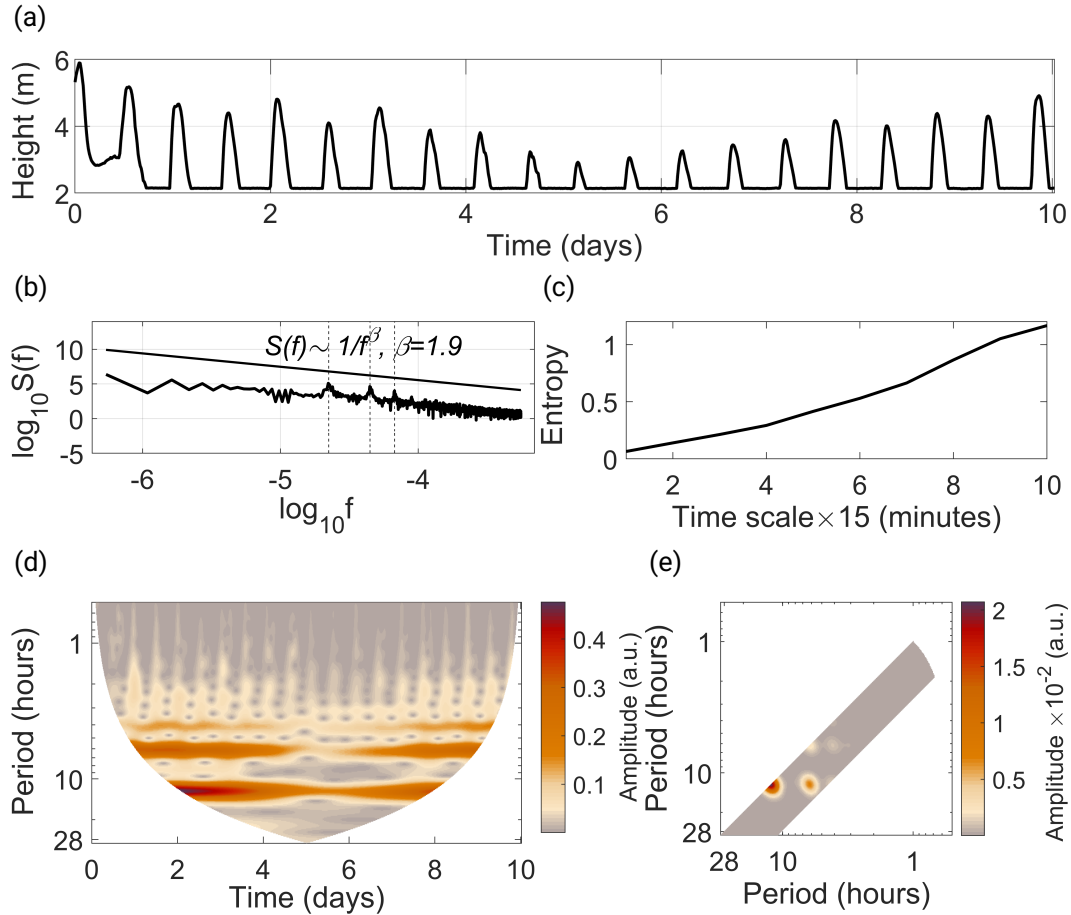
Figure 4.9: Tidal time-series recorded at Lancaster Quay, United Kingdom. The readings were made every 15 minutes from 16th–25th February 2022 (see the data availability statement for the data). The sensor is placed at 2.15 m, and unable to detect levels below this. (a) The time-series of the height of the water. (b) The PSD. (c) The multiscale sample entropy with $m = 2$ and $r = 0.15$. (d) The wavelet transform using the lognormal wavelet with a frequency resolution of 1.5. (e) The wavelet bispectrum using the lognormal wavelet with a frequency resolution of 1.5, tested (at 95% significance) against 59 surrogates generated from the data.

- we will indicate how time-frequency analysis can avoid the mischaracterisation of deterministic functioning as "noise" that would arise from applying to these experimental time-series a traditional PSD approach to separating oscillatory components from noise;

- and furthermore, for illustrative purposes, we will show how one might derive from our wavelet transform analysis a preliminary form of approximate model of the time-series according to our framework in Sec. 4.2.4 as represented by Eqs. (4.13)–(4.14).

By a "preliminary" form of model, we mean that this is simply based on our present analyses of the time-series; one can work towards more accurate and precise models through a combination of (a) applying additional time-resolved analysis methods to the signal, (b) recording further signals from the system or type of system being considered and applying suitable time-resolved analysis methods to those signals as well, and (c) incorporating any relevant already-existing physical knowledge regarding the system from which the signal is recorded.

We analyse, in Fig. 4.9, the height of water recorded by a monitoring station located at Lancaster Quay, United Kingdom; in Fig. 4.10, the magnetic field strength at the Earth's surface recorded by an observatory in Norway [216]; and in Fig. 4.11 the interplanetary magnetic field strenght, indicative of solar wind activity, recorded by a satellite in between the Earth and the Sun. All three of these systems are thermodynamically open systems with time-variable external influences—whether they be (respectively) the gravitational force of the moon or the plethora of electromagnetic forces that affect the magnetic fields at the Earth's surface and throughout the solar system, from solar winds, to electric currents in the Earth's atmosphere to plasma processes in the core of both the Earth and the Sun. These systems therefore all have the theoretical potential to have deterministic functioning that appears noise-like under a traditional PSD analysis.

The River Lune, the subject of Fig. 4.9, is known to be tidal at the point of measurement in Lancaster Quay. We would therefore expect to see the water levels oscillate with two peaks a day, and the wavelet transform therefore to show a significant oscillatory mode with a period of approximately twelve hours. The time-series itself, shown in plot (a),
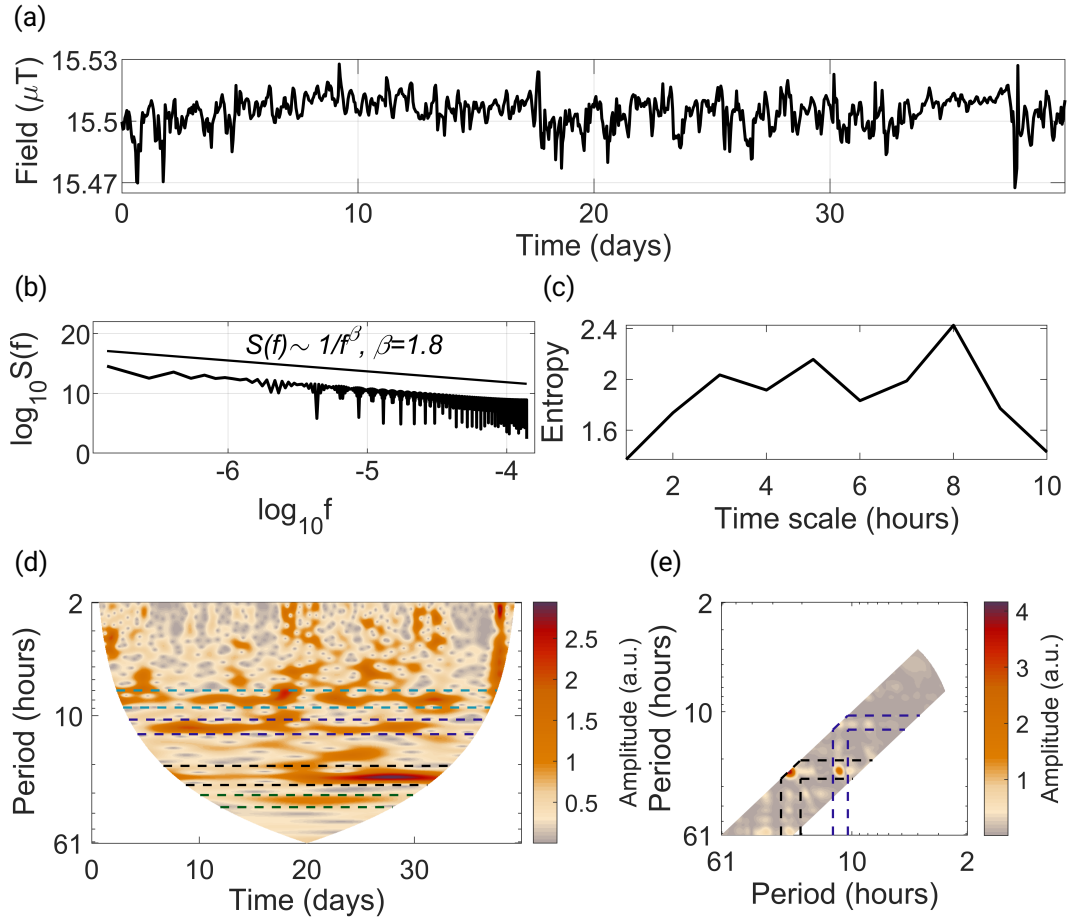
Figure 4.10: x-component of the ionospheric magnetic field recorded by UiT The Arctic University of Norway's KAR magnetogram station every hour for a period of 39 days and 23 hours, from 2nd December 2021 to 10th January 2022 [216]. (a) The time-series of the strength of the x-component of the ionospheric magnetic field. (b) The PSD. (c) The multiscale sample entropy, with $m = 2$ and $r = 0.15$. (d) The wavelet transform using the lognormal wavelet with a frequency resolution of 3. (e) The wavelet bispectrum using the lognormal wavelet with a frequency resolution of 3, tested (at 95% significance) against 59 surrogates generated from the data.

immediately makes clear that the river is indeed tidal, oscillating through two peaks and two troughs each day. The wavelet transform (plot (d)) shows three clear frequencies present in the signal, corresponding to periods of approximately twelve hours, six hours and four hours, in descending order of amplitude. The six-hour and four-hour peaks correspond to twice and three times the frequency of the fundamental twelve-hour peak; they are harmonics arising from the fact that the twelve-hour-period oscillations in the time-series are not of sinusoidal shape. (The bispectrum in plot (e) shows significant peaks at rationally related frequency-pairs arising from these harmonics. A procedure to determine whether frequency modes are harmonically related in less clear-cut cases is described in [162].)

From looking just at the wavelet transform, one could build a preliminary form of model for the time-series as

$$X(t) = A(t)h(\theta(t))$$
$$\dot{\theta}(t) = 2\pi/(12 \text{ hr}),$$

where h is a non-sinusoidal function as reflected by the presence of the harmonics of the 12-hour fundamental period, and $A(t)$ has fairly slow time-dependence on t as reflected by varying wavelet amplitude over time seen at the frequency $1/(12 \text{ hr})$ (and similarly at the harmonic frequencies). Of course, in this relatively simple example, we can see the behaviour directly from the time-series itself in plot (a), but in more complicated systems this would not be so. Since there is not much time-dependence in the frequency—although there is still significant time-dependence in the amplitude— the peaks at twelve, six and four hours that we saw in the wavelet transform are also present in the power-spectral density, indicated on plot (b) by the dotted lines. However such simple examples can be rare. In subsequent figures we will consider cases with increasingly complex frequency dynamics.

Magnetic field strength fluctuations at the Earth's surface are the subject of Fig. 4.10. There are many forces known to affect the magnetic field in the Earth's atmosphere, not least solar winds. It is already known that significant variations in the atmosphere, such as during a geomagnetic storm, also lead to variations at the Earth's surface, but the magnitude and significance of these surface variations, even during storm events, is still a matter of open research [218].

(a)

(b)

$S(f) \sim 1/f^{\beta}, \beta=1.8$

(c)

(d)

(e)
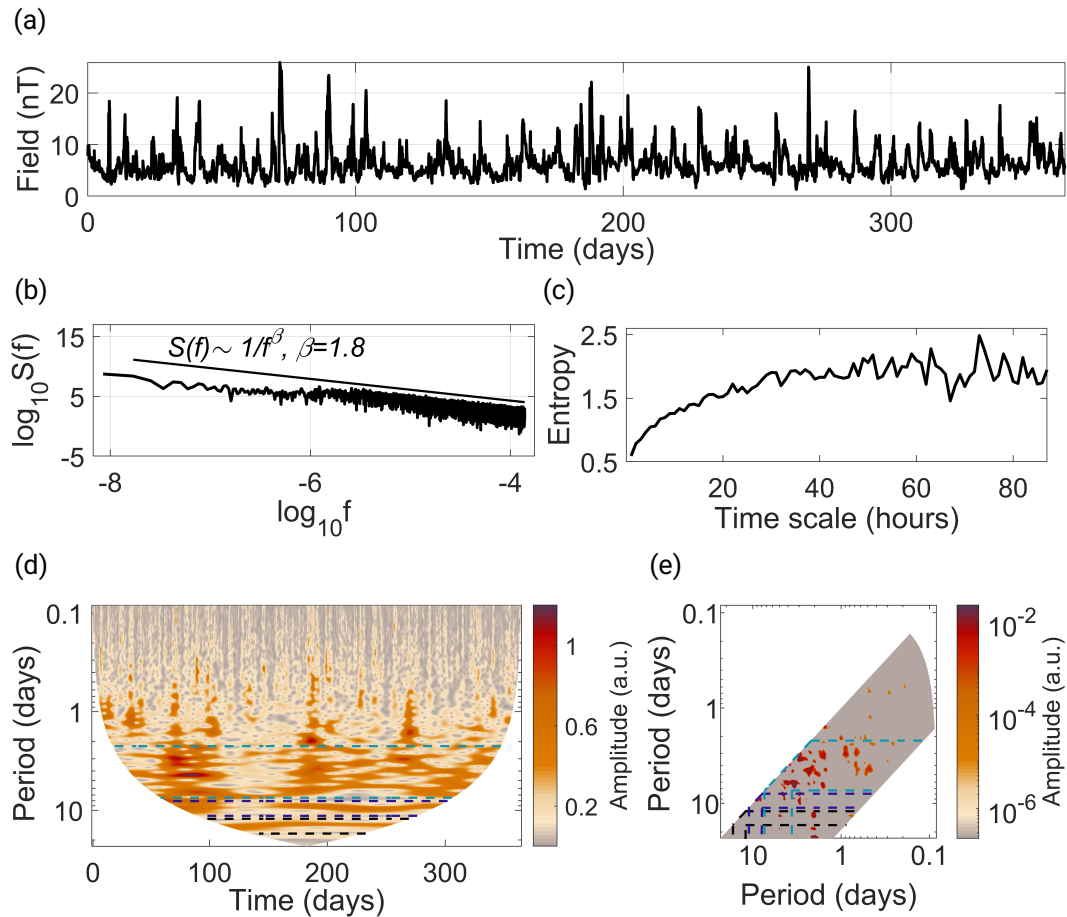
Figure 4.11: Average magnitude of the interplanetary magnetic field recorded by the WIND satellite, stationed at Lagrange point 1 of the Earth's orbit, for every hour for a period of 1 year, from 1st January 2022 to 31st December 2022 [217]. (a) The time-series of the strength of the magnitude of the interplanetary magnetic field. (b) The PSD. (c) The multiscale sample entropy, with $m = 2$ and $r = 0.15$. (d) The wavelet transform using the lognormal wavelet with a frequency resolution of 3. (e) The wavelet bispectrum using the lognormal wavelet with a frequency resolution of 3, tested (at 95% significance) against 59 surrogates generated from the data.

There are a variety of periodic fluctuations that have been found to take place in the geomagnetic field in absence of any solar event, primarily driven by electric currents resulting from solar winds and the moon's gravitational field moving against the geomagnetic field [219]. Such periods include 6 hours, 8 hours, 12 hours, 24 hours, 4 months and a year [220, 221].

In Fig. 4.10 we analyse magnetometer recordings over the space of 39 days and 23 hours, from the IMAGE magnetometer network. The purpose of this network is to detect ionospheric auroral electrojet events, but we have chosen a period in which no such events were detected. This period is hence more characteristic of so-called 'solar quiet' dynamics. The time domain of these recordings in (a) again does not immediately clarify whether the system is deterministic or noise-like, and the PSD shows no peaks. The wavelet transform, while more complex than in Fig. 4.9, shows four frequencies where a significant amplitude is maintained for a large majority of the examined time, corresponding to periods of approximately 24 hours, 12 hours, 8 hours, and 35 hours in descending order of amplitude. Three of these, 24 hours, 12 hours and 8 hours, are well-known already, as mentioned above. The 35-hour period however does not correspond to any known geomagnetic phenomenon. Besides these four frequency modes, the wavelet transform appears to show much other content in the signal that is somewhat noise-like, although with time-dependent intensity that is perhaps correlated with the amplitude of the 35-hour-period and/or 24-hour-period mode. The bispectrum shows very significant peaks at $((24 \text{ hr})^{-1}, (24 \text{ hr})^{-1})$ and $((24 \text{ hr})^{-1}, (12 \text{ hr})^{-1})$; but since the system contains distinct oscillatory processes of period 24 hours, 12 hours and 8 hours, it is difficult to conclude with confidence that the 24-hour component is significantly non-sinusoidal or that there is coupling between the 24-hour component and the 12-hour component, until first carrying out a much more detailed investigation of time-localised phase-bicoherence [63] (preferably with a longer time-series recording). The other regions where the bispectrum plot shows values slightly above the critical threshold may be due to the inherently far-from-sinusoidal nature of the apparent noise, or it could be that this "noise" genuinely includes many temporally intermittent cyclic processes with couplings between them. These are all issues that could be investigated with further time-resolved analysis of this time-series and further magnetic field strength time-series recordings together with physical considerations of the system itself; but as a preliminary

model according to our framework, we could model the time-series as

$$X(t) = \sum_{i=1}^{n} A_i(t) \sin(\theta_i(t)) + \varepsilon_\xi(t)\xi(t)$$

$$\dot{\theta}_i(t) = 2\pi(f_i + \varepsilon_i(t)),$$

where the frequencies $f_1, \ldots, f_n$ include the four frequencies $(8 \text{ hr})^{-1}$, $(12 \text{ hr})^{-1}$, $(24 \text{ hr})^{-1}$ and approximately $(35 \text{ hr})^{-1}$, the $\varepsilon_i(t)$ are functions representing the apparent slight time-dependence of the frequency in the wavelet transform, and $\varepsilon_\xi(t)\xi(t)$ represents a noise process with intensity proportional to a function $\varepsilon_\xi(t)$. Similarly to our first example in Fig. 4.9, the variations in amplitude $A_i(t)$ are much more substantial than the variations in frequency $\varepsilon_i(t)$. As we have indicated, it could be that $\varepsilon_\xi(t)$ itself should be taken to be proportional to one of the $A_i(t)$. Note that while our framework allows for a separation between deterministic oscillations and noise just like the traditional framework does, the classical PSD approach based on the traditional framework does not at all clearly detect the four oscillatory modes and risks leading to the *whole* signal being characterised as noise.

Finally, in Fig. 4.11, we analyse how the magnitude of the interplanetary magnetic field changes over time, measured at Lagrange point 1 in orbit of the Earth. This measures the varying strength of the solar wind, which causes the solar magnetic field to spread throughout the solar system. The wavelet transform in this case shows arguably the most complex behaviour of all three examples. There are two clear lower modes, of approximately 14.5 and 9.6 day periods, with clear time-variability. However, at shorter periods, the modes become so time-variable and similar that they are difficult to distinguish. Such a situation is another reason to next check for harmonic relations between potential modes using a harmonic finder, which will help to identify what the independent modes are, even despite their time-variability. These lower modes can be seen from other solar wind wavelet analysis investigations, such as in [222]. The higher modes however are less evident and studied, with most attention being shown to much longer periods more on the timescale of the solar period of 11 years. In the bispectrum however, there is shown to be significant potential interactions between these faster modes, and even these modes and the slower ones, that could be worth further investigation. Indeed, while other wavelet-based approaches have been used, the use of PSDs to identify solar wind events and mechanisms is widespread [223–225]. In the case

Table 4.1: How different types of processes within a system may be identified as being deterministically functional versus being noise, when their manifestation as components in a time-series is analysed from the perspective of the classical framework versus from the perspective of our framework. As has been evidenced in this paper, typical power-spectral density methodology based on the classical framework may fail to distinguish the manifestation of prominent forced oscillatory processes in a time-series from the manifestation of classical noise-emergence mechanisms.

Component	Appearance in traditional framework	Appearance in our framework
Isolated small collection of oscillatory processes	Determinism	Determinism
Forced small collection of oscillatory processes	Noise	Determinism
Net effect of immeasurably many independent microscopic influences	Noise	Noise

of Fig. 4.11, we see once again that the PSD gives no indication of the complexities identified in the wavelet transform and bispectrum, instead presenting a profile very similar to pink noise. Hence adopting a solely or predominantly PSD approach could again lead to missing potentially key aspects of solar wind dynamics.

In all three examples, we have also included the multiscale sample entropy. This does appear to indicate that our three examples, in the order that we have presented them, are of increasing complexity; and this would seem to agree with the pictures indicated by the wavelet transforms. Still, we would not have been able to arrive at a basic description of what is going on in each of these examples if we had not employed time-resolved methods such as the wavelet transform and had instead restricted ourselves to classical-framework methodologies such as power-spectral density and non-time-resolved statistical entropy measures.

We have given three examples of open systems where determinism can be missed or even misidentified as noise under traditional PSD analysis. The time-dependent dynamics at the heart of this mischaracterisation is typical of thermodynamically open systems, where

external forces influence the evolution of the system. These systems are the norm in the natural world, outside of any environment that is not artificially isolated. Therefore, it is essential that a suitably time-resolved framework of analysis is employed when analysing any such system. For one example from the field of biology, there has been much work to include noise in the Hodgkin-Huxley model on an understanding of the behaviour of cells as partially stochastic [45]. However, it may be the case that this complex dynamics could be produced by a model based in the time-dependent theory we have presented here, which may form both a more simple and experimentally accurate model. The advantages of this kind of model over high-dimensional autonomous ones in the context of cellular dynamics have already been demonstrated in [201].

4.5   Summary and conclusion

In this paper, we have shown that

- an ensemble of phase oscillators can produce a "$(1/f^\beta)$-noise-like" mean field time-series without the need for either a larger number of oscillators in the ensemble or the presence of chaotic dynamics, merely as a result of the presence of time-dependence in the parameters of the system (even if this time-dependence occurs on only relatively slow timescales);

- the same mischaracterisability of time-dependent, relatively non-complex, non-chaotic oscillatory dynamics as noise can occur in actual experimentally obtained time-series;

- in both cases, deterministic time-frequency analysis and related methods can be used to gain a picture of what is really going on in the behaviour of the system.

By "noise-like", we mean that the typical basic method of investigating noise in a signal in terms of a roughly linear trend in a log-log plot of a PSD estimate—as used widely by practitioners across the sciences—will yield results that look like white ($\beta = 0$) or pink ($\beta \in (0, 2)$) noise. We have identified and discussed in detail the key mathematical assumptions underlying this approach to investigating noise in a signal, and the key physical assumptions giving rise to those mathematical assumptions, that are fundamentally responsible for the mischaracterisation of relatively simple deterministically functioning

signal components as noise in the numerical and experimental scenarios considered in this paper. In essence, classical power-spectral density is a concept defined within the framework of stationary stochastic processes, whose application to time-series in turn presupposes that deterministic components in the time-series arise from autonomous dynamics, which itself in turn is the mathematical modelling assumption corresponding to the physical modelling assumption that the system does not have physical characteristics being modulated over time by external influences.

By contrast, systems throughout nature are thermodynamically open, exchanging matter and energy with their environment, and thus are bound to have temporally modulating characteristics. Starting from this observation, we have built a fairly general conceptual framework for describing the dynamics of thermodynamically open complex systems, in terms of non-autonomous finite-time oscillatory dynamics, represented by Eqs. (4.9)–(4.10). We have shown how deterministic time-frequency analysis can naturally arise as the appropriate methodology for analysing time-series generated by dynamics for which our framework is suitable; and we have both (a) used our framework to generate the numerical time-series in Sec. 4.3, and (b) in the inverse direction, used the experimental time-series in Sec. 4.4 to derive preliminary models within our framework, all towards illustrating what is learnt by deterministic time-frequency analysis that is profoundly obscured by classical PSD analysis (along with the entire rest of the toolbox of time-series analysis methods based on the assumption that the time-series comes from a stationary stochastic process). As discussed in some detail within Secs. 4.2.4 and 4.2.6, merely generalising the classical framework of parameter-estimation for stationary stochastic processes to that of time-dependent-parameter-estimation for nonstationary stochastic processes is not the appropriate treatment for time-series coming from general open systems.

The contrast between how signal components may be characterised when analysed by traditional PSD analysis as motivated by the classical framework for dynamical systems and their output time-series, versus when analysed by time-frequency analysis as motivated by our framework of finite-time non-autonomous oscillatory dynamics, is summarised in Table 4.1. In conclusion, as we have evidenced through numerics and experimental time-series data, apparent "noise to be filtered out" in a signal may provide crucial insight

into the deterministic properties of a system when analysed by methods that explicitly resolve the dimension of the progression of time such as time-frequency analysis and other methods described in, e.g., [207] and references therein.

4.6   Acknowledgements

4.7 Data availability

The wavelet transform and wavelet bispectrum analyses can be conducted using the Multiscale Oscillatory Dynamics Analysis (MODA) toolbox found at https://github.com/luphysics/MODA [211]. The source of the data in Fig. 4.9 is https://check-for-flooding.service.gov.uk/river-and-sea-levels, and the OMNI data analysed in Fig. 4.11 were obtained from the GSFC/SPDF OMNIWeb interface at https://omniweb.gsfc.nasa.gov.

4.8 Appendix

In this section we provide additional analysis of numerical time-series, based on the investigation presented in the rest of this chapter. Primarily, these analyses concern the variation of parameters of the analysis tools themselves, conducted to ensure that the previous figures were produced with the appropriate parameters.

First, in Fig. 4.12, we demonstrate the impact of the initial phases of the oscillators on the power-spectral density, in particular its gradient. In the previous sections the phases of each oscillator in an ensemble were set to be equidistant from one another around the circle from 0 to 2π. This results in every system initialising in a maximally disordered state. In Fig. 4.12, from left to right, we investigate whether initialising all phases at 0, π or a random number between 0 and 2π, generated by the Matlab function rand that draws from a uniform distribution, has a significant impact on the eventual PSD. These hence represent states of maximal order, in the first two cases, and a state most likely in between maximal order and disorder for the latter. Fig. 4.12 shows very little change between each of these cases, certainly not to the extent of changing the colour of the noise it represents, or whether it appears noise-like at all.

In Fig. 4.13 we investigate the quantity of zero padding added to the time-series in order that the PSD can accurately and consistently estimate the power content spectrum, as was briefly discussed earlier. In previous PSD estimations, enough zeros have been symmetrically added to the time-series that the new length of the time-series is double the next power of two of the original length, which is represented by the bottom row of Fig. 4.13. In the middle row, we add just enough zeros that the new length is
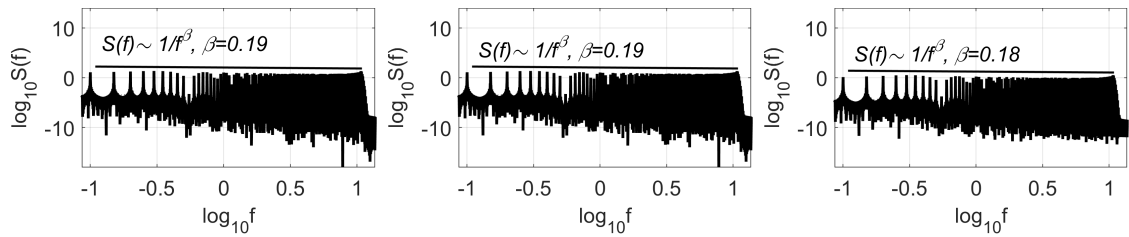
Figure 4.12: The role of initial phases. The power-spectral density is calculated for $n = 10$ oscillators described by the equation $f(t) = 5.05$ Hz $+4.95$ Hz $\sin{(0.1\pi t)}$ for three different methods of assigning the initial phases of the oscillators. From left to right: all equal to 0, all equal to π and each as a different random number between 0 and 2π generated by the Matlab function rand that draws from a uniform distribution, as opposed to being set equidistantly from one another between 0 and 2π.

the next power of two of the original, and in the top row no padding is added. The PSDs shown in the left hand column are averages of the PSDs of 100 time-series, each integrated from the same equation, but with randomised initial phases between 0 and 2π. In the right hand column, the standard deviation of these sets of PSDs is shown at each frequency. This shows a significant difference in the average power-spectral density between no and first and second next power zero-padding, and a higher standard deviation at lower frequencies in the former, though also somewhat lower at higher frequencies. This is evident to the extent of changing the colour of the noise suggested by the PSD gradient. There is little difference in either the average or the standard deviation between the first and second next powers however, indicating that first next power zero-padding may provide sufficient stability in these estimations. Out of abundance of caution, nevertheless, second next power zero-padding is used for all other PSD estimations in this chapter.

Next, we consider the parameters of the autocorrelation function. Fig. 4.14 varies the size of the windows that the correlation is calculated between. This variation increases and decreases from the period of non-autonomous modulation, which is the longest of the fundamental periods in the model. We see in the top row, as the window is reduced from right to left, below a single period of the modulation, there are significant changes in the profile and magnitude of the correlation. This is in contrast to the bottom row, where the window increases in multiples of the modulation period and there is no discernable

163
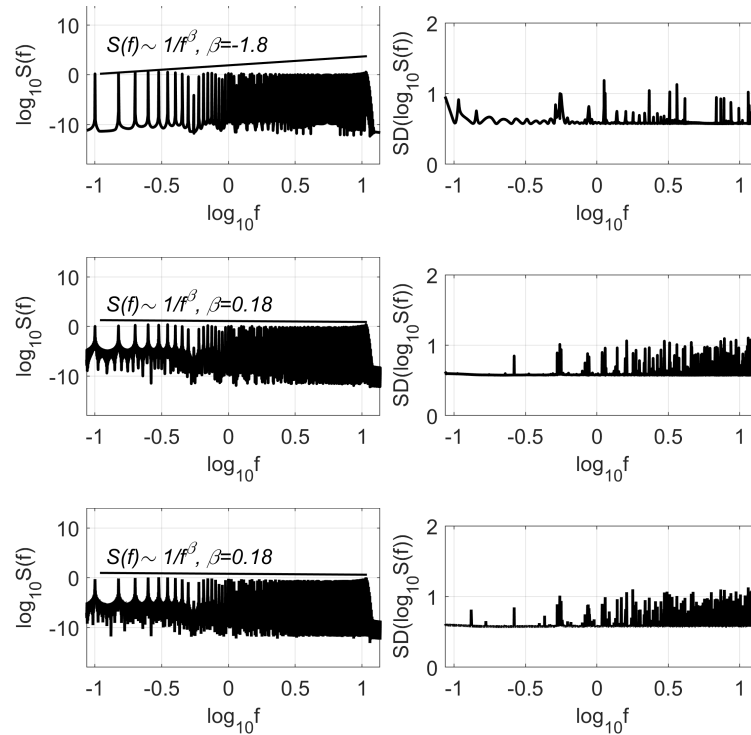
Figure 4.13: Role of zero-padding in the estimation of the power-spectral density. The power-spectral density is calculated for $n = 10$ oscillators described by the equation $f(t) = 5.05$ Hz $+4.95$ Hz $\sin{(0.1\pi t)}$, for three different zero-padding methods. From top to bottom, no zero-padding, the time series consists of t/h points, where $t = 6000s$ is the length of the simulation, and $h = 0.001$ is the numerical integration step, zero-padding to the first next power of 2 of t/h, and finally zero-padding to the second next power of 2 of t/h. On the left hand side are the average of the power-spectral densities of 100 simulated time series, each with different randomly selected initial oscillator phases between 0 and 2π. On the right hand side are the standard deviations of these 100 power-spectral densities.
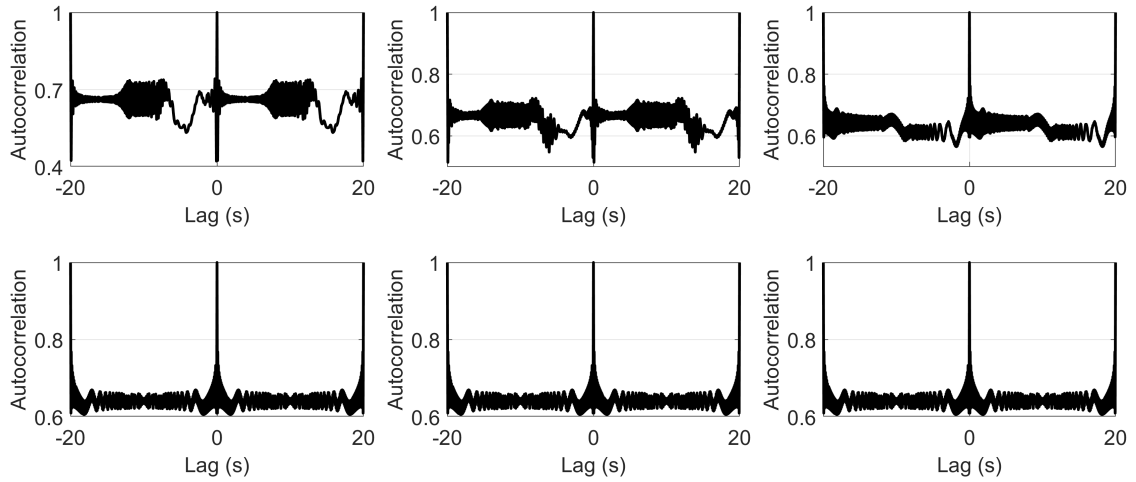
Figure 4.14: The role of the window length in the calculation of the autocorrelation. $n = 10$ oscillators with the equation $f(t) = 5.05$ Hz $+ 4.95$ Hz $\sin(0.1\pi t)$ are simulated. The window length of the autocorrelation function is set to, from left to right, bottom to top, $L = 0.125 \cdot \frac{1}{0.05}$ s, $0.25 \cdot \frac{1}{0.05}$ s, $0.5 \cdot \frac{1}{0.05}$ s, $\cdot \frac{1}{0.05}$ s, $4 \cdot \frac{1}{0.05}$ s, $6 \cdot \frac{1}{0.05}$ s.

change in the correlation. The symmetry between these cases is also transformed; in the latter the correlation is reflectively symmetrical about 0 lag, and in the former it is translationally symmetrical. This suggests that one of the most important factors in determining the correlation of this kind of system is whether the window is an integer or non-integer multiple of the various periods of the model.

The impact of the range of lags of the autocorrelation that is calculated is more predictable. As fewer lags are calculated, the changes from lag to lag can become clearer, but as more lags are included, longer-timescale features can be unveiled. In particular, in Fig. 4.15, spikes to a correlation of 1 appear at each lag equal to the period of the modulation, potentially revealing the existence of this periodicity, but are of course only visible if these lags are included.

Finally, we examine the variation of two parameters of the wavelet bispectrum calculations. First, a range of resolution frequencies is compared in Fig. 4.16. At reduced values of the resolution frequency, the biamplitude peaks become less well localised in frequency-frequency space, occupying a greater area in the graph. At higher frequencies however, the calculation of the bispectrum takes increasingly long times and consumes more computational resources, and hence a compromise is required.
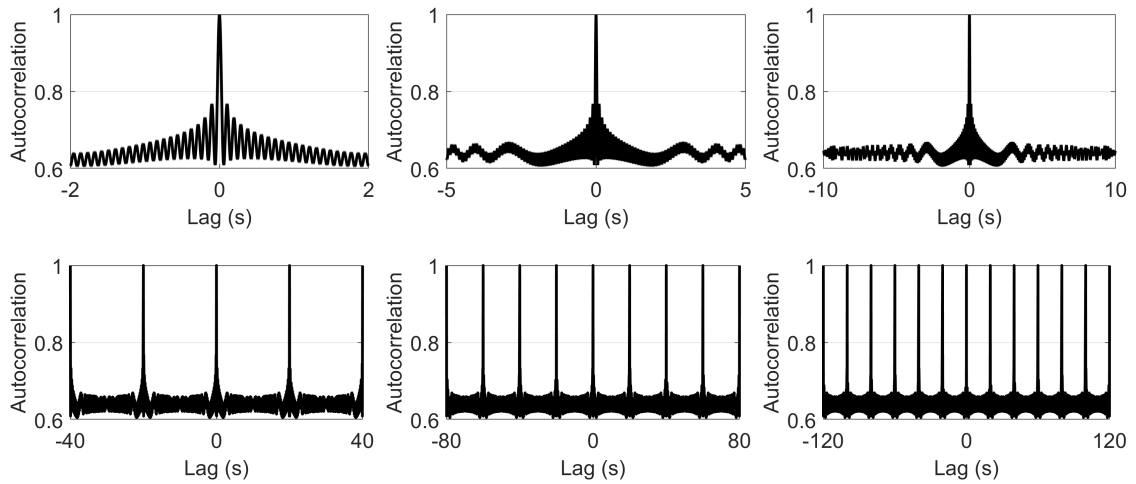
Figure 4.15: The role of the range of lags in the calculation of the autocorrelation. $n = 10$ oscillators with the equation $f(t) = 5.05\text{ Hz} + 4.95\text{ Hz}\sin(0.1\pi t)$ are simulated. The window length of the autocorrelation function is set to 10 s, and the range of lags, from left to right, bottom to top, is $0.125 \cdot \frac{1}{0.05}$ s, $0.25 \cdot \frac{1}{0.05}$ s, $0.5 \cdot \frac{1}{0.05}$ s, $2 \cdot \frac{1}{0.05}$ s, $4 \cdot \frac{1}{0.05}$ s, $6 \cdot \frac{1}{0.05}$ s.
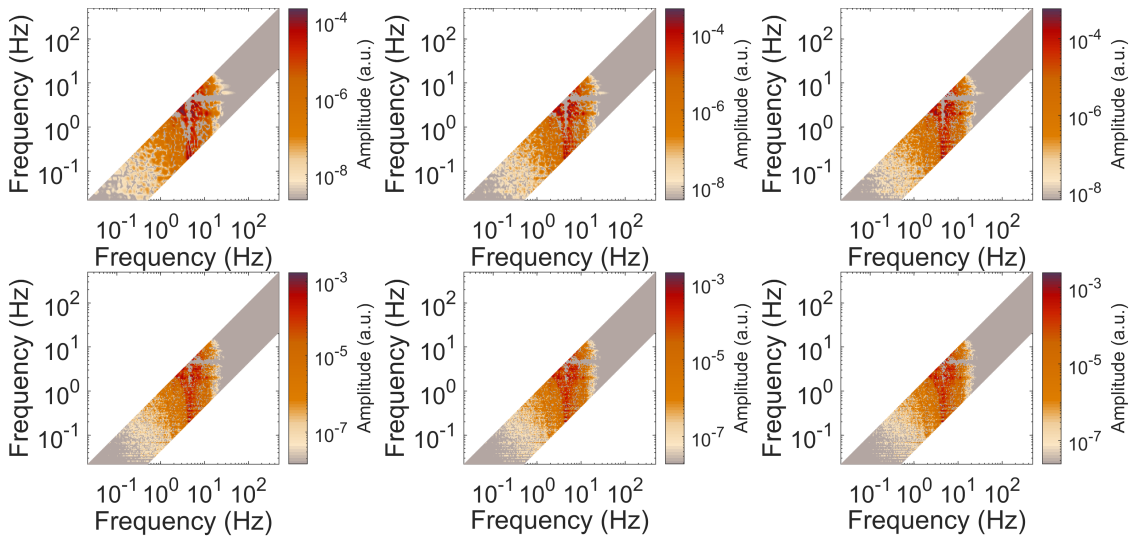
Figure 4.16: The role of the resolution frequency in the wavelet bispectrum. Considered for the model of Fig. 4.6(b), from left to right, top to bottom, a resolution frequency of $2, 3, 4, 6, 7, 8$ was used, rather than 5 as in Fig. 4.6(b).
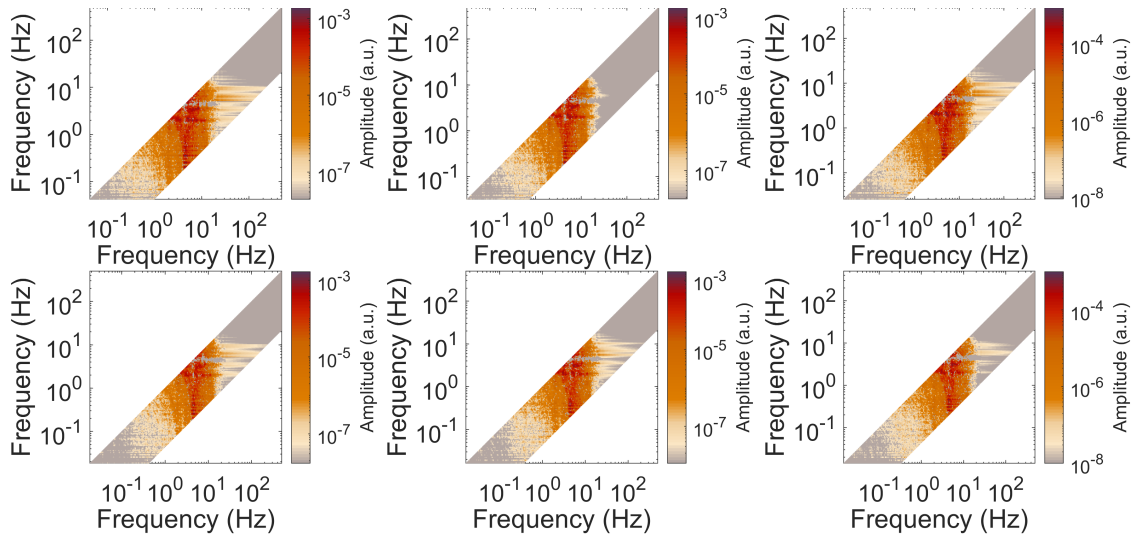
Figure 4.17: The role of the length of the time series from which the wavelet bispectrum is calculated. Considered for the model of Fig. 4.6(b), from left to right, top to bottom, the length of the time-series is 120 s, 160 s, 200 s, 280 s, 320 s, 360 s, rather than 240 s as in Fig 4.6.

The variation of the length of the time-series from which the wavelet bispectrum is calculated, shown in Fig. 4.17, shows less predictable, linear change than the variation of the resolution frequency. Between most of the different series lengths there appears to be a little, but not very significant, change, but this change does not appear to follow a particular pattern. The most pronounced change appears to be when the length of the time-series is 200 s, in the middle of the top row of Fig. 4.17, which is the only one that does not have biamplitude peaks spread across the higher frequencies of the x-axis between 1 and 10 Hz on the y-axis. There is, again, no obvious reason why this particular period should have such a difference to the others. Therefore, without any predictability to the effects of varying the length of the time-series established, in Fig. 4.6 240 s was used. This provided 12 periods of the modulation frequency and ensured the calculations were still computationally feasible.

4.8.1 Discrete Fourier transform

Estimating the Fourier transform of a discrete time-series inevitably involves the numerical calculation of the discrete Fourier transform, which is what we have applied in this Chapter. This is defined as

$$\mathcal{F}_j = h \sum_{k=0}^{n-1} x_k e^{-\frac{2\pi i k j}{n}}, \tag{4.27}$$

where n is the number of points in a time-series $x(t)$, and h is the time step separating the points of $x(t)$. Traditionally, this computation would require n^2 calculations. This was significantly improved upon with the introduction of the fast Fourier transform, which was used in this Chapter. This reduces the number of calculations to $n \log_2 n$ through the observation that transform can be computed as the sum of the transform of even points and odd points, like so

$$\mathcal{F}_j = \sum_{k=0}^{\frac{n}{2}-1} x_{2k} e^{\frac{2\pi i j k}{n/2}} + \sum_{k=0}^{\frac{n}{2}-1} x_{2k+1} e^{\frac{2\pi i j k)}{n/2}},$$
$$= \mathcal{F}_j^e + W_j F_j^o, \tag{4.28}$$

where $\mathcal{F}_j^e$ is the jth component of the Fourier transform of the even points of $x(t)$, F_j^o the corresponding transform of the odd points, and W_j the jth components of $W = e^{2\pi i n}$. This can be applied recursively to split the transform into odds and evens of length $\frac{n}{2}$, then into four odds and evens of length $\frac{n}{4}$ and so on. The recombination of each pair of this factorisation requires n operations, and given there will be $\log_2 n$ combinations, we obtain a total number of calculations of the order $n \log_2 n$, far fewer than n^2. This factorisation is optimal if n is a power of 2, and hence the efficiency and reliability of the algorithm is increased if $x(t)$ is padded with zeros up to the next power of 2, as we have done in this Chapter.

The performance of the Fourier transform, in its aim of identifying the spectral properties of the time-series analysed in this Chapter, may be improved via the application of windows. Windows apply the Fourier transform over only an interval of the time-series defined by the window's shape, which may take a variety of forms. The aim of windowing in this application would be to attempt to limit the extent of spectral leakage in the calculated Fourier transforms. Spectral leakage is the introduction of frequency components, which may cause the 'real' frequency components of the analysed signal to become hard to distinguish. In a worst case scenario, this therefore may lead to the

transform appearing noise-like through all of its frequency components becoming indistinguishable. A consideration of appropriate windows in the calculation of the Fourier transform may therefore be required to ensure that the noise-like spectrum of the analysis is inevitable, and not a product of preventable spectral leakage.

5. Summary and conclusions

5.1 Summary

The work presented in this thesis combined the study of non-autonomous processes, networks of processes and finite-time analysis of data to model far from equilibrium behaviour in thermodynamically open living systems. We have paid particular attention to the open question of how these systems can be best treated, and compared the approach we have developed here to the commonly applied frameworks of autonomous deterministic dynamics and random noise.

In Chapter 1, we introduced the topic of the thesis and outlined the background that underpins it. First and foremost, the concepts of autonomous and non-autonomous systems were introduced, which form the mathematical basis of our models, and the concepts of stability and synchronisation, which are essential to their ability to reflect the behaviour of living systems. Next, the motivation behind statistical physics was discussed, as well as the theories of ergodicity and stationarity, which form the crux of the difference between the finite-time and statistical approaches to analysis. Then, the relevance of thermodynamics to the dynamics of living systems was outlined, and we explained why we consider them to be thermodynamically open. The challenges of far from equilibrium behaviour that characterises these systems was discussed in the context of two major contributions to the field, synergetics and dissipative structures, and their overlaps with the theory we further developed here. The idea of complexity and its links to deterministic and stochastic dynamics was discussed, as well as random noise, which is explored further in Chapter 4. Then, the theory behind the numerical methods that we used was laid out. Finally, we discussed significant recent advancements and

contributions in the two core fields this thesis concerns — non-autonomous dynamical systems and network science.

In Chapter 2 a model for the energy metabolism of cells was introduced, consisting of inter-coupled networks of weighted non-autonomous phase oscillators. The basis of this model in the theory of non-autonomicity and thermodynamic openness, and how this differs to other contemporary models, was explained. The biological motivations and justifications for the choices made in this model were additionally discussed.

In Chapter 3, the model introduced in Chapter 1 was numerically analysed with wavelet phase coherence and Kuramoto order parameter algorithms. This was done both for the full model, and intermediate steps between it and the predecessor model in [138], for equivalent parameters spaces to those analysed in [138]. This provided a picture of the impact of each new element of the model presented here on its dynamics. A direct comparison between numerical outputs of this model and the one developed in [160], representative of more conventional and common biological modelling approaches, was also provided. This comparison was facilitated by analysis of data from the experiment presented in [132], which indicated the natural frequency of glycolysis in HeLa cells.

Finally, in Chapter 4, the framework of finite-time analysis that we based our modelling approaches on, and contributed to over the course of this thesis, was further explained, alongside the existing framework of statistical time-series analysis. Analysis tools based in both of these frameworks were applied to autonomous and non-autonomous oscillator models, and to experimental time-series recorded from thermodynamically open systems.

5.2   Original contributions

- A mathematical model was introduced that combined non-autonomous networks, inter-network coupling, and biologically-motivated intra-network weighted coupling for the first time

- A numerical process for identifying the recently-identified phenomenon of intermittent synchronisation was developed, which does not require user examination of each time-series

- Numerous new, complex synchronisation relations between each element of the model were identified

- A tendency of networked non-autonomous processes to create more stable systems than non-networked ones was identified

- Two fundamental frequency modes, 0.01 Hz and 0.07 Hz, were identified in experimental data of HeLa cells' glycolytic oscillations, the former of which is comparable to findings of the frequency of glycolysis in yeast cells [111, 161]

- The ability of the simple non-autonomous oscillator weighted network model to produce complex dynamics reflective of experimental time-series was demonstrated

- The mean fields of ensembles of non-autonomous oscillators can appear to be $1/f^\beta$ noise in their power-spectral densities, a characteristic tool of the statistical time-series analysis framework, and do so when they consist of only few oscillators. This is in contrast to autonomous ensembles, which appear noisy only when there are many oscillators. This behaviour even persists for non-autonomous oscillators with certain strengths of intra-network coupling

- Experimental time-series also appear to be noisy in the statistical framework, but finite-time analyses can identify informative deterministic frequency modes and couplings in these same series

5.3   Future work

In this thesis we have adopted to approach of analysing numerically generated time-series. This allowed us to assess the dynamics of equations for which the analytical stability is not well understood in a bespoke manner, or search for specific dynamics such as intermittent synchronisation. A comprehensive analytical understanding of the dynamics, however, would be a more powerful tool for predicting the behaviour of any given model. Developing such an understanding may additionally potentially identify dynamics that are not currently known at all. An approach for analytically understanding the stability of 1-dimensional cyclic processes was recently proposed in [58]. This could

provide a pathway to similar results for general n-dimensional processes, and beyond those subject to just slowly varying forcing.

We have also considered two network topologies — simple all-to-all connection of nodes, and weighted all-to-all connection. Further modifications to these may better represent yet further physical systems, and may lead to unknown dynamics. The interactions between topology and dynamics may also be better understood by a methodical investigation to this end. For instance, in [2], it was found that removing node connections can increase the parameter region where synchronisation is possible.

The model developed in Chapters 2 and 3 was done so with the purpose of representing the energy metabolism of a single cell. To model more complex, larger scale processes, extensions would be required. For instance, investigating methods for coupling the entire model to replications of itself could be used to understand the energy metabolism of multi-cellular systems.

The identification between synchronisation regimes of our model and healthy/unhealthy states of the biological system also has expansive potential for analysing pathologies. For instance, this conception of the model as examining energy metabolism could be applied to the brain, in the form of the astrocyte-neuronal lactate shuttle hypothesis [226, 227]. Taking advantage of the transformation to networks could allow variation of the amplitudes of metabolic supplies in this context. The resulting effects on the synchronisation regimes in the model could then be used to assess the contribution of each variation to pathologies such as dementia. This application could be experimentally supported with time-series measurements of brain blood flow for healthy and dementia patients.

Such an approach can be widely applied, beyond just energy metabolism, and even beyond biological systems. This model and data analytical approach can be made relevant to any thermodynamically open system that is characterised by many interacting processes. For instance, NASA has made available near-Earth solar wind magnetic field and plasma parameter data recorded simultaneously by several spacecraft in various different orbits [217]. This could be analysed to understand better the frequency the frequency dynamics of the solar wind and the atmospheric phenomena it gives rise to, and its

spatial and temporal variations. The resulting interactions in the Earth's atmosphere may then also be understood through application of the model we have proposed.

Ca^{2+} oscillations that occur in the cytosol of cells appear to be a robustly oscillating process that provides crucial regulation and communication to myriad cellular processes. This communication is thought to be hugely variable in its purpose, accomplished through significant modulation of both the oscillation frequency and amplitude [228]. This therefore makes it well suited to the application of the non-autonomous oscillator network model. The non-autonomicity of the oscillators allows for easy modulation of oscillatory frequency, while the introduction of networked interactions allow for amplitude modulations.

Finally, we have demonstrated in Chapter 4 that relatively low-dimensional non-autonomous periodic processes can produce high-dimensional dynamics that may be mistaken for noise. One of the implications of this, that also bears relevance to Chapters 1 and 3, is that modelling of experimental data that contains 'noise' could be done entirely deterministically. Developing such models could further reinforce the need to consider deterministic origins of 'noise', and provide much more information about the studied system than current noise-based approaches.

Glossary and Notation

Glossary

Autonomous dynamical system An individual or set of differential equations that do not explicitly depend on time, describing a system that is time-independent

Chronotaxic systems Driven non-autonomous dynamical systems that are stabilised against perturbations

Coherence A measure of the constancy of the relationship between two periodic processes

Dynamical equilibrium A state defined by a set of state variables from which the system will not deviate unless perturbed

Extended phase space The phase space of a system, including time

Finite-time analysis The approach of analysing a dynamical system over a finite interval of time

Harmonic A periodic component whose frequency is an integer multiple of the frequency of a different periodic component

Intermittent synchronisation The phenomenon of oscillators obtaining a common frequency at some times but not others, with no addition or subtraction of interactions

Jacobian matrix A matrix of all the first order partial derivatives of a function with respect to its state variables. Where it exists, its determinant may describe the dynamics of the function.

Non-autonomous dynamical system An individual or set of differential equations that explicitly depends on time, describing a system that is time-dependent

Nyquist frequency The maximum frequency that can be accurately represented by a discrete time-series, which is half the sampling frequency

Permanent synchronisation The phenomenon of oscillators obtaining a common frequency at all times

Phase The position of a process in its repeating cycle

Phase space The space of all the state variables of a system

Sampling frequency The frequency at which recordings are made in a discrete time-series

State variable A variable necessary to describe the behaviour of a system

Steady state A certain state of a dynamical system that does not change in time

Thermodynamically closed system A system that allows energy but not matter to cross its boundaries

Thermodynamically isolated system A system that allows neither energy nor matter to cross its boundaries

Thermodynamically open system A system that allows both energy and matter to cross its boundaries

Thermodynamic equilibrium A state between two or more systems where there is no net flow of energy or matter

Notation

$\dot{x}$ The derivative of the state variable(s) x with respect to time

x A set of state variables

t Time

F A continuous vector field

$\{X_t\}$ A set of random variables X_t

X_t A random variable indexed at time t

J The Jacobian matrix

x_f A set of fixed points of the state variables x

θ A phase

ω A natural frequency

ϵ A coupling strength to an external driver

ϕ A phase difference

F A coupling strength between two oscillators or networks

K An internal coupling strength of an oscillator network

r The Kuramoto order parameter

Ψ The mean phase of an oscillator network

x_0 A set of initial conditions of the state variables x

t_0 The initialisation time of a system

W_{ij} The weighting strength on the interaction between a phase oscillator indexed i and one indexed j

Bibliography

[1] Suprunenko YF, Clemson PT, Stefanovska A. Chronotaxic Systems: A New Class of Self-Sustained Nonautonomous Oscillators. Phys Rev Lett. 2013;111(2):024101.

[2] Lucas M, Fanelli D, Stefanovska A. Nonautonomous driving induces stability in network of identical oscillators. Phys Rev E. 2019;99(1):012309.

[3] Kuramoto Y. Self-entrainment of a population of coupled non-linear oscillators. In: Araki H, editor. Lecture Notes in Physics. vol. 39. New York: Springer; 1975. p. 420-2.

[4] Strogatz SH. Nonlinear Dynamics And Chaos. Boulder: Westview Press; 2001.

[5] Pikovsky A, Rosenblum M, Kurths J. Synchronization – A Universal Concept in Nonlinear Sciences. Cambridge: Cambridge University Press; 2001.

[6] Kuramoto Y. Chemical Oscillations, Waves, and Turbulence. Berlin: Springer-Verlag; 1984.

[7] Boccaletti S, Latora V, Moreno Y, Chavez M, Hwang DU. Complex networks: Structure and dynamics. Phys Rep. 2006;424(4):175-308.

[8] Kloeden PE, Rasmussen M. Nonautonomous Dynamical Systems. New York: AMS Mathematical Surveys and Monographs; 2011.

[9] Blair RH, Trichler DL, Gaille DP. Mathematical and statistical modeling in cancer systems biology. Front Physio. 2012;3:227.

[10] Bose I. Emergent phenomena in living systems: A statistical mechanical perspective. J Biosci. 2022;47(2):22.

[11] Ghosh A, Spakowitz AJ. Statistical behavior of nonequilibrium and living biological systems subjected to active and thermal fluctuations. Phys Rev E. 2022;105(1):014415.

[12] Fodor E, Marchetti MC. The statistical physics of active matter: From self-catalytic colloids to living cells. Phys A: Stat Mech Appl,. 2019;504:106-20.

[13] Kondepudi D, Prigogine I. Modern Thermodynamics: From Heat Engines to Dissipative Structures. New York: John Wiley & Sons, Incorporated; 2014.

[14] Onsager L. Reciprocal Relations in Irreversible Processes. I. Phys Rev. 1931;38:2265.

[15] Progogine I. Time, Structure and Fluctuations; 1977. Available from: https://www.nobelprize.org/prizes/chemistry/1977/prigogine/lecture/.

[16] Prigogine I. What is entropy? Naturwissenschaften. 1989;76:1-8.

[17] Nicolis G, Prigogine I. Self-organization in nonequilibrium systems. New York: Wiley; 1977.

[18] Haken H. Cooperative phenomena in systems far from thermal equilibrium and in nonphysical systems. Rev Mod Phys. 1975;47:67-121.

[19] Nicolis G, Nicolis C. Foundations of Complex Systems. World Scientific; 2012.

[20] Simon HA. The Sciences of the Artificial. MIT Press: Cambridge; 1981.

[21] Prigogine I. Exploring complexity. Eur J Oper Res. 1987;30:97-103.

[22] Amaral LAN, Ottino JM. Complex networks. Eur Phys J B. 2000;38:147-62.

[23] Crutchfield JP, Young K. Inferring statistical complexity. Phys Rev Lett. 1989;63:105-9.

[24] Grassberger P. Toward a quantitative theory of self-generated complexity. Int J Theor Phys. 1986;25:907-28.

[25] Kolmogorov AN. Three approaches to the quantitative definition of information. Problems of Information Transmission. 1965;1:1-17.

[26] Bennett CH. In: Herken R, editor. Logical depth and physical complexity. Oxford: Oxford University Press; 1988. p. 227-57.

[27] Lloyd S, Pagels H. Complexity as thermodynamic depth. Annals of Physics. 1988;188:186-213.

[28] Ladbury JE, Arold ST. Noise in cellular signaling pathways: causes and effects. Trends Biochem Sci. 2012;37(5):173-8.

[29] Howard R. Pervasive randomness in physics: an introduction to its modelling and spectral characterisation. Contemp Phys. 2017;58(4):303-30.

[30] Réfrégier P. Noise Theory and Application to Physics: From Fluctuations to Information. Springer New York; 2004.

[31] Milotti E. The Physics of Noise. Morgan & Claypool Publishers; 2019.

[32] Kasdin NJ. Discrete Simulation of Colored Noise and Stochastic Processes and $1/f^\alpha$ Power Law Noise Generation. Proc IEEE. 1995;83:802-27.

[33] Engelberg S. Random Signals and Noise: A Mathematical Introduction. CRC Press Inc; 2006.

[34] Faisal AA, Selen LPJ, Wolpert DM. Noise in the nervous system. Nat Rev Neurosci. 2008;9:292-303.

[35] Horowitz JM, Gingrich TR. Thermodynamic uncertainty relations constrain non-equilibrium fluctuations. Nat Phys. 2020;16(1):15-20.

[36] Colbeck R, Renner R. Free randomness can be amplified. Nat Phys. 2012;8:450-3.

[37] Dobrin MB, Savit CH. Introduction to Geophysical Prospecting. McGraw-Hill; 1988.

[38] Yuan X, Zhou H, Cao Z, Ma X. Intrinsic randomness as a measure of quantum coherence. Phys Rev A. 2015;92:022124.

[39] Parzen E. Modern Probability Theory and Its Applications. John Wiley and Sons; 1960.

[40] Newman JRS, Ghaemmaghami S, Ihmels J, Breslow DK, Noble M, DeRisi JL, et al. Single-cell proteomic analysis of S. cerevisiae reveals the architecture of biological noise. Nature. 2006;441:840-6.

[41] Scales JA, Snieder R. What is noise? Geophysics. 1998;63(4):1122-4.

[42] Britten AJ, Crotty M, Kiremidjian H, Grundy A, Adam EJ. The addition of computer simulated noise to investigate radiation dose and image quality in images with spatial correlation of statistical noise: an example application to X-ray CT of the brain. BJR. 2004;77(916):323-8.

[43] Goldie DJ, Brink PL, Patel C, Booth NE, Salmon GL. Statistical noise due to tunneling in superconducting tunnel junction detectors. Appl Phys Lett. 1994;64:3169.

[44] Nicolis C. Solar variability and stochastic effects on climate. Sol Phys. 1981;74:473-8.

[45] Goldwyn JH, Shea-Brown E. The What and Where of Adding Channel Noise to the Hodgkin-Huxley Equations. PLoS Comput Biol. 2011;7(11):e1002247.

[46] Einstein A. Uber die von der molekularkinetischen theorie der wärme geforderte bewegung von in ruhenden flüssigkeiten suspendierten teilchen. Ann Phys. 1905;322:549.

[47] Cencini M, Falcioni M, Olbrich E, Kantz H, Vulpiani A. Chaos or noise: Difficulties of a distinction. Phys Rev E. 2000;62(1):427-37.

[48] Battiston F, Amico E, Barrat A, Bianconi G, de Arruda GF, Franceschiello B, et al. The physics of higher-order interactions in complex systems. Nat Phys. 2021;17(10):1093-8.

[49] Casdagli M. Chaos and deterministic versus stochastic non-linear modelling. J R Statist Soc B. 1992;54:303-28.

[50] Gaspard P. Cycles, randomness, and transport from chaotic dynamics to stochastic processes. Chaos. 2015;25:097606.

[51] Gaspard P, Briggs ME, Francis MK, Sengers JV, Gammon RW, Dorfman JR, et al. Experimental evidence for microscopic chaos. Nature. 1998;394:865-8.

[52] Kelly D, Melbourne I. Deterministic homogenization for fast-slow systems with chaotic noise. J Funct Anal. 2017;272:4063.

[53] Grassberger P. In: Atmanspacher H, editor. Information and Complexity Measures in Dynamical Systems. Boston, MA: Springer; 1991. p. 15-33.

[54] Shannon CE. A mathematical theory of communication. Bell Syst Tech J. 1948;27(3):379-423.

[55] Yaneer BY. Dynamics of Complex Systems. Addison–Wesley; 1997.

[56] Costa M, Goldberger AL, Peng CK. Broken asymmetry of the human heartbeat: Loss of time irreversibility in aging and disease. Phys Rev Lett. 2005;95:198102.

[57] Courtiol J, Perdikis D, Petkoski S, Müller V, Huys R, Sleimen-Malkoun R, et al. The multiscale entropy: Guidelines for use and interpretation in brain signal analysis. J Neurosci Methods. 2016;273:175-90.

[58] Newman J, Lucas M, Stefanovska A. Stabilization of cyclic processes by slowly varying forcing. Chaos. 2021;31:123129.

[59] Nyquist H. Certain topics in telegraph transmission theory. Trans AIEE. 1928;47:617-44.

[60] Shannon CE. Communication in the presence of noise. Proc IRE. 1949;37(1):10-21.

[61] Epperson JF. An Introduction to Numerical Methods and Analysis. Wiley; 2021.

[62] Shampine LF, Reichelt MW. The Matlab ODE Suite. SIAM J Sci Comput. 1997;18(1):1-22.

[63] Newman J, Pidde A, Stefanovska A. Defining the wavelet bispectrum. Appl Comput Harmon Anal. 2021;51:171-224.

[64] Lancaster G, Iatsenko D, Pidde A, Ticcinelli V, Stefanovska A. Surrogate data for hypothesis testing of physical systems. Phys Rep. 2018;748:1-60.

[65] England JL. Dissipative adaptation in driven self-assembly. Nat Nanotechnol. 2015;10(11):919-23.

[66] Crooks GE. Entropy production fluctuation theorem and the nonequilibrium work relation for free energy differences. Phys Rev E. 1999;60(11):2721.

[67] Herpich T, Cossetto T, Falasco G, Esposito M. Stochastic thermodynamics of all-to-all interacting many-body systems. New J Phys. 2020;22:063005.

[68] Ali MM, Huang WM, Zhang WM. Quantum thermodynamics of single particle systems. Sci Rep. 2020;10:13500.

[69] Kosloff R. Quantum thermodynamics and open-systems modeling. J Chem Phys. 2019;150:204105.

[70] Manzano G, Zambrini R. Quantum thermodynamics under continuous monitoring: A general framework. AVS Quantum Sci. 2022;4:025302.

[71] Valente D, Brito F, Werlang T. Quantum dissipative adaptation. Commun Phys. 2021;4(11):1-8.

[72] Delvenne JC, Sandberg H. Dissipative open systems theory as a foundation for the thermodynamics of linear systems. Phil Trans R Soc A. 2017;375:20160218.

[73] van der Schaft A. In: Sanz-Solé M, Soria J, Varona JL, Verdadera J, editors. Port-Hamiltonian systems: an introductory survey. EMS Press; 2007. p. 1339—1365.

[74] Zhang X, Lu Z, Yuan X, Wang Y, Shen X. L2-Gain Adaptive Robust Control for Hybrid Energy Storage System in Electric Vehicles. IEEE Trans Power Electron. 2021;36(6):63-73.

[75] Wang ZM, Zhao X, Li X, Wei A. Finite-time adaptive control for uncertain switched port-controlled Hamiltonian systems. Commun Nonlinear Sci Numer Simul. 2023;119:107129.

[76] Menara T, Baggio G, Bassett D, Pasqualetti F. Functional control of oscillator networks. Nat Commun. 2022;13(0):4721.

[77] Yuvan S, Bier M. Synchronisation and Coupled Oscillators — Phase Transitions and Entropy Production. In: Stefanovska A, McClintock PVE, editors. Physics of Biological Oscillations. Cham: Springer, Cham; 2021. p. 131-49.

[78] Strogatz SH. From Kuramoto to Crawford: exploring the onset of synchronization in populations of coupled oscillators. Physica D. 2000;143:1-20.

[79] Cheban DN, Kloeden PE, Schmalfuss B. The relationship between pullback, forward and global attractors of nonautonomous dynamical systems. Nonlinear Dyn Syst Theory. 2002;2:125-44.

[80] Rasmussen M. Attractivity and Bifurcation for Nonautonomous Dynamical Systems. Berlin: Springer; 2007.

[81] Kloeden PE, Yang M. Introduction to Nonautonomous Dynamical Systems and their Attractors. Singapore: World Scientific Publishing Co. Inc.; 2021.

[82] Kloeden PE, Lorenz T. Bohner M, Ding Y, Dosly O, editors. Pullback and forward attractors of nonautonomous difference equations. Springer Heidelberg; 2014.

[83] Kloeden PE, Lorenz T. Construction of nonautonomous forward attractors. Proc Amer Mat Soc. 2016;144(1):259-68.

[84] Fenichel N. Persistance and Smoothness of of Invariant Manifolds for Flows. Indiana Univ Math J. 1972;21(3):193-226.

[85] Gin AH. Aperiodically forced oscillators. University of Warwick; 2013.

[86] Doan TS, Karrasch D, Nguyen TY, Siegmund S. A unified approach to finite-time hyperbolicity which extends finite-time Lyapunov exponents. J of Diff Equations. 2012;252(10):5535 5554.

[87] MacKay RS. Normal Hyperbolicity for Non-autonomous Oscillators and Oscillator Networks. In: Stefanovska A, McClintock PVE, editors. Physics of Biological Oscillations. Cham: Springer, Cham; 2021. p. 71-85.

[88] Karrasch D. Linearization of hyperbolic finite-time processes. J Differ Equ. 2013;254(1):256-82.

[89] Stefanovska A, Clemson PT, Suprunenko YF. In: Wunner G, Pelster A, editors. Introduction to Chronotaxic Systems – Systems Far from Thermodynamics Equilibrium that Adjust Their Clocks. Springer, Cham; 2016. p. 227-46.

[90] Shadden SC, Lekien F, Marsden JE. Definition and properties of Lagrangian coherent structures from finite-time Lyapunov exponents in two-dimensional aperiodic flows. Physica D. 2005;212:271-304.

[91] Lekien F. Lagrangian coherent structures in n-dimensional systems. J Math Phys. 2007;48:065404.

[92] Ndour M, Padberg-Gehle K, Rasmussen M. Spectral Early-Warning Signals for Sudden Changes in Time-Dependent Flow Patterns. Fluids. 2021;6(2):49.

[93] Krishna K, Song Z, Brunton SL. Finite-horizon, energy-efficient trajectories in unsteady flows. Proc R Soc A. 2022;478(2258):20210255.

[94] Haller G. Lagrangian Coherent Structures. Annu Rev Fluid Mech. 2015;47:137-62.

[95] Haller G. A variational theory of hyperbolic Lagrangian Coherent Structures. Phys D: Nonlinear Phenom. 2011;240(7):574-98.

[96] Lucas M, Newman J, Stefanovska A. Stabilization of dynamics of oscillatory systems by nonautonomous perturbation. Phys Rev E. 2018;97:042209.

[97] Mazuski C, Herzog ED. Circadian rhythms: to sync or not to sync. Curr Biol. 2015;25(8):R337-9.

[98] Newman J, Lucas M, Stefanovska A. Non-asymptotic-time Dynamics. In: Stefanovska A, McClintock PVE, editors. Physics of Biological Oscillations. Cham: Springer, Cham; 2021. p. 111-29.

[99] Stefanovska A, Bračič M. Physics of the human cardiovascular system. Contemp Phys. 1999;40(1):31-55.

[100] Kraikivski P. In: Kraikivski P, editor. Glycolytic Oscillations. Springer, Cham; 2021. p. 59—68.

[101] Chandra FA, Buzi G, Doyle JC. Glycolytic Oscillations and Limits on Robust Efficiency. Science. 2011;333(6039):187-92.

[102] Duysens LNM, Amesz J. Fluorescence spectrophotometry of reduced phosphopyridine nucleotide in intact cells in the near-ultraviolet and visible region. Biochim Biophys Acta. 1957;24:19-26.

[103] Hauser MJB. Synchronisation of glycolytic activity in yeast cells. Curr Genet. 2022;68(1):69-81.

[104] Goldbeter A. Biochemical Oscillations and Cellular Rhythms. Cambridge University Press; 1996.

[105] Kennedy RT, Kauri LM, Dahlgren GM, Jung S. Metabolic Oscillations in beta-Cells. Diabetes. 2002;51(1):S152-61.

[106] Ainscow EK, Rutter GA. Glucose-Stimulated Oscillations in Free Cytosolic ATP Concentration Imaged in Single Islet β-Cells: Evidence for a Ca^{2+}-Dependent Mechanism. Diabetes. 2002;51(1):S162-70.

[107] Jung S, Kauri LM, Qian W, Kennedy RT. Correlated Oscillations in Glucose Consumption, Oxygen Consumption, and Intracellular Free Ca2+ in Single Islets of Langerhans. J Biol Chem. 2000;275(9):6642-50.

[108] Betz A, Chance B. Phase relationship of glycolytic intermediates in yeast cells with oscillatory metabolic control. Archives of Biochemistry and Biophysics. 1965;109(3):585-94.

[109] Ganitkevich V, Mattea V, Benndorf K. Glycolytic oscillations in single ischemic cardiomyocytes at near anoxia. J Gen Physiol. 2010;135(4):307-19.

[110] Olsen LF, Andersen AZ, Lunding A, Brasen JC, Poulsen AK. Regulation of glycolytic oscillations by mitochondrial and plasma membrane H$^+$-ATPases. Biophys J. 2009;96(9):3850-61.

[111] Olsen LF, Stock RP, Bagatolli LA. Glycolytic oscillations and intracellular K+ concentration are strongly coupled in the yeast Saccharomyces cerevisiae. Arch Biochem Biophys. 2020;681:108257.

[112] Richard P. The rhythm of yeast. FEMS Microbiol Rev. 2003;27(4):547-57.

[113] Ozalp VC, Pedersen TR, Nielsen LJ, Olsen LF. Time-resolved measurements of intracellular ATP in the yeast Saccharomyces cerevisiae using a new type of nanobiosensor. J Biol Chem. 2010;285(48):37579-88.

[114] Thoke HS, Tobiesen A, Brewer J, Hansen PL, Stock RP, Olsen LF, et al. Tight coupling of metabolic oscillations and intracellular water dynamics in Saccharomyces cerevisiae. PLoS ONE. 2015;10(2):e0117308.

[115] Kurz FT, Aon MA, O'Rourke B, Armoundas AA. Spatio-temporal oscillations of individual mitochondria in cardiac myocytes reveal modulation of synchronized mitochondrial clusters. Proc Natl Acad Sci USA. 2010;107(32):14315-20.

[116] Kurz FT, Aon MA, O'Rourke B, Armoundas AA. Wavelet analysis reveals heterogeneous time-dependent oscillations of individual mitochondria. Am J Physiol Heart Circ Physiol. 2010;299(5):H1736-40.

[117] Aon MA, Cortassa S, Marbán E, O'Rourke B. Synchronized whole cell oscillations in mitochondrial metabolism triggered by a local release of reactive oxygen species in cardiac myocytes. J Biol Chem. 2003;278:44735—44744.

[118] Cortassa S, Sollott SJ, Aon MA. Computational Modeling of Mitochondrial Function from a Systems Biology Perspective. Mitochondrial Bioenergetics Methods in Molecular Biology. 2018;1782:249-65.

[119] Aon MA, Cortassa S, O'Rourke B. Mitochondrial oscillations in physiology and pathophysiology. Adv Exp Med Biol. 2008;641:98-117.

[120] Kohnhorst CL, Kyoung M, Jeon M, Schmitt DL, Kennedy EL, Ramirez J, et al. Identification of a multienzyme complex for glucose metabolism in living cells. J Biol Chem. 2017;292(22):9191-203.

[121] Weber A, Prokazov Y, Zuschratter W, Hauser MJB, Kurths J. Desynchronisation of Glycolytic Oscillations in Yeast Cell Populations. PLoS ONE. 2012;7(9):e43276.

[122] Gustavsson A, van Niekerk DD, Adiels CB, du Preez FB, Goksör M, Snoep JL. Sustained glycolytic oscillations in individual isolated yeast cells. FEBS J. 2012;279(16):2837-47.

[123] Madsen MF, Danø S, Sørensen PG. On the mechanisms of glycolytic oscillations in yeast: Mechanisms of glycolytic oscillations. FEBS Journal. 2005;272(11):2648-60.

[124] Vincent AE, Turnbull DM, Eisner V, Hajnóczky G, Picard M. Mitochondrial Nanotunnels. Trends Cell Biol. 2017;27(11):787-99.

[125] Aon MA, Cortassa S, O'Rourke B. Percolation and criticality in a mitochondrial network. PNAS. 2004;101:4447-52.

[126] Iotti S, Borsari M, Bendahan D. Oscillations in energy metabolism. Biochim Biophys Acta. 2010;1797:1353-61.

[127] Jafri MS. Modeling the mechanism of metabolic oscillations in ischemic cardiac myocytes. Journal of Theoretical Biology. 2006;242(4):801-17.

[128] Tu BP, McKnight SL. Metabolic cycles as an underlying basis of biological oscillations. Nat Rev Mol Cell Biol. 2006;7(9):696-701.

[129] Tu BP, Kudlicki A, Rowicka M, McKnight SL. Logic of the Yeast Metabolic Cycle: Temporal Compartmentalization of Cellular Processes. Science. 2005;310(5751):1152-8.

[130] Bechtel W, Abrahamsen A. Complex Biological Mechanisms: Cyclic, Oscillatory, and Autonomous. Amsterdam: North-Holland; 2011.

[131] Porat-Shliom N, Chen Y, Tora M, Shitara A, Masedunskas A, Weigert R. In Vivo Tissue-wide Synchronization of Mitochondrial Metabolic Oscillations. Cell Reports. 2014;9(2):514-21.

[132] Amemiya T, Shibata K, Itoh Y, Itoh K, Watanabe M, Yamaguchi T. Primordial oscillations in life: Direct observation of glycolytic oscillations in individual HeLa cervical cancer cells. Chaos. 2017;27(10):104602.

[133] O'Rourke B, Ramza BM, Marban E. Oscillations of membrane current and excitability driven by metabolic oscillations in heart cells. Science. 1994;265(5174):962-6.

[134] Chaudhry R, Varacallo M. Biochemistry, Glycolysis. Treasure Island (FL): Stat-Pearls Publishing; 2020.

[135] Wilson DF. Oxidative phosphorylation: regulation and role in cellular and tissue metabolism. The Journal of Physiology. 2017;595(23):7023-38.

[136] Muoio V, Persson PB, Sendeski MM. The neurovascular unit — concept review. Acta Physiologica. 2014;210:790-8.

[137] Carballido-Landeira J, Escribano B. Nonlinear Dynamics in Biological Systems. New York: Springer International Publishing; 2016.

[138] Lancaster G, Suprunenko YF, Jenkins K, Stefanovska A. Modelling chronotaxicity of cellular energy metabolism to facilitate the identification of altered metabolic states. Sci Rep. 2016;6:29584.

[139] Hagos Z, Stankovski T, Newman J, Pereira T, McClintock PVE, Stefanovska A. Synchronisation transitions caused by time-varying coupling functions. Phil Trans R Soc A. 2019;377:20190275.

[140] Strogatz SH, Mirollo RE. Stability of incoherence in a population of coupled oscillators. J Stat Phys. 1991;63(3-4):613-35.

[141] Akter K, Lanza EA, Martin SA, Myronyuk N, Rua M, Raffa RB. Diabetes mellitus and Alzheimer's disease: shared pathology and treatment? British Journal of Clinical Pharmacology. 2011;71(3):365-76.

[142] Bosco D, Fava A, Plastino M, Montalcini T, Pujia A. Possible implications of insulin resistance and glucose metabolism in Alzheimer's disease pathogenesis. Journal of Cellular and Molecular Medicine. 2011;15(9):1807-21.

[143] Seyfried TN, Shelton LM. Cancer as a metabolic disease. Nutrition & Metabolism. 2010;7(1):7.

[144] Kembro JM, Cortassa S, Lloyd D, Sollot SJ, Aon MA. Mitochondrial chaotic dynamics: Redox-energetic behavior at the edge of stability. Scientific Reports. 2018;11:15422.

[145] Macknight ADC. Principles of Cell Volume Regulation. Kidney and Blood Pressure Research. 1988;21(3–5):114-41.

[146] Kuwahata T. Effects of adenosine and ATP on the membrane potential and synaptic transmission in neurons of the rat locus coeruleus. The Kurume Medical Journal. 2004;51(2):109-23.

[147] Battle C, Broedersz CP, Fakhri N, Geyer VF, Howard J, Schmidt CF, et al. Broken detailed balance at mesoscopic scales in active biological systems. Science. 2016;352(6285):604-7.

[148] Rupprecht J, Prost J. A fresh eye on nonequilibrium system. Science. 2016;352(6285):514-5.

[149] Kurz FT, Aon MA, O'Rourke B, Armoundas AA. Assessing Spatiotemporal and Functional Organization of Mitochondrial Networks. Mitochondrial Bioenergetics Methods in Molecular Biology. 2018;1782:383-402.

[150] Kurz FT, Kembro JM, Flesia AG, Armoundas AA, Cortassa S, Aon MA, et al. Network dynamics: quantitativeanalysis of complex behavior inmetabolism, organelles, and cells,from experiments to modelsand back. WIREs Syst Biol Med. 2017;9(1).

[151] Vetter L, Cortassa S, O'Rourke B, Armoundas AA, Bedja D, Jende JME, et al. Diabetes Increases the Vulnerability of the Cardiac Mitochondrial Network to Criticality. Front Physiol. 2020;11:175.

[152] Bier M, Bakker BM, Westerhoff HV. How yeast cells synchronize their glycolytic oscillations: a perturbation analytic treatment. Biophys J. 2000;78(3):1087-93.

[153] Petkoski S, Stefanovska A. Kuramoto model with time-varying parameters. Phys Rev E. 2012;86:046212.

[154] Petkoski S, Iatsenko D, Basnarkov L, Stefanovska A. Differences between Mean Field and Mean Ensemble Frequencies of a System of Coupled Oscillators. Phys Rev E. 2013;87:032908.

[155] Catterall WA, Raman IM, Robinson HPC, Sejnowski TJ, Paulsen O. The Hodgkin-Huxley heritage: from channels to circuits. J Neurosci. 2012;32(41):14064-73.

[156] Lloyd D, Murray DB, Aon MA, Cortassa S, Roussel MR, Beckmann M, et al. Temporal metabolic partitioning of the yeast and protist cellular networks: the cell is a global scale-invariant (fractal or self-similar) multioscillator. J of Biomedical Optics. 2018;24(5):051404.

[157] Bandrivskyy A, Bernjak A, McClintock PVE, Stefanovska A. Wavelet phase coherence analysis: Application to skin temperature and blood flow. Cardiovasc Engin. 2004;4(1):89-93.

[158] Sheppard LW, Stefanovska A, McClintock PVE. Testing for time-localised coherence in bivariate data. Phys Rev E. 2012;85:046205.

[159] Sheppard LW, Bell JR, Harrington R, Reuman DC. Changes in large-scale climate alter spatial synchrony of aphid pests. Nature Clim Change. 2016;6:610-3.

[160] Amemiya T, Shibata K, Du Y, Nakata S, Yamaguchi T. Modeling studies of heterogeneities in glycolytic oscillations in HeLa cervical cancer cells. Chaos. 2019;29(3):033132.

[161] Weber A, Zuschratter W, Hauser MJB. Partial synchronisation of glycolytic oscillations in yeast cell populations. Sci Rep. 2020;10:19714.

[162] Sheppard LW, Stefanovska A, McClintock PVE. Detecting the harmonics of oscillations with time-variable frequencies. Phys Rev E. 2011;83:016206.

[163] Paluš M, Stefanovska A. Direction of coupling from phases of interacting oscillators: An information-theoretic approach. Phys Rev E. 2003;67:055201(R).

[164] Paluš M, Vejmelka M. Directionality of coupling from bivariate time series: How to avoid false causalities and missed connections. Phys Rev E. 2007;75(5):056211.

[165] Musizza B, Stefanovska A, McClintock PVE, Paluš M, Petrovčič J, Ribarič S, et al. Interactions between cardiac, respiratory, and EEG-δ oscillations in rats during anæsthesia. J Physiol (London). 2007;580(1):315-26.

[166] Barnes SJK, Stefanovska A. Physics of cellular energy metabolism. Adv Exp Med Biol. 2022;62:125-43.

[167] Xiong H, Pandey G, Steinbach M, Kumar V. Enhancing data analysis with noise removal. IEEE Trans Knowl Data Eng. 2006;18(3):304-19.

[168] Schreiber T, Grassberger P. A simple noise-reduction method for real data. Phys Lett A. 1991;160(5):411-8.

[169] Osborne AR, Pastorello A. Simultaneous occurence of low-dimensional chaos and colored random noise in nonlinear physical systems. Phys Lett A. 1993;181(2):159-71.

[170] Scott SG, Hutchinson DAW. Incoherence of Bose-Einstein condensates at supersonic speeds due to quantum noise. Phys Rev A. 2008;72:063614.

[171] Kuhlmann AV, Houel J, Ludwig A, Greuter L, Reuter D, Wieck AD, et al. Charge noise and spin noise in a semiconductor quantum device. Nat Phys. 2013;9(9):570-5.

[172] Brückner DB, Fink A, Schreiber C, Röttgermann PJF, Rädler JO, Broedersz CP. Stochastic nonlinear dynamics of confined cell migration in two-state systems. Nat Phys. 2019;15(6):595-601.

[173] Nassif SR, Fakhouri O. Technology Trends in Power-Grid-Induced Noise. Association for Computing Machinery; 2002. p. 55–59.

[174] Black F. Noise. J Finance. 1986;41(3):528-43.

[175] Pikovskii AS. Solar variability and stochastic effects on climate. Radiophys Quantum Electron. 1984;27:390-5.

[176] Antonov VA. Modeling of processes of cyclic evolution type. Synchronization by a random signal. Vestnik Leningrad Univ Mat Mekh Astronom. 1984;vyp. 2:67-76.

[177] Johnson JB. The Schottky effect in low frequency circuits. Phys Rev. 1925;26:71-85.

[178] Schottky W. Small-Shot Effect and Flicker Effect. Phys Rev. 1926;28:74-103.

[179] von Smoluchowski M. Zur kinetischen Theorie der Brownschen Molekularbewegung und der Suspensionen. Ann Phys. 1906;21(14):756-80.

[180] Mandelbrot BB. Multifractals and 1/f Noise. 1st ed. Springer New York; 1999.

[181] Chen Y. Zipf's law, 1/f noise, and fractal hierarchy. Chaos, Solitons and Fractals. 2012;45(1):63-73.

[182] Bak P, Tang C, Wiesenfeld K. Self-organized criticality: An explanation of the 1/f noise. Phys Rev Lett. 1987;59(4):381-4.

[183] Rao TS. The Fitting of Non-Stationary Time-Series Models with Time-Dependent Parameters. J R Stat Soc Ser B Methodol. 1970;32(2):312-22.

[184] Haslbeck JMB, Bringmann LF, Waldorp LJ. A Tutorial on Estimating Time-Varying Vector Autoregressive Models. Multivariate Behavioral Research. 2021;56(1):120-49.

[185] Crisan D. The stochastic filtering problem: a brief historical account. J Appl Probab. 2014;51(A):13-22.

[186] Dutta P, Horn PM. Low-frequency fluctuations in solids: 1/f noise. Rev Mod Phys. 1981;53:497.

[187] Weissman MB. 1/f noise and other slow, nonexponential kinetics in condensed matter. Rev Mod Phys. 1988;60:537.

[188] Balandin AA. Low-frequency 1/f noise in graphene devices. Nat Nanotech. 2013;8:549.

[189] Burnett J, Faoro L, Wisby I, Gurtovoi VL, Chernykh AV, Mikhailov GM, et al. Evidence for interacting two-level systems from the 1/f noise of a superconducting resonator. Nat Commun. 2014;5:4119.

[190] Mishin Y. Thermodynamic theory of equilibrium fluctuations. Ann Phys. 2015;363:48.

[191] Costanzi BN, Dahlberg ED. Emergent 1/f noise in ensembles of random telegraph noise oscillators. Phys Rev Lett. 2017;119:097201.

[192] Peng CK, Buldyrev SV, Havlin S, Simons M, Stanley HE, Goldberger AL. Mosaic organisation of DNA Nucleotides. Phys Rev E. 1994;49(2):1685-9.

[193] Hasselmann K. Stochastic climate models Part I. Theory. Tellus. 1976;28(6):473-85.

[194] Arnold L. Hasselmann's program revisited: the analysis of stochasticity in deterministic climate models. In: Imkeller P, von Storch JS, editors. Stochastic Climate Models. Basel: Birkhäuser Basel; 2001. p. 141-57.

[195] Zhang X, Kuehn C, Hallerberg S. Predictability of critical transitions. Phys Rev E. 2015 Nov;92:052905.

[196] Lotrič MB, Stefanovska A, Štajer D, Urbančič-Rovan V. Spectral components of heart rate variability determined by wavelet analysis. Physiol Meas. 2000;21:441-57.

[197] Huang NE, Shen Z, Long SR, Wu MC, Shih HH, Zheng Q, et al. The empirical mode decomposition and the Hilbert spectrum for nonlinear and non-stationary time series analysis. Proc R Soc Lond A. 1998;454:903-95.

[198] Rasmussen M. Finite-time attractivity and bifurcation for nonautonomous differential equations. Differ Equ Dyn Syst. 2010;18(1):57-78.

[199] Giesl P, McMichen J. Determination of the area of exponential attraction in one-dimensional finite-time systems using meshless collocation. Discret Contin Dyn Sys B. 2018;23(4):1835-50.

[200] Kaszás B, Feudel U, Tél T. Leaking in history space: A way to analyze systems subjected to arbitrary driving. Chaos. 2018;28(3):033612.

[201] Rowland Adams J, Stefanovska A. Modeling Cell Energy Metabolism as Weighted Networks of Non-autonomous Oscillators. Front Physiol. 2021;11:1845.

[202] Melbourne I, Gottwald GA. Power spectra for deterministic chaotic dynamical systems. Nonlinearity. 2008;21:179-89.

[203] Anishchenko VS, Vadivasova TE, Okrokvertskhov GA, Strelkova GI. Statistical properties of dynamical chaos. Phys-Usp. 2005;48(2):151.

[204] Alberts B, Johnson A, Lewis J, Raff M, Roberts K, Walter P. Molecular Biology of the Cell. CRC Press Inc; 2002.

[205] Juniper MPN, Straube AV, Besseling R, Aarts DGAL, Dullens RPA. Microscopic dynamics of synchronization in driven colloids. Nat Commun. 2015;6:7187.

[206] Kvale M, Hebboul SE. Theory of Shapiro steps in Josephson-junction arrays and their topology. Phys Rev B. 1991;43(4):3720-3.

[207] Clemson PT, Stefanovska A. Discerning non-autonomous dynamics. Phys Rep. 2014;542(4):297-368.

[208] Kaiser G. A Friendly Guide to Wavelets. Boston: Birkhäuser; 1994.

[209] van Milligen BP, Sanchez E, Estrada T, Hidalgo C, Branas B, Carreras B, et al. Wavelet bicoherence – a new turbulence analysis tool. Phys, of Plasmas. 1995;2(8):3017-32.

[210] Stankovski T, Pereira T, McClintock PVE, Stefanovska A. Coupling functions: Universal insights into dynamical interaction mechanisms. Rev Mod Phys. 2017;89:045001.

[211] Newman J, Lancaster G, Stefanovska A. Multiscale Oscillatory Dynamics Analysis, User Manual, Version 1.01; 2018.

[212] Smith III JO. Mathematics of the Discrete Fourier Transform (DFT): With Audio Applications. 2nd ed. W3K Publishing; 2007.

[213] Iatsenko D, McClintock PVE, Stefanovska A. Linear and synchrosqueezed time-frequency representations revisited: Overview, standards of use, resolution, reconstruction, concentration, and algorithms. Dig Sig Proc. 2015;42:1-26.

[214] Costa M, Goldberger AL, Peng CK. Multiscale entropy analysis of biological signals. Phys Rev E. 2005;71:021906.

[215] Richman JS, Moorman JR. Physiological time-series analysis using approximate entropy and sample entropy. Am J Physiol Heart Circ Physiol. 2000;278(6):H2039-49.

[216] Tanskanen EI. A comprehensive high-throughput analysis of substorms observed by IMAGE magnetometer network: Years 1993–2003 examined. J Geophys Res Space Phys. 2009;114(A5).

[217] King J, Papitashvili N. Solar wind spatial scales in and comparisons of hourly Wind and ACE plasma and magnetic field data. J Geophys Res. 2005;110:A02104.

[218] Orr L, Chapman SC, Beggan CD. Wavelet and Network Analysis of Magnetic Field Variation and Geomagnetically Induced Currents During Large Storms. Space Weather. 2021;19:e2021SW002772.

[219] Heelis RA. Electrodynamics in the low and middle latitude ionosphere: a tutorial. J Atmos Sol Terr Phys. 2004;66(10):825-38.

[220] Rabiu AB, Mamukuyomi AI, Joshua EO. Variability of equatorial ionosphere inferred from geomagnetic field measurements. Bull Astr Soc India. 2007;35:607-18.

[221] Campbell WH. An introduction to quiet daily geomagnetic fields. Pure Appl Geophys. 1989;131:315-31.

[222] Choi KE, Yung DY. Origin of Solar Rotational Periodicity and Harmonics Identified in the Interplanetary Magnetic Field B_z Component Near the Earth During Solar Cycles 23 and 24. Solar Phys. 2019;294(4):44.

[223] Roberts OW, Alexandrova O, Sorriso-Valvo L, Vörös Z, Nakamura R, Fischer D, et al. Scale-Dependent Kurtosis of Magnetic Field Fluctuations in the Solar Wind: A Multi-Scale Study With Cluster 2003–2015. J Geophys Res. 2022;127(9):e2021JA029483.

[224] Matteo MD, Villante U. The identification of solar wind waves at discrete frequencies and the role of the spectral analysis techniques. J Geophys Res. 2017;122(5):4905-20.

[225] Echer E, dS Franco AM, da Costa Junior E, Hajra R, José M, Bolzan A. Solar-Wind High-Speed Stream (HSS) Alfvén Wave Fluctuations at High Heliospheric Latitudes: Ulysses Observations During Two Solar-Cycle Minima. Solar Phys. 2022;297(11):143.

[226] Pellerin L, Magistretti P. Sweet Sixteen for ANLS. J Cereb Blood Flow Metab. 2012;32(7):1152-66.

[227] Magistretti P, Allaman I. A Cellular Perspective on Brain Energy Metabolism and Functional Imaging. Neuron. 2015;86(4):883-901.

[228] Smedler E, Uhlén P. Frequency decoding of calcium oscillations. Biochim Biophys Acta. 2014;1840(3):964-9.